Technical Report Documentation Page

1. Report No.	2. Government Accession No.	3. Recipient's Catalog No.
FHWA/TX-98/1404-2		

4. Title and Subtitle	5. Report Date
MEASURED BEHAVIOR OF A CURVED PRECAST SEGMENTAL CONCRETE BRIDGE ERECTED BY BALANCED CANTILEVERING	January 1998
	6. Performing Organization Code

7. Author(s)	8. Performing Organization Report No.
M. Keith Thompson, Rodney T. Davis, John E. Breen, and Michael E. Kreger	Research Report 1404-2

9. Performing Organization Name and Address	10. Work Unit No. (TRAIS)
Center for Transportation Research The University of Texas at Austin 3208 Red River, Suite 200 Austin, TX 78705-2650	11. Contract or Grant No. Project 0-1404

12. Sponsoring Agency Name and Address	13. Type of Report and Period Covered
Texas Department of Transportation Construction Division/Research Section P.O. Box 5080 Austin, TX 78763-5080	Research Report (9/96-8/97)
	14. Sponsoring Agency Code

15. Supplementary Notes

Project conducted in cooperation with the U. S. Department of Transportation

16. Abstract

A five-span continuous precast segmental horizontally curved concrete bridge erected in balanced cantilever as part of the US Highway 183 interchange with Interstate Highway 35 in Austin, Texas, was instrumented with concrete strain gauge devices, thermocouples, and tilt meters. The response of the structure was studied during erection, during live load test, and under the actions of daily applied thermal gradients that occurred over a period of nine months. Measured data are presented and compared with calculated values. The measured data are also used to evaluate design specifications in current highway bridge codes. Observations of the construction process and comments regarding improvements in design and in the efficiency of the construction methods used to build the bridge are also presented. Recommendations are made concerning bridge design specifications and construction practices.

17. Key Words	18. Distribution Statement
Field measurements, precast concrete piers, segmental bridges, cantilever erection, bridge instrumentation, thermal gradients, live load tests	No restrictions. This document is available to the public through the National Technical Information Service, Springfield, Virginia 22161.

19. Security Classif. (of report)	20. Security Classif. (of this page)	21. No. of pages	22. Price
Unclassified	Unclassified	168	

Form DOT F 1700.7 (8-72) Reproduction of completed page authorized

MEASURED BEHAVIOR OF A CURVED PRECAST SEGMENTAL CONCRETE BRIDGE ERECTED BY BALANCED CANTILEVERING

by

Keith Thompson,
Rodney T. Davis,
John E. Breen,
and
Michael E. Kreger

Research Report 1404-2

Research Project 0-1404
Instrumentation of Precast Segmental Box Girder Bridges on US 183 in Austin

Conducted for the

TEXAS DEPARTMENT OF TRANSPORTATION

in cooperation with the

U. S. DEPARTMENT OF TRANSPORTATION
Federal Highway Administration

by the

CENTER FOR TRANSPORTATION RESEARCH
Bureau of Engineering Research
THE UNIVERSITY OF TEXAS AT AUSTIN

January 1998

IMPLEMENTATION

This report documents observations and measurements made during the construction of balanced cantilevering of a five-span, continuous segmental concrete, curved box-girder bridge. Based on observations made during construction, and on measurements taken of concrete strains, tendon strains, temperature distributions, and slopes, a series of detailed design-, construction-, and inspection-related recommendations are made. While the behavior of the bridge as designed and constructed was excellent, there are a number of improvements that could make the construction of this type of structure even more efficient. These improvements include:

(1) more sensitivity in design to the need for access for construction operations,

(2) limits on the length of tendons in order to avoid high-friction losses and tangling, and

(3) more attention to the constructor and his erection engineers to detailing and test runs of innovative erection methods.

Numerous suggestions are made for improvements in detailing, erection procedures, and inspection procedures to correct observed problems and difficulties. A number of comments and recommendations are made for improvements and clarifications to American Association of State Highway and Transportation Officials (AASHTO) specifications. Adoption of these recommendations should help designers and constructors improve the efficiency of segmental bridge construction, resulting in both lower initial costs and improved durability.

ACKNOWLEDGMENTS

The authors express appreciation for the guidance provided by the Texas Department of Transportation (TxDOT) Project Director, T. E. Rummel (Design), and by the TxDOT Project Monitoring Committee, which included D. Harley (FHWA) and C. Titus (CMD).

DISCLAIMERS

The contents of this report reflect the views of the authors, who are responsible for the facts and the accuracy of the data presented herein. The contents do not necessarily reflect the official views or policies of the Federal Highway Administration or the Texas Department of Transportation. This report does not constitute a standard, specification, or regulation.

There was no invention or discovery conceived or first actually reduced to practice in the course of or under this contract, including any art, method, process, machine, manufacture, design or composition of matter, or any new and useful improvement thereof, or any variety of plant, which is or may be patentable under the patent laws of the United States of America or any foreign country.

NOT INTENDED FOR CONSTRUCTION, BIDDING, OR PERMIT PURPOSES

John E. Breen, P.E. (Texas No. 18479)
Michael E. Kreger, P.E. (Texas No. 65541)
Research Supervisors

TABLE OF CONTENTS

CHAPTER 1. INTRODUCTION

1.1 General

This report presents results from the study of a five-span, continuous precast, segmented horizontally curved, concrete bridge structure constructed in balanced cantilever. This structure is part of a flyover ramp between northbound IH-35 and northbound US 183 in Austin, Texas. This research has been conducted by the Phil M. Ferguson Structural Engineering Laboratory as part of a study sponsored by the Texas Department of Transportation (TxDOT) to investigate the structural performance of the US 183 elevated highway recently completed in north central Austin. The results of this research will be furnished to TxDOT engineers to improve the design and construction of segmental bridges in Texas and in the rest of the U.S. The overall study focused on the performance of four structures within the US 183 project: an innovative Y-shaped, cast-in-place pier, a three-span semicontinuous precast segmental superstructure unit constructed span-by-span, a tall precast segmental pier, and the five-span, continuous precast segmental bridge structure constructed in balanced cantilever that will be the topic of this report. This report is based on the master's thesis of the senior author (22). The other three types of structures have been reported in detail by Andres (4), Bonzon (6), Wood (23), and Davis (7). These studies are summarized in Reports 1404-1 and 1404-3F.

1.2 Project Overview

US 183 passes through the northern part of Austin, Texas, and serves as an important piece of the arterial viaducts carrying traffic in and around the city. Elevated lanes were constructed on the portion of US 183 that runs through north Austin to alleviate congestion by separating through traffic from local traffic. The project was designed by TxDOT and contracted by Martin K. Eby Construction in a joint venture with Flatiron Structures Company.

An important design consideration for the TxDOT bridge engineers who worked on US 183 was the aesthetics of the project. Negative public response to the previously built IH-35 elevated freeway on the eastern edge of Austin prompted designers to give careful consideration to the appearance of the US 183 project. The size of the project (over 10 kilometers of bridge structure) and the need to reduce the amount of substructure for ground level right-of-way limitations made a precast segmental box girder solution optimal. The simple form and lightweight appearance of this type of superstructure was deemed a more aesthetically pleasing structure than the typical pretensioned I-girder superstructures used in most Texas bridges. The box girder choice also allowed for longer spans and a reduction of project substructure, which in turn provided economic benefits and opened up the space beneath the bridge for less intrusion of the structure on local businesses and residential communities. Architectural details of the piers and the superstructure were chosen to further improve the appearance of the bridge.

The solution chosen by the TxDOT designers proved to be very cost effective as well as aesthetic. The average cost of the project that had spans in the 39.6-m (130-ft) range was

420 $/m^2 (39 $/ft^2), as compared with the Texas average of 344 $/m^2 (32 $/ft^2) and the U.S. average of 743 $/m^2 (69 $/ft^2). The latter averages are for a wide range of girder bridges, frequently with much shorter span lengths. The project encompassed 121,000 m^2 (1,300,000 ft^2) of deck space. One hundred ninety-eight spans of the elevated highway were constructed span-by-span. Fifteen transition spans were cast-in-place because it was too difficult to modify the precast forms for these structures. Five spans that had much longer lengths were built in balanced cantilever that helped reduce traffic interruptions in a key intersection. The five spans built in balanced cantilever formed one part of a ramp structure connecting northbound IH-35 with northbound US 183. This ramp was designated as Ramp P in contract drawings. Figure 1.1 shows the location of the US 183 project and the portion known as Ramp P.

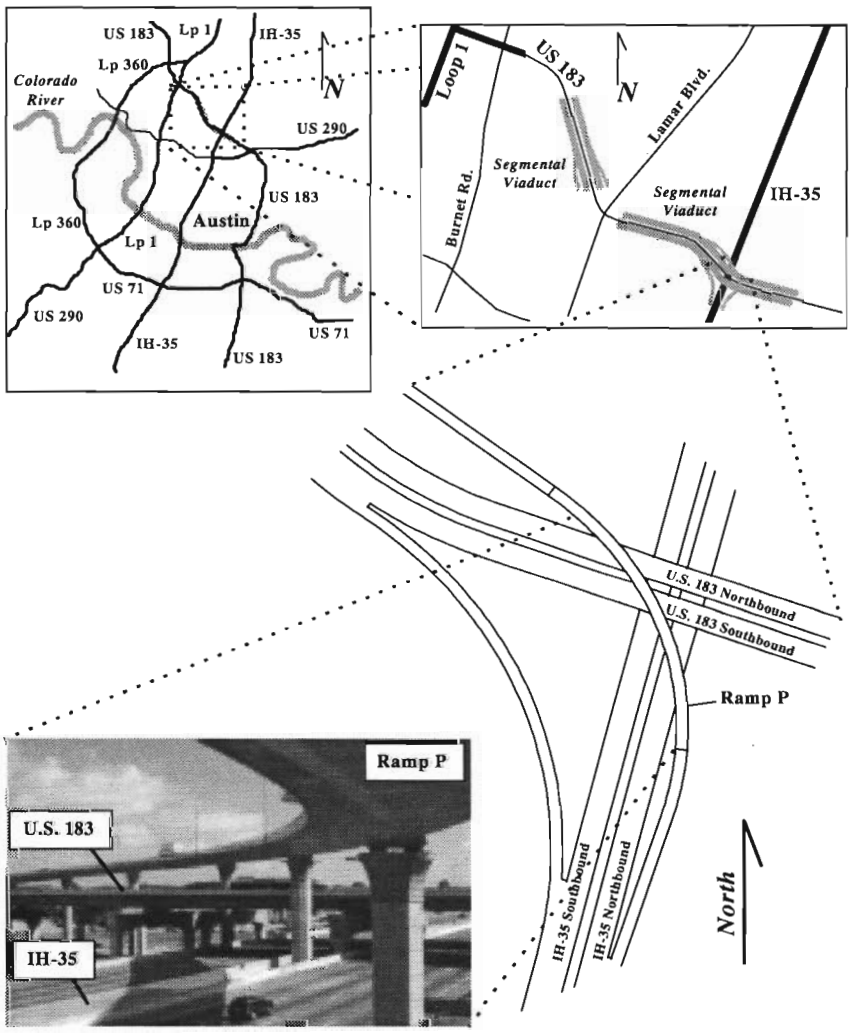

Figure 1.1 US 183 project location

1.3 Description of Ramp P

The alignment of the flyover ramp between northbound IH-35 and northbound US 183 (Ramp P) required the structure to pass over the main lanes and frontage roads of both of those highways. The congestion in the area beneath the ramp reduced the space available for supporting substructure requiring longer spans in the ramp than were typical of the rest of the project. The alignment of the ramp also followed a fairly tight radius of 221 m (726 ft). Both of these constrictions made use of the span-by-span construction method — which was used extensively through the rest of the US 183 project — impractical for construction of Ramp P. Therefore, balanced cantilever construction was used to build the ramp.

Figure 1.2 shows the span arrangement of Ramp P. The ramp had heavy anchorage diaphragms for post-tensioning tendons over each pier. The dimensions of the segments that had these diaphragms (four total) are given in Figure 1.3. Typical segments had an increasing bottom-flange thickness near the interior piers. The bottom-flange modification was necessitated by the heavy negative moment from the free cantilever construction load. Figure 1.4 shows the typical segment dimensions. Figure 1.5 shows the dimensions of the pier cross section.

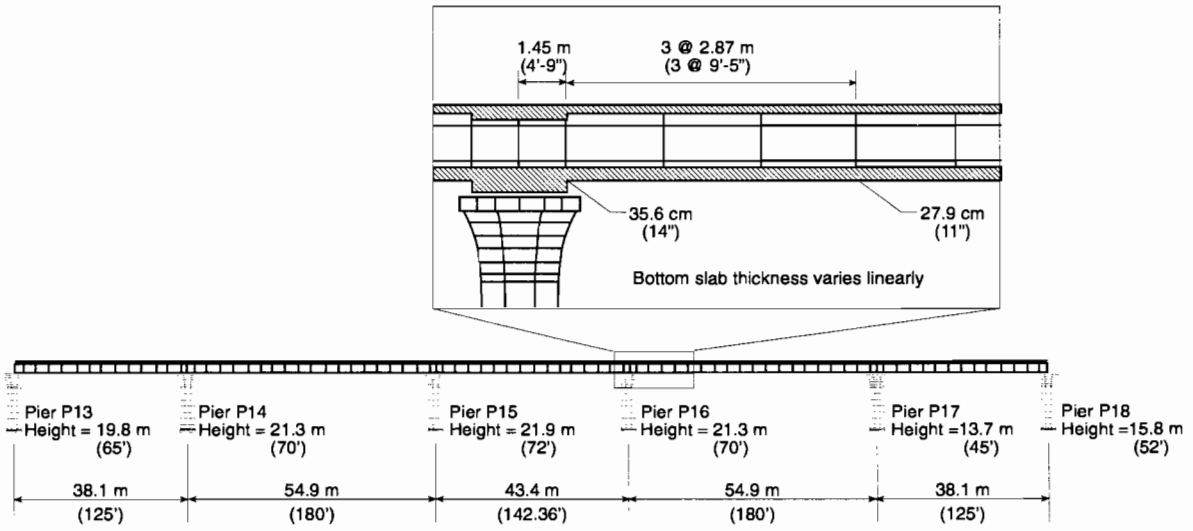

Figure 1.2 Layout of Ramp P

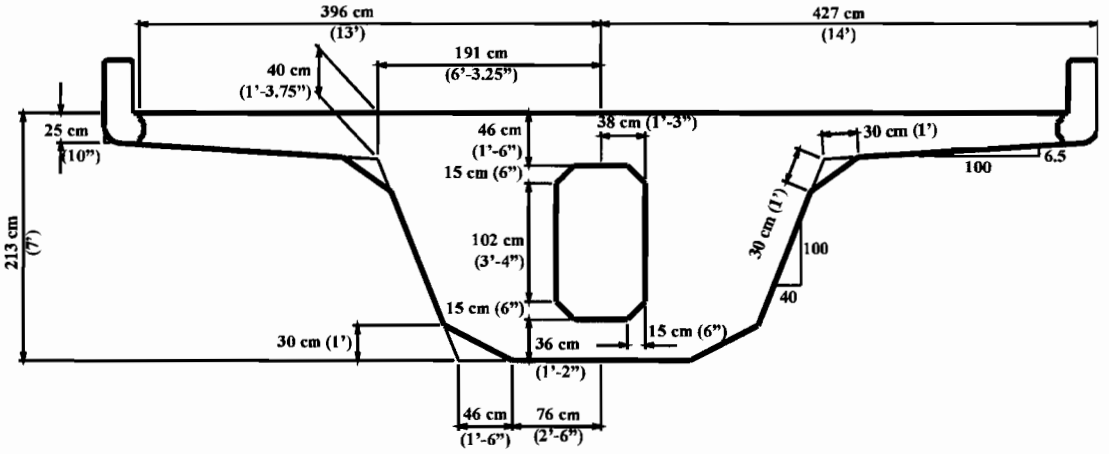

Figure 1.3 Dimensions for Ramp P interior anchorage segment cross section

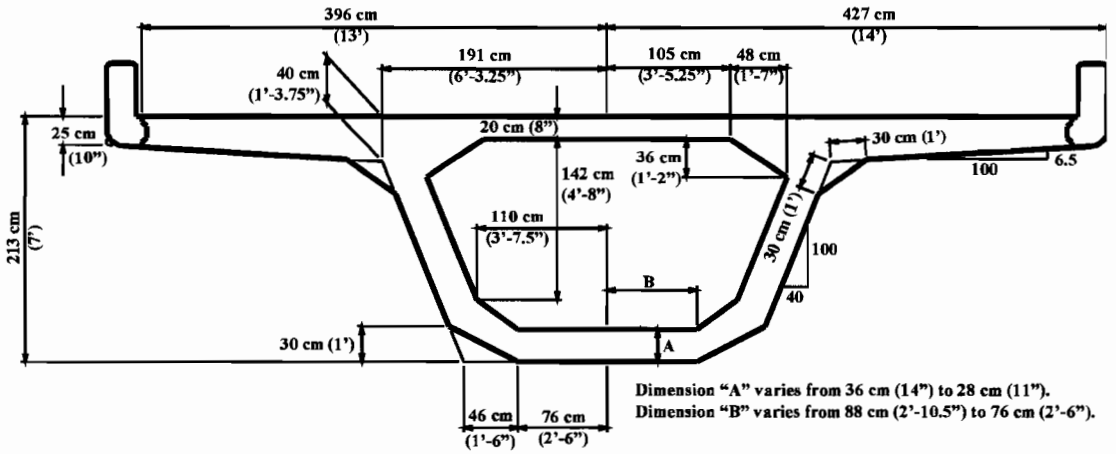

Figure 1.4 Dimensions for Ramp P typical segment cross section

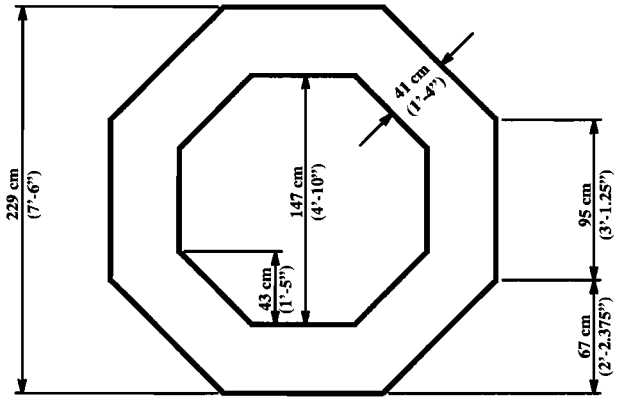

Figure 1.5 Dimensions for large ramp pier cross-section

1.4 Problem Statement and Objectives

Segmental bridge construction is still a relatively new form of technology for many engineers in the U.S. Education of engineering students with respect to design or erection of precast, post-tensioned construction of any form is not common in the curriculum of most U.S. universities. TxDOT has sponsored a broad program of research into segmental bridge topics that began in 1970 with the construction and study of the JFK Memorial Causeway in Corpus Christi, Texas. Over the years TxDOT has invested much money into research projects designed to advance the knowledge of the actual behavior of segmental bridges. Most of the information gained from this research has been implemented in the provisions of the AASHTO Guide Specifications for Design and Construction of Segmental Bridges (1). The AASHTO Guide Specifications are one of the only texts available to bridge engineers that provides guidance in the design of segmental bridges. Many of the guidelines in the AASHTO Guide Specifications are derived from analytical studies or laboratory research of reduced scale bridge models. Studies from actual bridge structures are not numerous enough to provide confirmation of all of the guidelines, nor do they include the full range of bridge structures covered under the AASHTO Guide Specifications. The purpose of the study of the US 183 project is to provide data from an actual bridge structure that can be used to verify commonly used analytical methods for bridge design and to point out problem areas that may have escaped the attention of engineers in the past. Specifically, the study of Ramp P is intended to satisfy the following objectives:

1. To comprehensively instrument the ramp so that its flexural and torsional behavior under various loading conditions could be fully determined.
2. To determine the behavior of the ramp under construction loads.
3. To observe the construction of the ramp and report on constructability problems related to segmental balanced cantilever construction.
4. To determine the behavior of the completed ramp under live load.

5. To measure thermal gradients and creep effects in the ramp over an extended period of time.
6. To determine the response of the ramp to these applied thermal gradients.
7. To make recommendations to TXDOT and AASHTO of any needed changes in design procedures or design specifications based on the indications from the recorded data and the observations of the researchers involved in the study.

1.5 Scope of Work

The scope of work encompassed by this report includes the instrumentation of one span of a five-span continuous precast segmental horizontally curved concrete box girder bridge constructed in balanced cantilever. Instruments were monitored at two-minute intervals during the construction process and during a live load test performed on the completed structure. Instruments were monitored hourly at all other times (during construction and since completion of the structure) to determine the thermal gradients occurring in the structure and the response to these gradients. Data measured with the instrumentation were then compared to simple analytical calculations of predicted behavior. When applicable, calculations were based on recommended methods from the *Proposed AASHTO LRFD Guide Specifications for Design and Construction of Segmental Bridges* (17) or the *AASHTO LRFD Bridge Design Specifications* (2). Recommendations for changes in design practices are given when deemed necessary.

1.6 Organization of Report

The organization of this report is as follows:

Chapter 1 - Introduction
Chapter 2 - Background and Previous Studies
Chapter 3 - Superstructure Instrumentation
Chapter 4 - Superstructure Construction Process
Chapter 5 - Construction Sequence Data
Chapter 6 - Live-Load Test
Chapter 7 - Thermal Behavior
Chapter 8 - Conclusions and Recommendations

Chapters 1, 2, and 3 provide background information that will facilitate the reader's comprehension of the chapters that present data and observations (Chapters 4 through 7). Chapters 4 through 7 each contain their own conclusions and recommendations that are relevant to the topics discussed in those chapters. Chapter 8 summarizes the conclusions and recommendations from Chapters 4 through 7. Detailed data and fuller documentation are included (22).

CHAPTER 2. BACKGROUND

2.1 Introduction

This chapter presents the reader with background information pertinent to the topics that will be discussed in this report. Therefore, this chapter contains discussions on:

- the historical background of prestressed segmental construction with emphasis on balanced cantilever construction
- stress distributions in segmental hollow box girder bridges,
- thermal effects on bridges,
- the behavior of curved girders, and
- analysis methods for segmental concrete box girder bridges.

2.2 Prestressed Segmental Construction

A number of previous reports produced by the Ferguson Structural Engineering Laboratory (FSEL) have included detailed descriptions of the development of segmental bridge construction. Particularly, Arréllaga (5) provides a thorough background summary of prestressed segmental bridge development. In addition, the texts by Podolny and Müller (5) and Menn (11) have served as the traditional resources on segmental bridge design and construction for many years. Both contain very good descriptions of the development of prestressed segmental bridges. However, both of these texts were published in the 1980s and have already become out-of-date with regard to the latest accomplishments in this rapidly advancing industry.

2.2.1 Evolution

The modern state of prestressed concrete segmental box girder bridges is the result of developments in materials and techniques used for prestressing and of the technology used in segmental construction.

Prestressing

Prestressing was first applied to bridges between 1910 and 1912 by Eugene Freyssinet with the La Veurde Bridge, a three-span arch bridge over the Allier River in France. Freyssinet used jacks placed at the apexes of the arches to push the two halves apart and remove creep deflections from the bridge (Figure 2.1). The applied deformations were maintained in the bridge by placing mortar permanently in the apexes of the arches. Freyssinet continued to pursue the idea of using applied forces to enhance the structural performance of bridge structures and eventually patented a steel wire system for prestressing in 1928 (5).

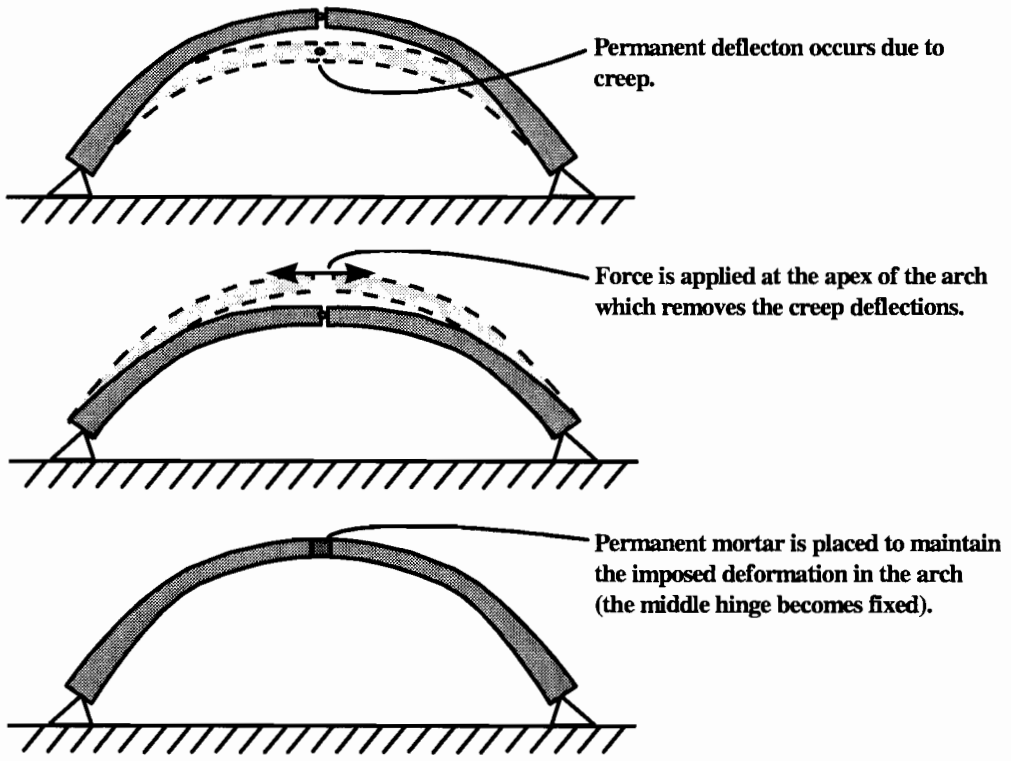

Figure 2.1 The beginnings of prestressing in bridges

The first modern use of tensioned steel for prestressing of a bridge occurred in 1928. Dischinger used large diameter steel rods to post-tension the 61 m (200 ft) long concrete span of the Saale-Brucke Bridge in Germany. These rods were of the relatively low-strength steel that was available at the time. Eventually, creep and shrinkage of the concrete and relaxation of the steel resulted in losses of 75% of the initial prestress force in the bars. Prestressed concrete was hampered by these phenomena and the difficulties of stressing in the field. However, advances in technology produced higher strength steel at economical costs as well as better anchorage and jacking systems for steel bars and wires. Such advances occurred quickly. By 1939, prestressing in concrete structures began to rapidly infiltrate into bridge designs.

Segmental Construction

Segmental construction had been in practice in Europe since the twelfth century. The process evolved from masonry structures to reinforced concrete structures. By 1901, hollow box reinforced concrete sections were being used for arch bridges (11).

Precasting of concrete, which was first applied to short-span beam bridges, was combined with segmental construction by Eugene Freyssinet in the early 1940s. The Pont de Luzancy was a precast, prestressed, segmental girder bridge. It was completed in 1946.

Cantilever Construction

The first recorded use of the cantilever construction method for bridges was in the fourth century with the Shogun's Bridge in the city of Nikko, Japan (15). Cantilever construction had been used extensively for the construction of steel bridges in the late 1800s. The St. Louis Bridge, a steel truss arch designed by James Eads, was constructed in cantilever so that falsework, which would block the flow of river traffic on the Mississippi River, could be avoided (14). Elimination of falsework has been the traditional reason for building bridges in cantilever.

The first application of cantilever construction to reinforced concrete was the Rio do Peixe Bridge in Herval, Brazil built in 1930 (11, 15). Cantilever construction with cast-in-place prestressed concrete first occurred in 1951 with the Lahn Bridge in Balduistein, Germany (11). Precast segmental bridges erected in balanced cantilever were built in the 1960s in the former Soviet Union (5).

In 1964 the Choisy-le-Roi Bridge was built over the Seine River in Paris. This bridge designed by Jean Muller represented the first use of balanced cantilever construction combined with precast segments having epoxied match-cast joints (11, 15). Since the construction of the Choisy-le-Roi Bridge, use of segmental balanced cantilever construction has become a common construction method for segmental bridges. The typical span ranges of bridges built in balanced cantilever compared with other segmental construction methods are shown in Figure 2.2. Cantilever construction is generally used for the following reasons:

- Congestion in the area beneath the bridge construction or environmental reasons prevent the use of falsework.
- Span lengths set by the spacing of the substructure elements are too long to build an economical erection truss for span-by-span construction or the size of the project is too small to make an erection truss a cost-effective expenditure.
- The method of construction leaves the bridge with a favorable distribution of dead load forces.

2.2.2 Segmental Bridge Codes in the United States

In the U.S., design and construction of segmental bridges is currently controlled by two manuals. The first is the *AASHTO Guide Specifications for Design and Construction of Segmental Bridges* (1), a specific set of code provisions focused on segmental issues only. The second is the *AASHTO Standard Specifications for Highway Bridges* (3), the general set of code provisions intended to govern the design of all bridge types in the U.S.

Currently, a proposed Load and Resistance Factor Design (LRFD) revision of the *AASHTO Guide Specifications* is under the process of review. The new *AASHTO LRFD Guide Specifications for Design of Segmental Bridges* (17) (as yet unpublished) will rely on the provisions of the new *AASHTO LRFD Bridge Design Specifications (1994 Edition)* (2).

These two manuals will shortly replace the previous *AASHTO Guide Specifications* and the *AASHTO Standard Bridge Design Specifications* as the controlling codes for segmental bridge design. Eventually, the *AASHTO LRFD Guide Specifications* will be completely incorporated into the *AASHTO LRFD Bridge Design Specifications*, and only one code manual will be used. This report will thus reference the two LRFD codes when discussing code provisions for segmental design.

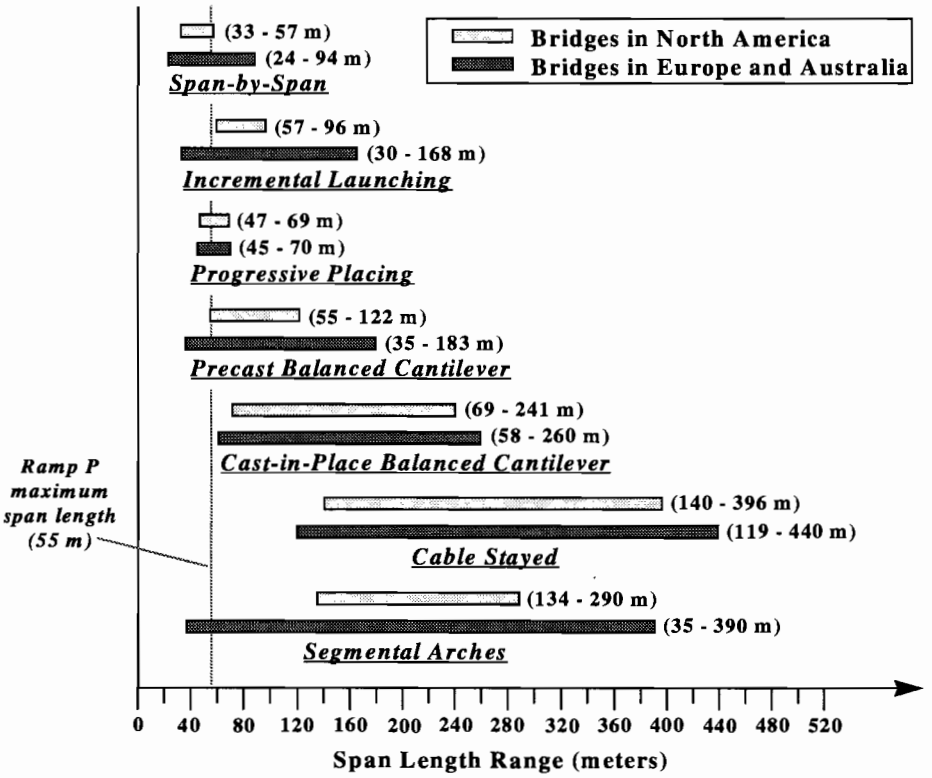

Figure 2.2 ***Span ranges for various segmental construction methods (after Arrélaga [5])***

2.3 Stress Distributions in Box Girders

Three phenomena cause nonlinear stress distributions in box girder cross sections. The first is the diffusion of post-tensioning that occurs near anchorage zones. The second is shear lag. The third is nonlinear thermal gradients. The first two of these topics will be covered in this section. The last will be covered in the subsequent section dealing with thermal effects on bridges.

2.3.1 Diffusion of Post-tensioning Forces

The concentrated force that is applied to the concrete from a post-tensioning anchorage takes a certain distance to distribute into the full cross section of the girder. Near the anchorages, only a small portion of the cross section will be active in resistance against the concentrated force. Thus, peaks occur in the stress distribution near those locations. Figure 2.3 taken from Kristek (10) shows an elastic, folded plate solution for the cross section pictured. Longitudinal normal stress and transverse splitting stress distributions are shown. The effect of the diffusion of the concentrated loads into the section is clearly seen. Away from the concentrated load, beam theory can be used to calculate the linear stress distribution. However, near the loads, the peak stresses in the cross section are much greater than would be calculated with beam theory assumptions. Furthermore, transverse splitting stresses are produced by the post-tensioning forces.

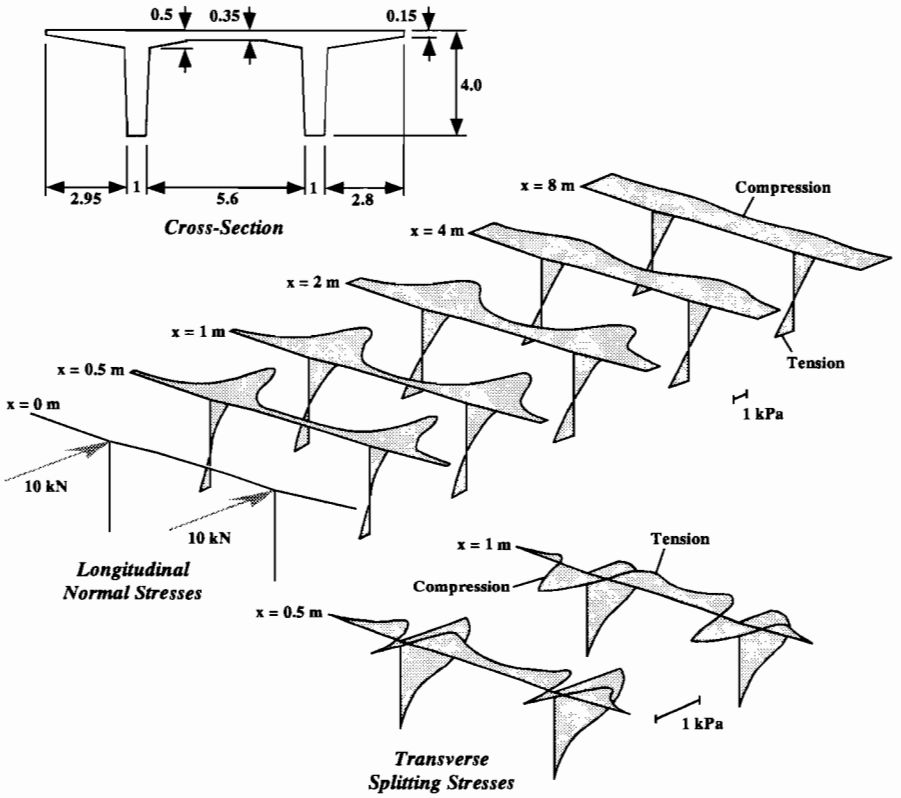

Figure 2.3 Example of the effects of the diffusion of post-tensioning forces (after Kristek [10])

Elastic solutions such as Figure 2.3 are rarely used for design. One approximate solution that is often used is to assume that the force diffuses into the girder in the form of a wedge projected outward from the anchorage zone. A typical angle of diffusion that would be used to define the wedge would be $\pm 30^{\circ}$ from the line of action of the post-tensioning concentrated force. The area inside of the wedge would be taken as the effective cross section used to calculate the normal and flexural stresses caused by the concentrated load. Such a method is recommended in the *AASHTO LRFD Bridge Design Specifications* (2).

2.3.2 Shear Lag

Shear lag is an effect caused by warping of the box girder section under applied shear loads. A cut taken between the top flange and the top of the webs shows that there must be a large force resultant transferred into the flange from the shear in the web (Figure 2.4). This force resultant causes deformations in the flange that bend it out of the plane of the cross section. The force creates a distribution of normal stresses that is non-uniform across the transverse width of the web.

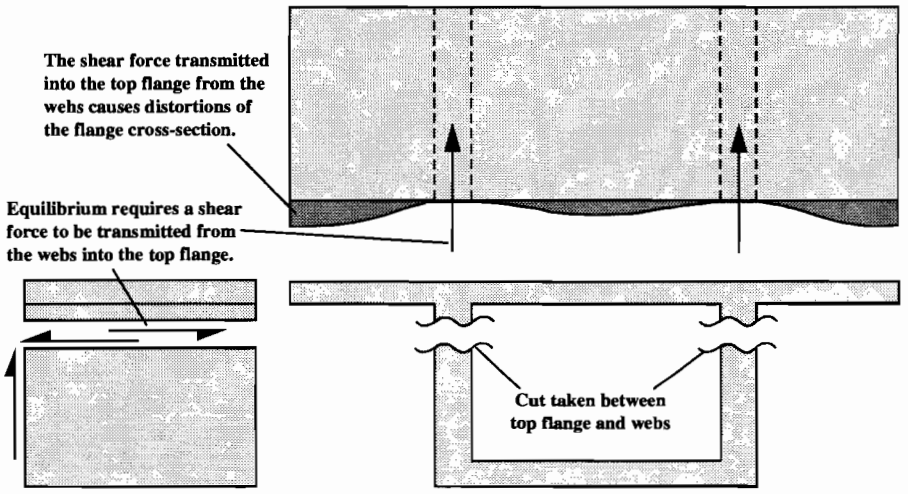

Figure 2.4 The effects of shear lag

Folded plate or finite element analyses will show shear lag effects directly. However, normal beam theory analysis will miss the effects of shear lag because it assumes plane sections remain plane. Thus, designers generally handle shear lag by using the approximate effective flange width method. This method reduces the areas of the top and bottom flanges that are considered effective for resisting normal and flexural forces. Thus, higher stresses will be calculated for the section in the flanges than if the entire section were considered effective. The effective width is chosen so that the peak stresses calculated using the effective section match those that would be calculated using more exact methods.

2.3.3 AASHTO Specifications

The *AASHTO LRFD Bridge Design Specifications* (2) deal with nonuniform stress distributions from concentrated axial forces and shear lag using effective flange width methods. These specifications are presented in Section 4.6.2.6.2 of the code. The provisions of Clause 3-10.2 of the *1983 Ontario Highway Bridge Design Code* (13) are also allowed as an alternative.

The effective flange width requirements for box girders are defined by four figures in Section 4.6.2.6.2 that are reproduced in Figures 2.5 through 2.8. The variables used are:

- d_o = depth of superstructure (in.)
- b = flange width on each side of the web (in.)
- b_m = generalized effective flange width used in conjunction with Figure 2.6 to determine b_{mf} and b_{ms} depending on the position of the section of interest in the span (in.)
- b_{mf} = effective flange width for interior portions of a span (in.)
- b_{ms} = effective flange width at interior support or for a cantilever arm (in.)
- a = portion of span subject to a transition in effective flange width taken as the lesser of the physical flange width on each side of the web shown in Figure 2.7 or one quarter of the span length in inches (in.)
- l_i = a notional span length specified in Figure 2.5 for the purpose of determining b_f and b_s specified in Figure 2.6
- b_s = coefficient for determining effective flange width at supports and for cantilever arms
- b_f = coefficient for determining effective flange width for interior portions of spans

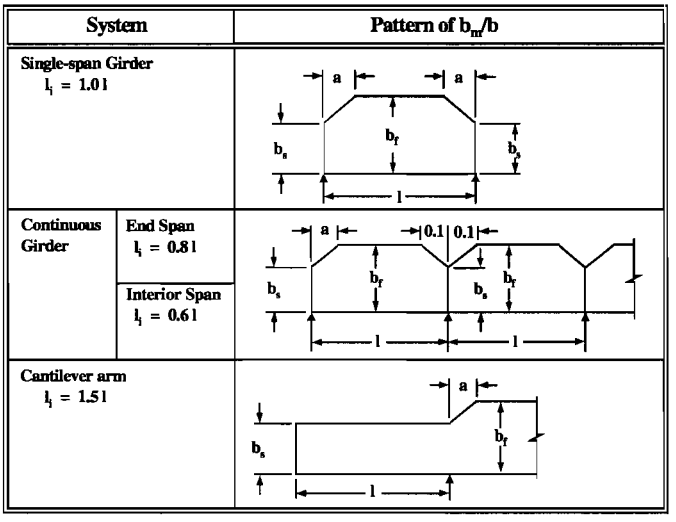

Figure 2.5 Pattern of effective flange width coefficients, b_f and b_s (Figure 4.6.2.6.2-1 from the AASHTO LRFD Bridge Design Specifications [2]

The effective flange widths b_{mf} and b_{ms} are determined as the product of the coefficient b_f and b_s, given as b_m/b in Figure 2.6, and the physical distance b, as given in Figure 2.7. The following interpretations apply:

- The b shall be taken as the flange width either side of the web, i.e., b_1, b_2, or b_3 in Figure 2.7.
- For $b \leq 0.3d_o$, no reduction in flange width need be considered.
- For $b > 0.3d_o$, the effective width may be determined in accordance with Figures 2.5 and 2.6.
- In any event, neither b_{mf} nor b_{ms} shall be taken as greater than b.
- The effects of unsymmetrical loading on the effective flange width may be disregarded.
- The value of b_{ms} shall be determined using the greater of the effective span lengths adjacent to the support.
- If b_{mf} is less than b_{ms} in a span, the pattern of the effective width within the span may be determined by the connecting line of the effective widths b_{ms} at the adjoining support points.

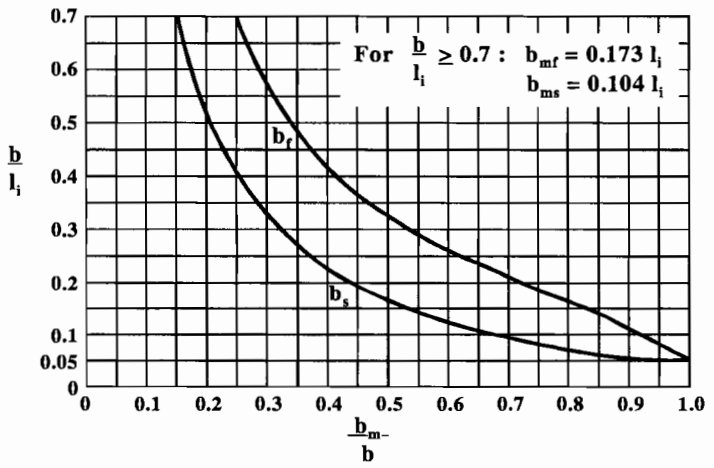

Figure 2.6 ***Values of the effective flange width coefficient b_m/b, for the given values of b/l_i (Figure 4.6.2.6.2-2 from the AASHTO LRFD Bridge Design Specifications [2])***

For the superposition of local and global force effects, the distribution of stresses due to the global force effects may be assumed to have a straight line pattern in accordance with Figure 2.7c). The linear stress distribution should be determined from the constant stress distribution using the conditions that the flange force remains unchanged, and that the maximum width of the linear stress distribution on each side of a web is 2.0 times the effective flange width.

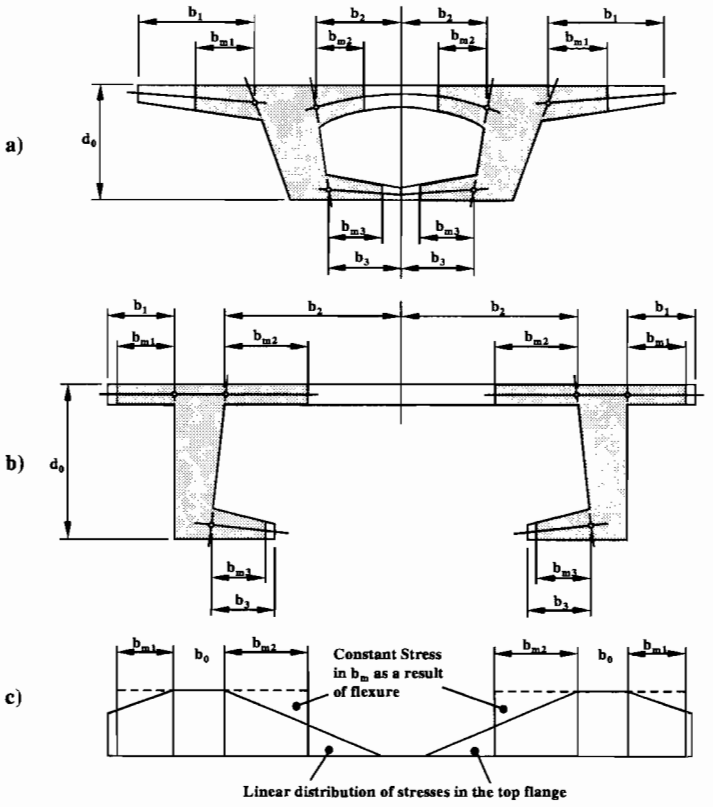

Figure 2.7 ***Cross sections and corresponding effective flange widths, b_m, for flexure and shear (Figure 4.6.2.6.2-3 from the AASHTO LRFD Bridge Design Specifications [2])***

The flange properties for normal forces (such a concentrated post-tensioning loads) may either be based on the pattern according to Figure 2.8, or be determined by more rigorous analysis.

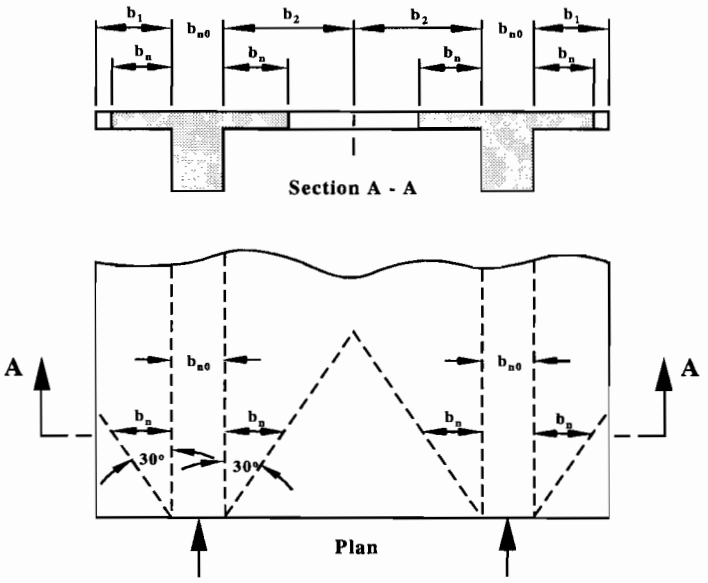

Figure 2.8 Effective flange widths, b_n, for normal forces (Figure 2.6.2.6.2-4 from the AASHTO LRFD Bridge Design Specifications [2])

2.4 Thermal Effects on Bridge Structures

There are two types of thermal activity that occur in bridges that are of interest for design. The first is the annual variation of the average temperature of the bridge. This variation causes expansion and contraction of the bridge's length over the course of the year. This effect is well understood, and designers know how to accommodate it.

The second effect is the daily variation of the thermal gradient in the bridge. The daily rising and setting of the sun as well as other climatic factors tend to heat and cool a bridge's superstructure unevenly through its depth. During the day, the solar radiation causes the exposed deck of the bridge to heat up. However, concrete is a relatively poor heat conductor. Thus, the top of the cross section tends to get much warmer than the lower parts of the cross section. At night, most of the heat is dissipated through the external perimeter of the cross section causing the interior of the cross section to be much warmer than the exterior. These phenomena are known as nonlinear thermal gradients. Little is known about the magnitudes of these gradients and what effects they have on bridges. This section will discuss thermal effects on bridges in two parts: the shape of the thermal distribution in the

cross section, and then the structural effects from the application of the temperature distribution to the superstructure cross section.

2.4.1 Shapes of Thermal Gradients

Factors Affecting Thermal Gradient

Typically, designers are interested in two types of nonlinear thermal gradients: a positive gradient, defined where the temperature of the top deck is warmer than the temperature of the webs; and a negative gradient, defined where the webs have higher temperatures than the deck and the bottom flange. Two types of factors affect the shape and magnitude of these thermal gradients:

1. Climatic factors that affect the amounts of thermal energy that are being applied to the bridge.
2. Material and shape properties of the cross section that affect how the section conducts the applied thermal energy.

The major climatic factors that affect thermal gradients are solar radiation, ambient temperature, wind speed, and precipitation. Figure 2.9 shows how the climatic factors affect the shape and magnitude of the thermal gradient. Solar radiation strikes the top deck and warms it up over the course of the day. Solar radiation is the primary contributor to the magnitude of the top spike in a positive gradient. Precipitation can suddenly cool the top deck and decrease the magnitude of the top spike, potentially adding to the severity of a negative gradient. Over the day, the ambient temperature rises and becomes warmer than the average temperature of the bridge. The ambient temperature will then begin to heat up the exterior of the bridge cross section while the inside of the cross section generally stays at a relatively stable temperature. At night, the ambient temperature drops below the average temperature of the bridge and starts to cool the exterior of the cross section. Wind blowing over the exterior surface of the cross section helps the concrete to re-radiate energy into the surrounding atmosphere.

A maximum positive gradient is expected when clear warm weather, with very light winds, follows a period of cool overcast weather. A maximum negative gradient is expected when a harsh cold front, accompanied by precipitation, follows several days of warm weather.

The material properties that affect the gradient are the conductivity, density, absorptivity, and specific heat. Concrete has a low conductivity that allows large nonlinear gradients to occur because the external portions of the structure can be heated or cooled quickly by the external environment while the concrete will not transfer thermal energy to or from the interior quickly enough to even out the temperature distribution through the cross section. Asphalt on the deck tends to insulate the concrete underneath, thus reducing the magnitudes of the thermal gradients.

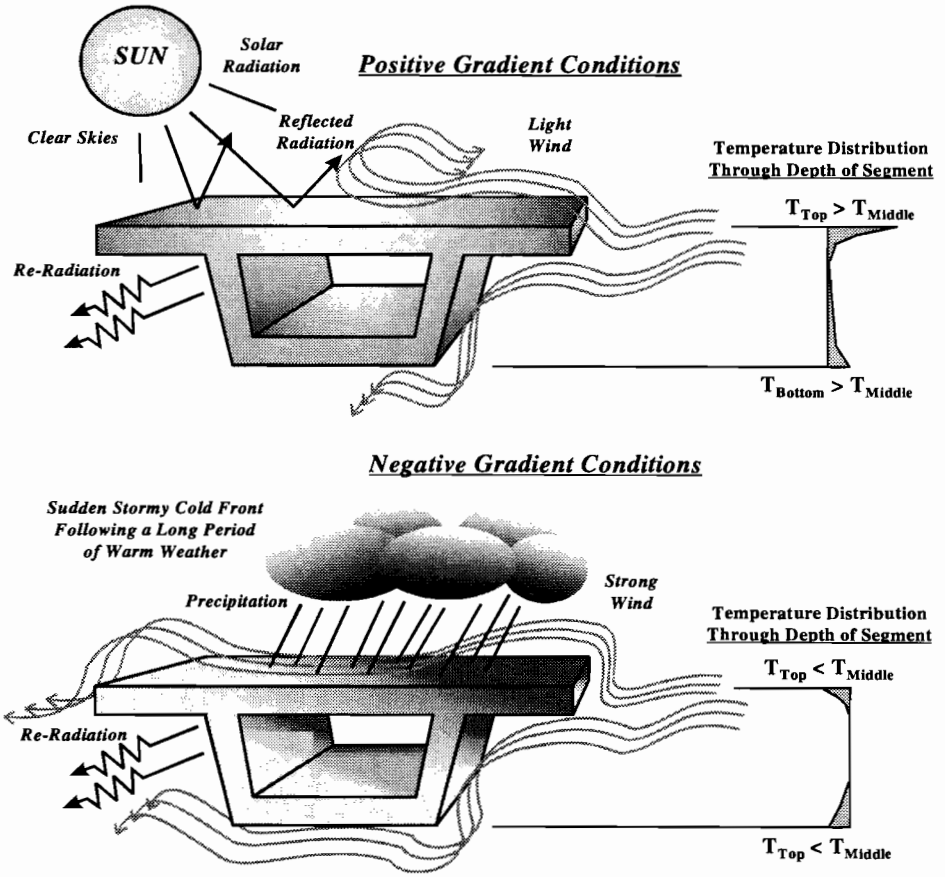

Figure 2.9 Climatic effects on thermal gradients

The shape of the cross section also has complex effects on the shape of the thermal gradient. In a box girder section, the wide top flange provides a large surface for absorbing solar radiation, but this thermal energy can only be transferred into the depth of the cross section at the webs. The webs act as heat sinks for the top flange. The spacing, thickness, and number of webs plus the thickness of the top flange at the junction to the webs affect the efficiency of the webs to conduct heat out of the top flange. More webs or thicker webs obviously allow more heat to be conducted out of the top flange. A greater spacing between webs requires the thermal energy to travel further across the top flange before it can be conducted into the webs. As the junctions of the top flange with the webs become thicker, more thermal energy can be passed into the webs at the junction points. Across the width of the top flange, the temperature will drop off over the webs during a positive gradient. As the webs become more efficient at conducting thermal energy out of the top flange, the top peak of the positive gradient will be reduced and distributed further into the depth of the cross section. Figure 2.10 illustrates these points. Thick web and flange walls also result in large

transverse gradients through the thickness of the web walls. As a result, the interior of the box girder tends to remain at a fairly constant temperature through the course of the day while the exterior fibers of the section change temperature significantly. A low concrete conductivity mitigates the effects of cross section proportioning on the shape of thermal gradients.

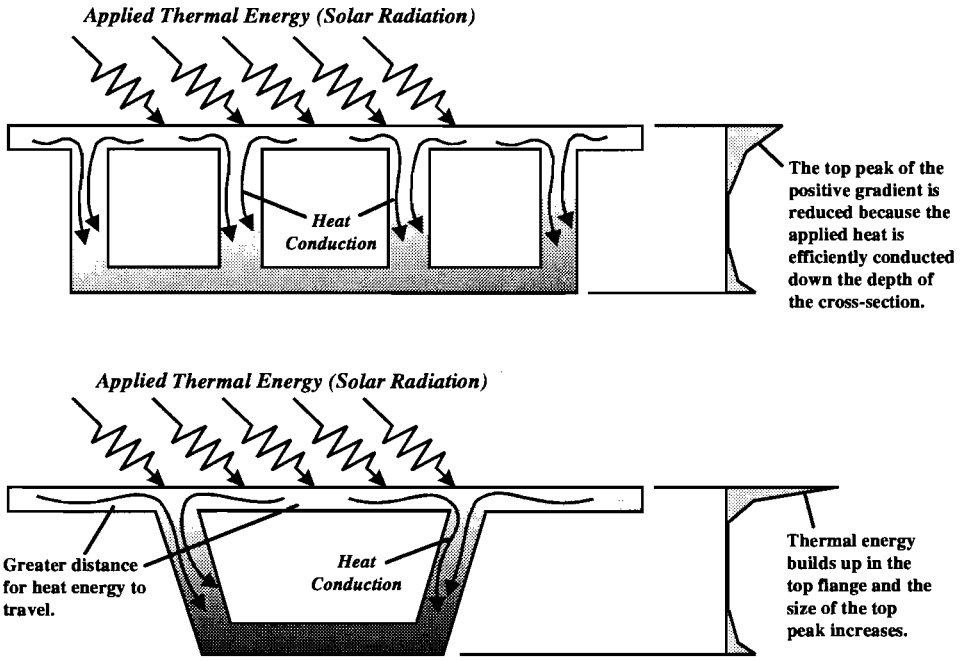

Figure 2.10 The effects of cross section on thermal gradient shape

The result of the material and cross-sectional affects on thermal gradient shape is that two box-girder sections of the same depth and with the same amount of asphalt blacktop on their decks can experience very different thermal gradients under the same climatic conditions if they have very different cross-sectional proportions or concrete properties.

AASHTO Recommended Gradient Shapes

A thorough review of literature on thermal gradients will reveal several recommended shapes for design gradients. This section will not deal with all of the design gradients that have been recommended, nor will it summarize all of the research that has been conducted. Such literature studies have already been conducted in the works of Roberts (19), Bonzon (6), and Wood (23). This section will instead focus on the current recommended gradients in the *AASHTO LRFD Bridge Design Specifications* (2), on how they were developed, and on some questionable aspects of these gradients.

The *AASHTO LRFD Bridge Design Specifications* provides recommended design gradients in Section 3.12.3. This section contains items, a map of solar radiation zones for the U.S., and a diagram of the proposed gradient shape with a table. These figures are reproduced in Figures 2.11 and 2.12. Values for positive gradient T_1 and T_2 come from the table. Negative gradient values are calculated by multiplying the positive gradient values by -0.5. T_3 is specified to be 0.0°C (0.0°F) unless a site-specific study is performed to determine an appropriate value, but shall not exceed 2.8°C (5°F) for the positive gradient and -1.4°C (-2.5°F) for the negative gradient. The dimension "A" is specified to be:

- 300 mm (12 in.) for concrete superstructures that are 400 mm (16 in.) in depth or greater,
- 100 mm (4 in.) for concrete superstructures that are less than 400 mm (16 in.) in depth, or
- 300 mm (12 in.) for steel superstructures, where the value "t" is equal to the thickness of the concrete deck.

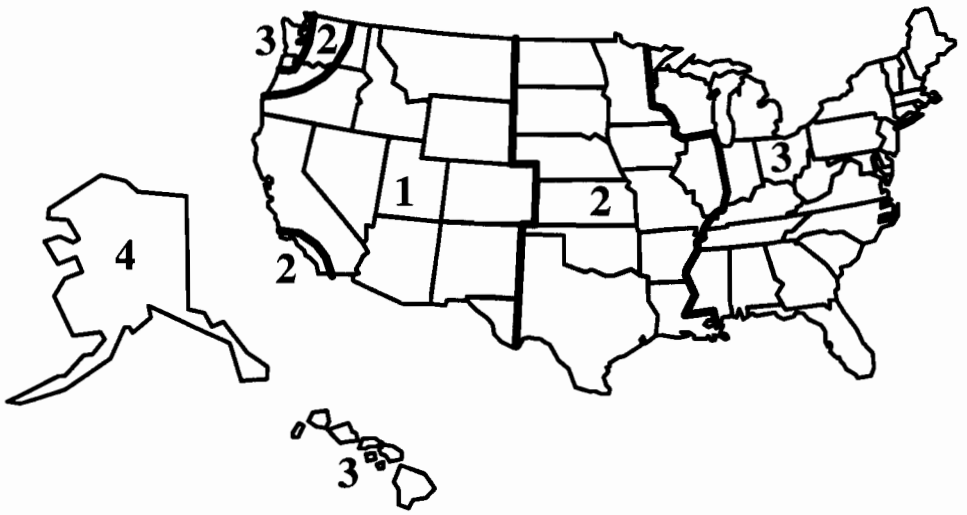

Figure 2.11 Solar radiation zones for the United States (Figure 3.12.3-1 from the AASHTO LRFD Bridge Design Specifications [2])

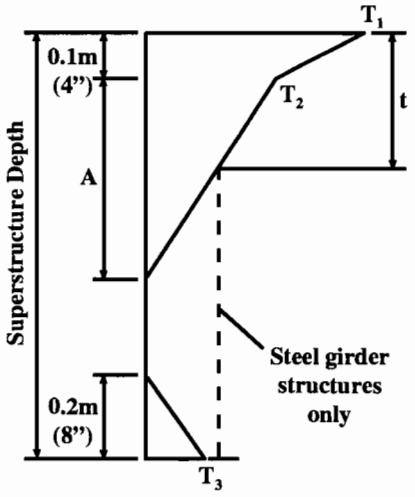

Plain Concrete Surface			50 mm Asphalt (2" Asphalt)		10 mm Asphalt (4" Asphalt)	
Zone	T_1 °C (°F)	T_2 °C (°F)	T_1 °C (°F)	T_2 °C (°F)	T_1 °C (°F)	T_2 °C (°F)
1	30 (54)	7.8 (14)	23.9 (43)	7.8 (14)	17.2 (31)	5 (9)
2	25.6 (46)	6.7 (12)	20 (36)	6.7 (12)	13.9 (25)	5.6 (10)
3	22.8 (41)	6.1 (11)	18.3 (33)	6.1 (11)	12.8 (23)	6.1 (11)
4	21.1 (38)	5 (9)	16.1 (29)	5 (9)	12.2 (22)	6.1 (11)

Figure 2.12 Positive vertical temperature gradient in concrete and steel superstructures (Figure 3.12.3-2 and Table 3.12.3-1 from the AASHTO LRFD Bridge Design Specifications [2])

Thus, for the US 183 elevated highway in Austin, Texas, the design positive gradient would have values for T_1, T_2, and A of 20.0°C (36°F), 6.7°C (12°F), and 300 mm (12 in.), respectively. The design negative gradient, then, would have values of -10.0°C (-18°F), -3.35°C (-6°F), and 300 mm (12 in.), respectively. The value of T_3 will most likely be chosen as 0.0°C (0.0°F) for any bridge design gradient because it is unlikely that many engineers will have access to site-specific data that would justify otherwise.

The recommended design gradients from the *AASHTO LRFD Bridge design Specifications* were developed based on research from Potgieter and Gamble (16) and the British Standard BS 5400 (21). Potgieter and Gamble performed analytical studies based on weather station data from around the U.S. in conjunction with a finite-difference, one-dimensional, heat-flow program. From these studies they determined what conditions would produce maximum positive nonlinear temperature gradients and what the shapes and magnitudes of these gradients would be. The results of their theoretical work were verified against four measured positive thermal gradients from the Kishwaukee River Bridge. The negative gradient was developed from the recommendations in the British Standard BS 5400 code that have no analytical or recorded field data to substantiate them (19). The recommended design gradients were first published in the *1989 AASHTO Bridge Guide Specifications for Design and Construction of Segmental Highway Bridges* (1). Since then, field studies have been performed that have not always measured maximum thermal gradients with magnitudes as high as the recommended gradients. The majority of these studies have not agreed with each other on a definitive set of maximum magnitudes nor shapes for the gradients. When the *AASHTO LRFD Bridge Design Specifications* (2) was published in 1994, the magnitudes of the original design gradients were kept, though the shapes were simplified slightly to make design calculations easier to perform.

The philosophy that has previously been applied to the choice of recommended gradient shapes has been to instrument a bridge structure with thermocouple gauges, and then to choose the maximum positive and negative gradients measured in the bridge over a period of observations as design gradients. This philosophy is questionable for several reasons. The first question is whether the gradient should be chosen from the absolutely worst measured case or whether the design gradients should instead be chosen based on a reasonable rate of occurrence from a database of thermal gradients measured over a sufficient period of time with a sufficient frequency of measurements. Most design loads are specified based on probabilistic rates of occurrence such that the actions will represent the 95th fractile. That is, only five percent of actions that might occur would be greater. The choice of design thermal gradients should follow the same pattern. Absolute maximum, measured thermal gradients are unnecessarily severe for design purposes because they actually occur infrequently over the service life of a bridge. Thermal stresses are a service limit state condition. During the relief of such restraint-induced actions because of cracking and creep, the effects of temperature stresses will be negligible at factored loads (11). Secondly, in the past, no consideration has been given for the effects of cross-sectional shape except for the depth of the member. As discussed earlier, the shape and proportioning of a box girder cross-section affects the way heat is conducted through the section. Thus, they affect the shape of the thermal gradient that occurs. This problem raises three questions:

- If design gradients are to be verified by comparison with field measured data, how can a gradient measured in one bridge superstructure be applied to the design of another bridge superstructure that has substantially different cross-sectional proportions?
- How can the effects of cross-sectional variations be used in determining a single pair of positive and negative design gradients for the AASHTO code?
- Is the influence of cross-sectional shape and proportion significant enough that different design gradients should be specified for significant variations in box girder proportions?

Lastly, measurement of thermal gradients in the field has previously focused only on the collection of temperature data. Measurement of the stresses caused by these thermal gradients has largely been ignored. Thus, there is little confirmation that the gradients that have been assumed as the most severe are actually the thermal gradients that cause the highest stresses. Possibly, different shapes of the applied gradient will cause different behavior of the structure such that one applied positive gradient may produce critical stresses for one part or one type of a bridge structure while another (with a different shape) may cause critical stresses at a different part or in a different type of bridge structure. The problem is analogous to placing live load on a structure in different patterns to produce an envelope of critical stresses. Are the current provisions for thermal design adequate in this respect?

2.4.2 *Structural Response to Thermal Gradients*

Factors That Affect Structural Response

For analysis purposes, nonlinear thermal gradients are typically divided into three components. First, a uniform temperature component is removed from the initial gradient. Second, a linear thermal gradient is removed. The remainder after removing these first two components is a self-equilibrating temperature distribution. Figure 2.13 shows the three components of the nonlinear thermal gradient. The effects of these components on the bridge structure depends on three factors: the statical determinacy of the structure, the susceptibility of the cross section to warping, and the stress range of the concrete under which the loading occurs that determines whether the behavior will be elastic or inelastic.

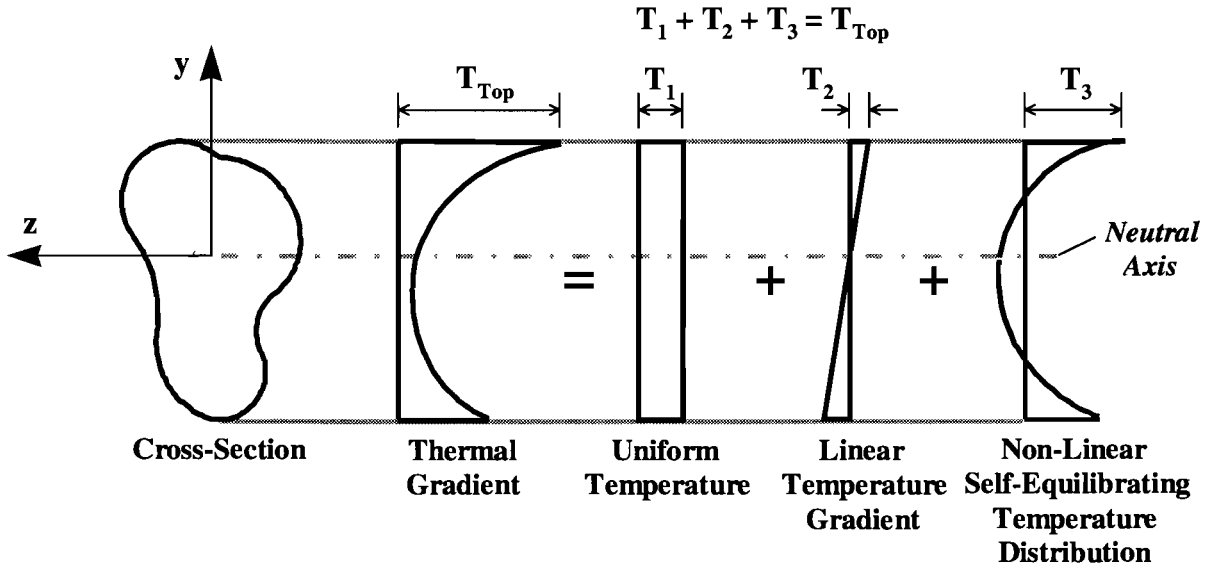

Figure 2.13 Components of a nonlinear thermal gradient

The effects of the first two components of the thermal gradient depend primarily on the statical determinacy of the structure. The first component, the uniform temperature, causes a uniform expansion or contraction of the unrestrained superstructure. Generally, this phenomenon is accommodated by expansion joints or rolling bearings. If the structure is continuous and two or more of the interior supporting piers are rigidly fixed to the superstructure, they will provide restraint against such movement. This restraint will produce moments and axial forces in the structure. The second component, the linear thermal gradient, will produce a uniform curvature in the unrestrained superstructure. Only if the superstructure is a simply supported single span can the bridge deform freely (Figure 2.14). Otherwise, if the structure is continuous over two or more spans, the internal piers will

restrain the superstructure from deforming in such a manner. Thus, secondary moments are introduced into the structure. This effect is shown in Figure 2.15.

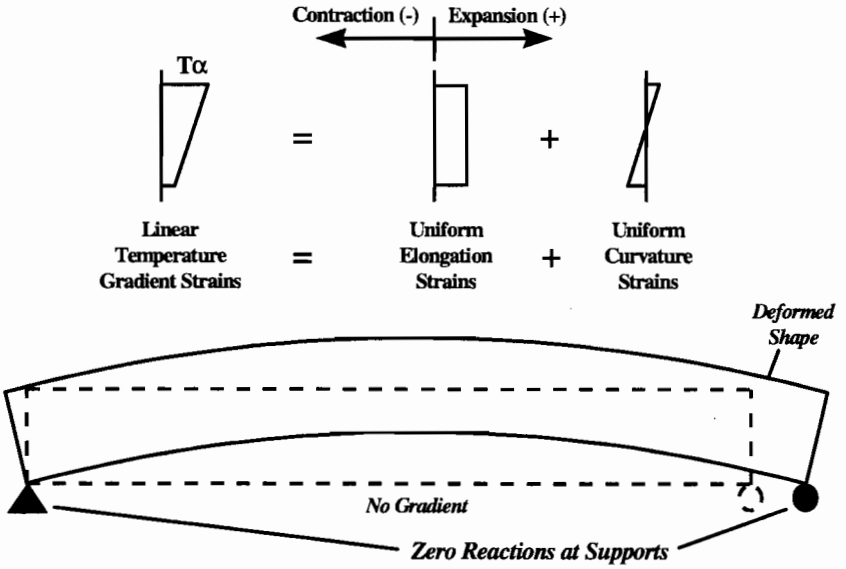

Figure 2.14 Effect of linear thermal gradient components on a statically determinate span

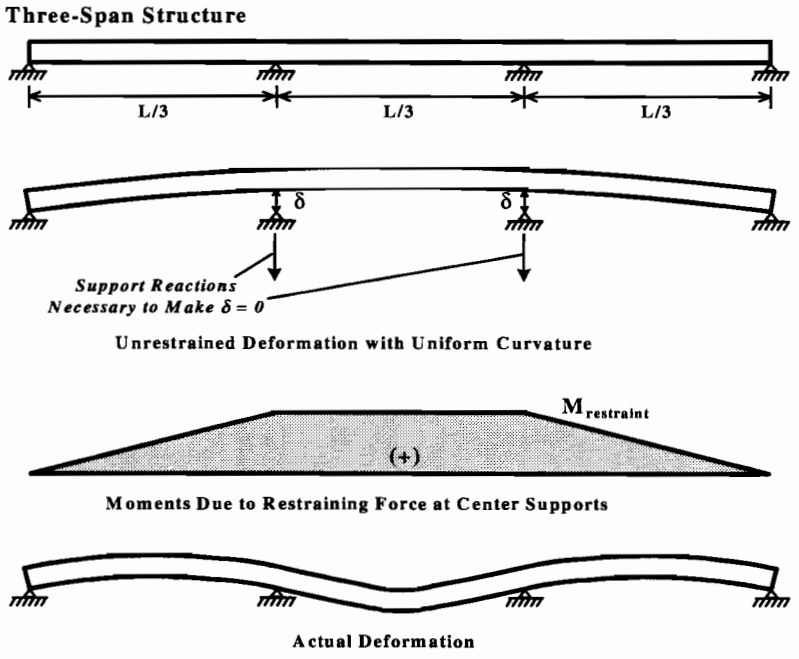

Figure 2.15 Effects of linear thermal gradient components on a statically indeterminate bridge structure

The third component, the self-equilibrating temperature distribution, will cause self-equilibrating internal stresses in the bridge cross section. The effect of this component depends on the susceptibility of the cross section to warping. If plane sections remain plane, the stresses produced by the remaining component of the thermal gradient can be solved for fairly easily. Under this assumption, the self-equilibrating stresses can be calculated by assuming that the member is fully restrained against any thermal deformation as in Figure 2.16. The following variables are used in the calculation:

y	=	distance measured perpendicular to the longitudinal axis at the center of gravity of the cross section
T(y)	=	temperature at a depth y
b(y)	=	net section width at a depth y
E	=	modulus of elasticity
α	=	coefficient of thermal expansion
$\sigma_{SE}(y)$	=	self-equilibrating stress at a depth y
A	=	cross-sectional area
I	=	moment of inertia

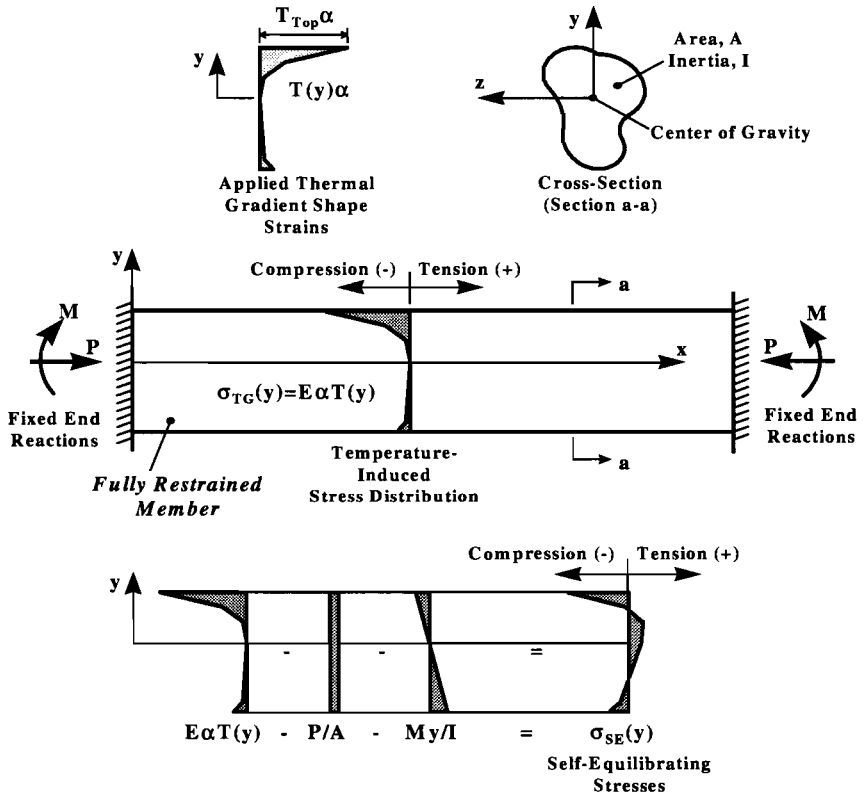

Figure 2.16 Calculation of self-equilibrating stresses from a nonlinear thermal gradient when plane section remain plane

In all calculations, the z and y axes are assumed to be principal axes of the cross section. The force necessary to restrain the member axially at the fixed ends is calculated by:

$$\text{Restrained Axial Load, } P = \int_{depth} E\alpha T(y)b(y)dy \tag{2-1}$$

The moment necessary to restrain the member rotationally at the fixed ends is calculated by:

$$\text{Restrained Moment, } M = \int_{depth} E\alpha T(y)b(y)ydy \tag{2-2}$$

In the unrestrained case, however, these loads will not be acting on the member. Thus they must be removed. The stresses obtained after removing the fully restrained moment and axial force are then the self-equilibrating stresses acting to keep all sections plane through the member:

$$\sigma_{SE}(y) = E\alpha T(y) - P/A - My/I \tag{2-3}$$

This calculation method is applicable for calculating internal stresses in continuous- or simple- span structures so long as warping does not occur.

In a continuous bridge, the problem of determining the secondary moments caused by constraint from the piers is solved by applying a deformed shape to the superstructure consistent with the axial elongation (or contraction) and the constant curvature that would be caused by the uniform temperature and linear thermal gradient components of the applied thermal gradient. The forces in the interior piers would then be the forces necessary to bring the structure back to a zero deflection at the pier locations (already shown in Figure 2.15). The unrestrained axial strain and curvature of the superstructure are calculated as:

$$\text{Axial Strain, } \varepsilon_{axial} = P/EA \tag{2-4}$$

$$\text{Curvature, } \phi = M/EI \tag{2-5}$$

The above discussion has focused on the equations used to solve the one-dimensional gradient problem. If the gradient varies across the width of the cross section as well as the depth (Figure 2.17), then the equations are simply modified as:

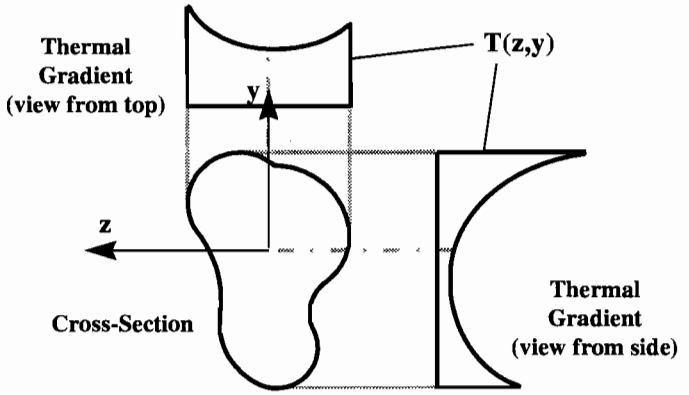

Figure 2.17 Thermal gradient that varies across the width and depth of a cross section

y	=	vertical distance measured to the center of gravity of the cross section
z	=	transverse distance measured to the center of gravity of the cross section
T(z,y)	=	temperature at transverse distance z and depth y
$\sigma_{SE}(z,y)$	=	self-equilibrating stress at transverse distance z and depth y
I_z	=	moment of inertia about z axis
I_y	=	moment of inertia about y axis

$$\text{Restrained Axial Load, } P = \int_{depth}\int_{width} E\alpha T(z,y)\,dz\,dy \tag{2-6}$$

$$\text{Restrained Moment about z axis, } M_z = \int_{depth}\int_{width} E\alpha T(z,y)\,y\,dz\,dy \tag{2-7}$$

$$\text{Restrained Moment about y axis, } M_y = \int_{depth}\int_{width} E\alpha T(z,y)\,z\,dz\,dy \tag{2-8}$$

$$\sigma_{SE}(z,y) = E\alpha T(z,y) - P/A - M_z y/I_z - M_y z/I_y \tag{2-9}$$

Generally, most engineers would ignore the moment about the y axis because the linear gradient component across the width of the cross section is likely to be small, and the moment of inertia about the y axis is likely to be large. However, the variation in the self-equilibrating internal stresses across the width of a cross section may not be negligible for some bridges' structures.

Thermal gradients may also act across the section transversely. In the box-girder section, the temperature distribution varies not only through the depth of the section, but from the inside perimeter to the outside perimeter as well. Thus, thermal gradients will be present through the thickness of the flanges and webs (Figure 2.18). These gradients cause transverse stresses through the girder cross section. A simplified method to solve for these

stresses is to take a transverse slice of unit width out of the girder and analyze it as a two-dimensional frame. The slice is broken into individual members as shown in Figure 2.18, and appropriate thermal gradients are applied to each member. Each member can be treated in the same manner that was described for the longitudinal behavior, and the stresses caused by the transverse gradients can be solved for.

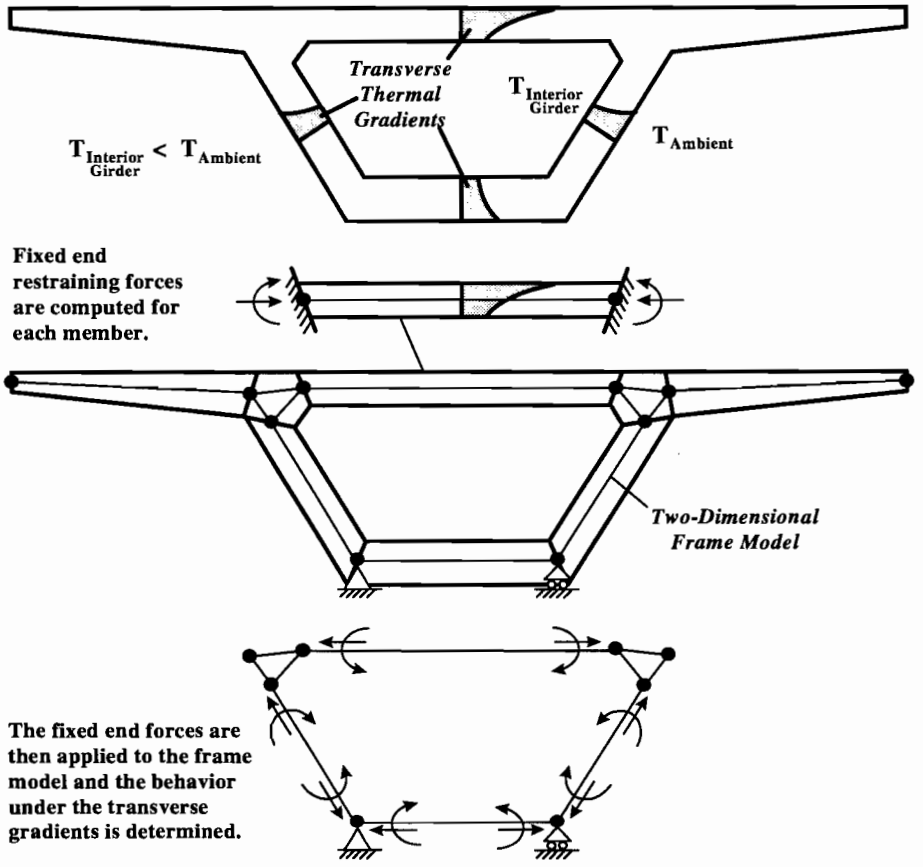

Figure 2.18 Analysis of transverse thermal gradients

The structural response to thermal gradients has been discussed for simple span and continuous box girders for sections that do not warp. The next step is to consider what happens to the stress distribution in the box girder if warping does occur. In Figure 2.19a, a cut is made between the top flange and the rest of the section shown in the figure. When a positive gradient is applied to the span, the upper portion of the gradient causes the top flange to bow and elongate much more than the lower portion of the gradient causes the bottom part of the span to bow and elongate. In order to bring the two halves of the span into a consistent shape, stresses like the ones shown in Figure 2.19a must be produced. Thus, local bending and axial load occur in the top flange just over the webs. Furthermore, the lower portion of the span is much stiffer than the top flange by itself, so one can expect that the top flange will undergo most of the deformation necessary when the two halves of the span are brought

together into a consistent shape. Figure 2.19b shows the resulting distribution of normal stresses in the top flange of the span. Transverse stresses across the top flange are produced as well because the top flange must bend across its width to achieve the final shape shown in Figure 2.19b. The peak normal stresses produced by the warping are then greater than would be expected if the plane sections remained plane. This occurs because less of the stress concentrates in the top flange over the webs. The phenomenon has results similar to shear lag though the mechanism of the distortion is different.

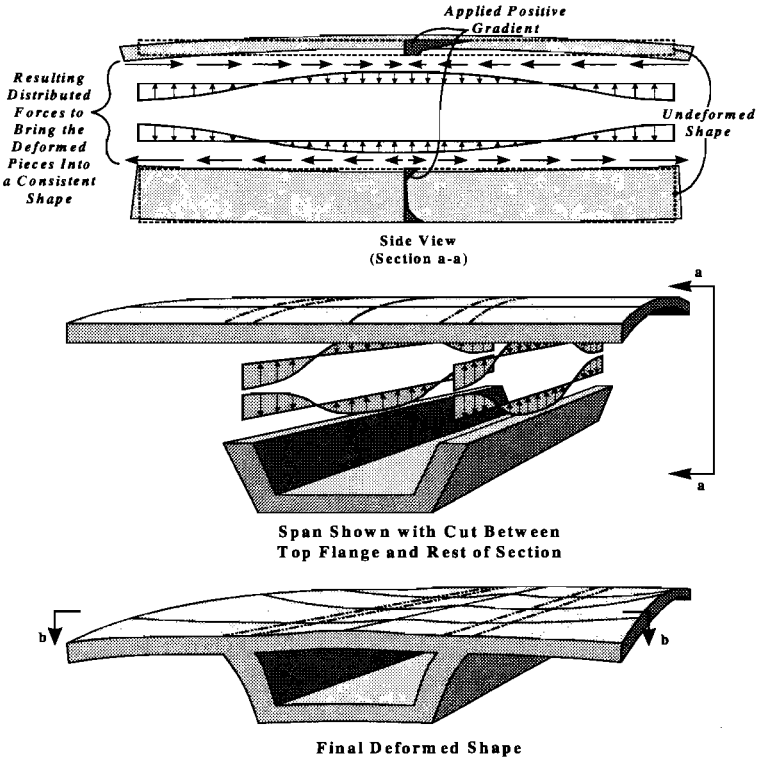

Figure 2.19a Effect of an applied positive gradient when warping occurs

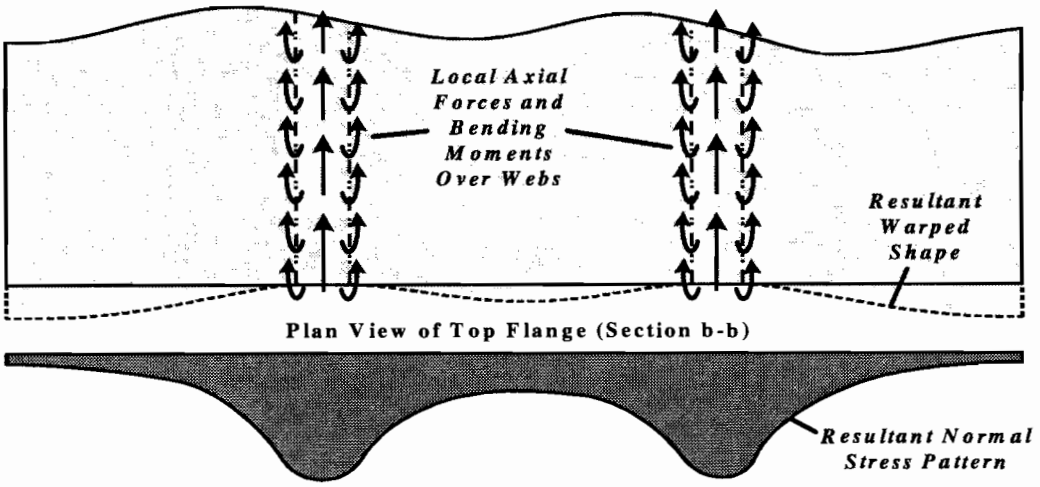

Figure 2.19b Effect of an applied positive gradient when warping occurs (continued)

Finally, all of the above discussion has been for elastic response in the lower ranges of the service limit state. For concrete near the ultimate limit state, the behavior becomes very different. Because the structure is trying to satisfy strain compatibility and not external load equilibrium, the stresses will be greatly reduced by cracking or even microcracking of the concrete. Under such conditions, the concrete is free to expand and contract much more freely than under perfectly homogeneous conditions. For this reason, analysis of thermal gradients is generally only performed for service load cases. The effects of thermal gradients are greatly relieved by cracking and hence are usually ignored for ultimate loading conditions.

AASHTO Recommended Method of Analysis

The AASHTO LRFD Bridge Design Specifications (2) recommend a method for analysis of structures with applied thermal gradients in Section 4.6.6. Analysis for all three components of the thermal gradient is required. The recommended method is provided in the commentary and follows the procedure that was outlined in the previous section for elastic behavior without warping. Design for thermal effects is only required under load combinations Service I through V in Section 3.4.1 of the *AASHTO LRFD Bridge Design Specifications*.

2.5 Curved Girders

The problem of solving for the internal forces in a curved girder is difficult. The mechanics of a curved member require an interdependency between the moments and torques in the member. This results in analysis problems that many engineers do not know how to solve. In bridge design, curved horizontal alignments are quite common. However, in general, the radius of curvature of most bridges is large compared with the span lengths. Thus, the horizontal curvature along any single span is often negligible. This allows design

engineers to neglect the moment and torsion interdependency in most designs. The exception to this pattern usually occurs with freeway interchanges in urban or environmentally sensitive areas where tight radii are required in the alignment of the interchange ramps and little ground space is available for supporting substructure. The US 183 Ramp P is such a bridge. The problem of the moment and torsion interdependency was of some concern for the designers of Ramp P.

2.5.1 General Curved Girder Theory

The proceeding derivation will follow the form given in Nakai and Yoo (12). A similar derivation can be found in Kristek (10).

Consider the curved differential segment shown in Figure 2.20. The right hand rule should be used for interpretation of all moment and torque vectors shown in the figure. The variables in the figure are defined as:

ds	=	the arc length of the curved differential segment
$d\theta$	=	the angle subtended by the arc of the curved differential segment
R	=	the radius of curvature of the curved differential segment
w	=	the distributed load over the length of the curved differential segment (only the resultant is shown in the figure)
t	=	the distributed torque over the length of the differential curved segment (only the resultant is shown in the figure)
V_0	=	the shear at the downstation face of the curved differential segment
M_0	=	the moment at the downstation face of the curved differential segment
T_0	=	the torque at the downstation face of the curved differential segment
V_1	=	the shear at the upstation face of the curved differential segment
M_1	=	the moment at the upstation face of the curved differential segment
T_1	=	the torque at the upstation face of the curved differential segment

a, b, c, and d are dimensions defined in the figure.

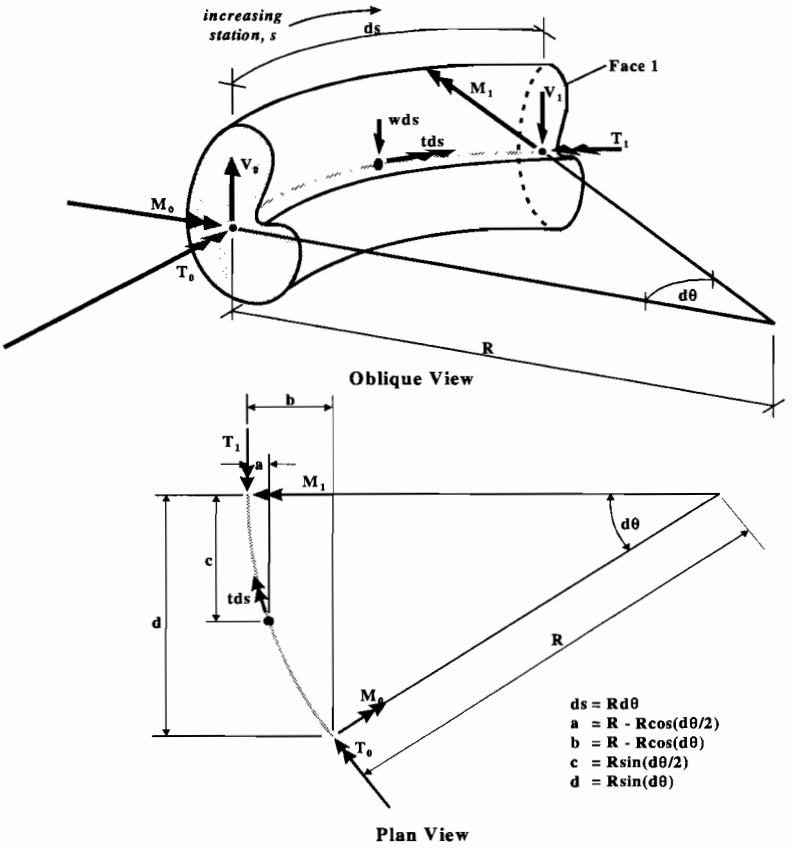

Figure 2.20 Curved differential segment with applied loads

External equilibrium at face 1 of the segment requires the following relationships:

$$V_1 = V_0 - wds \tag{2-10}$$

$$M_1 = - T_0\sin(d\theta) + M_0\cos(d\theta) - V_0R\sin(d\theta) - tds*\sin(d\theta/2) + wds*R\sin(d\theta/2) \tag{2-11}$$

$$T_1 = T_0\cos(d\theta) + M_0\sin(d\theta) - V_0(R-R\cos d\theta) + tds*\cos(d\theta/2) + wds*(R-R\cos(d\theta/2)) \tag{2-12}$$

Small angle theory is then used to make the following simplifications:

$$\cos(d\theta) \cong 1$$

$$\sin(d\theta) \cong d\theta$$

$$\cos(d\theta/2) \cong 1$$

$$\sin(d\theta/2) \cong 0$$

When these approximations are applied to equations (2-11), and (2-12), they reduce to:

$$M_1 = -T_0d\theta + M_0 - V_0Rd\theta \tag{2-13}$$

$$T_1 = T_0 + M_0d\theta + tds \tag{2-14}$$

Equations (2-10), (2-13), and (2-14) are rearranged so that like terms are moved to the left-hand sides of the equations, and the substitution ds/R is made for dθ throughout:

$$dV = V_1 - V_0 = -wds \tag{2-15}$$

$$dM = M_1 - M_0 = -T_0ds/R - V_0ds \tag{2-16}$$

$$dT = T_1 - T_0 = M_0ds/R + tds \tag{2-17}$$

Equations (2-15), (2-16), and (2-17) are then put in their final form by a division of ds:

$$\frac{dV}{ds} = -w \tag{2-18}$$

$$\frac{dM}{ds} = -\frac{T}{R} - V \tag{2-19}$$

$$\frac{dT}{ds} = \frac{M}{R} + t \tag{2-20}$$

Differentiation of equation (2-19) and substitution with equation (2-20) yields the following differential equation and solution:

$$\frac{d^2M}{ds^2} + \frac{M}{R^2} = \frac{t}{R} - w \tag{2-21}$$

$$M = A\sin\theta + B\cos\theta - wR^2 + tR \tag{2-22}$$

where A and B are constants determined from boundary conditions.

The forces in equations (2-18) through (2-22) are related to deformations in a curved girder by the relations:

$$-\frac{M}{EI} = \frac{d^2y}{ds^2} - \frac{\hat{a}}{R} \tag{2-23}$$

$$\frac{T}{GK} = \frac{d\ddot{o}}{ds} \tag{2-24}$$

$$\varphi = \beta + y/R \tag{2-25}$$

The variables in the above equations are defined as:

E	=	the modulus of elasticity of the girder
I	=	the moment of inertia about the horizontal axis of the girder cross section
G	=	the shear modulus of the girder
K	=	the torsional constant of the girder cross section
y	=	the deflection of the girder at a station, s, along its length
β	=	the tile of the girder at a station, s, along its length
φ	=	the torsional angle of the girder at a station, s, along its length

The torsional constant, K, is generally defined for a concrete box girder according to Bredt's formula (9):

$$K = \frac{4A^2t_{avg}}{P} \tag{2-26}$$

A	=	the area enclosed by the centerline of the box-girder walls
t_{avg}	=	the average thickness of the box-girder walls
P	=	the perimeter measured along the centerlines of the box-girder walls

Figure 2.21 shows the geometric relations between β, y, and φ.

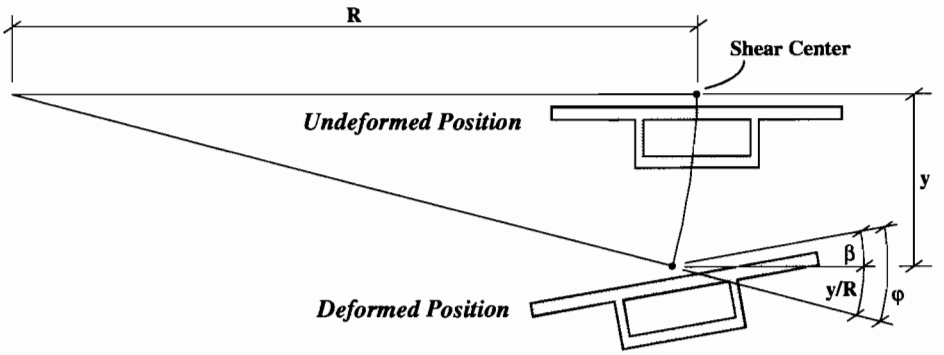

Figure 2.21 Variables used to define the deformation of a curved girder

One of the important results that can be determined from curved girder theory regards the torsional effect of internal post-tensioning on a curved girder. Figure 2.22 shows the forces transmitted into a curved girder from an internal post-tensioned tendon. The following variables are used in the figure and in this discussion:

P	=	the axial load from the post-tensioning
u	=	the uniformly distributed transverse load caused by redirection of the post-tensioning tendon around the horizontal curve of the girder
e	=	the eccentricity of the post-tensioning tendon measured from the cross-sectional center of gravity
$e_{S.C.}$	=	the eccentricity of the cross-sectional shear center measured from the cross-sectional center of gravity
M_{PT}	=	the total moment from post-tensioning = M_{sec} + Pe
M_{sec}	=	the secondary moments from post-tensioning
R_u	=	the radially oriented resultant concentrated force from the sum of the distributed load, u, over a differential length of girder, ds
R_P	=	the radially oriented resultant concentrated load from the axial stresses on both faces of a differential length of girder, ds

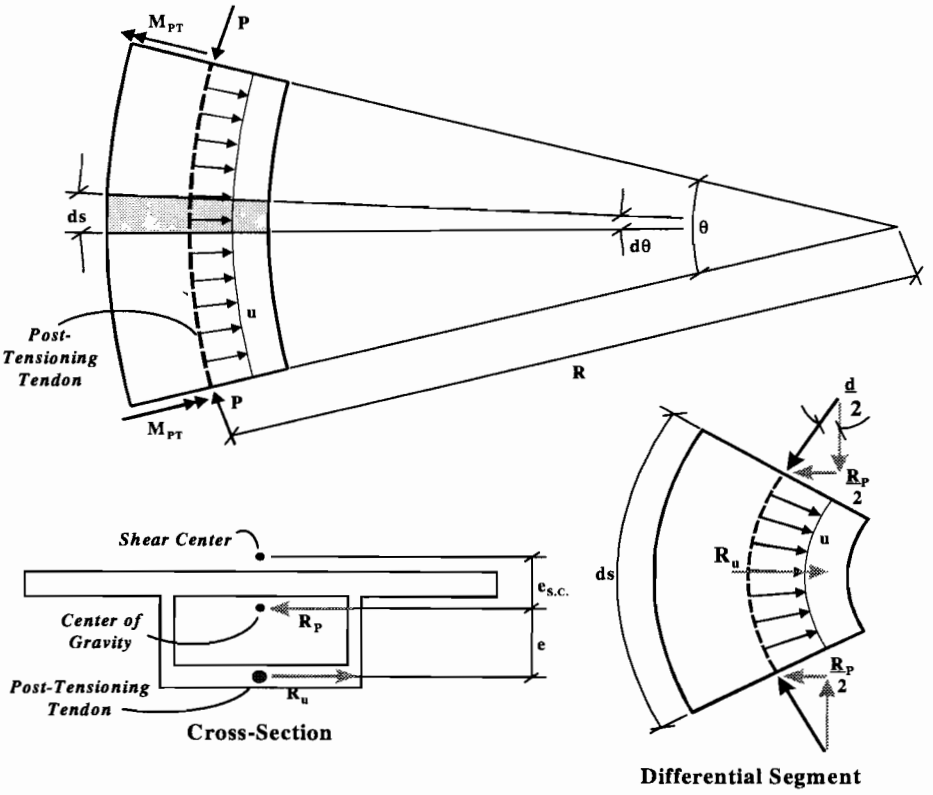

Figure 2.22 Internal post-tensioning in a curved girder

From Figure 2.22, the following relationships are determined:

$$u = \frac{P}{R} \tag{2-27}$$

$$R_u = uds = \frac{P}{R}ds \tag{2-28}$$

$$R_p = 2(P\sin(\frac{d\grave{e}}{2})) \cong Pd\theta = \frac{P}{R}ds \tag{2-29}$$

Thus, the distributed torque resultant from a differential curved segment is:

$$tds = (\frac{P}{R}ds)e_{s.c.} - (\frac{P}{R}ds)(e + e_{s.c.}) = -\frac{Pe}{R}ds$$

or

$$t = -\frac{Pe}{R} \tag{2-30}$$

Substituting this result into Equation 2-20 leads to:

$$\frac{dT}{ds} = \frac{M_{PT}}{R} + t = \frac{M_{sec}}{R} + \frac{Pe}{R} - \frac{Pe}{R}$$

$$\frac{dT}{ds} = \frac{M_{sec}}{R} \tag{2-31}$$

Thus, no torsion should be produced by internal prestressing except by the secondary moments from the prestressing. The preceding result does not apply to external tendons that transmit forces into the girder at discrete locations.

2.5.2 AASHTO Specifications and Analysis Approaches

The requirements for torsional analysis of curved girders are governed by Section 4.6.1.2 of the *AASHTO LRFD Bridge Design Specifications* (2). No methods for analysis are recommended in that section. The section gives criteria defining when horizontal curvature in a girder must be considered in design analysis and how permanent loads must be treated on such a girder. Curved girders must be analyzed as curved if the central angle subtended by a span is greater than 12.0°. The section also requires that analysis of such girders shall consider the transverse eccentricity of dead and live loads in the curved configuration. No requirements are given for the precision of techniques to be used for the analysis of curved girders.

Software that is capable of three-dimensional analysis of segmental prestressed concrete bridges is not common in the design industry. Many segmental bridge design firms and state transportation agencies usually treat curved box girders as straight for flexural design and perform a separate torsion analysis using any convenient three-dimensional frame solver. Thus, the flexural design will reflect the effects of creep, shrinkage, and prestressing, but the torsional analysis may not include such effects or will treat such effects in approximate ways.

In general, neglect of the torsional contribution to moment is conservative, but neglect of the moment contribution to torsion is not. Thus, designers sometimes perform flexural analysis on an equivalent straightened bridge rather than the curved bridge. The torsional analysis can then be performed by inserting the approximate straight bridge moment diagram into Equation 2-20 for dT/ds and treating the M/R result as an equivalent distributed torsion. This approximation uncouples the relationship between the moment and torque distributions and allows torsional analysis to be performed as if the bridge were straight (Note: All distributed torsion loads are still determined from the curved geometry).

CHAPTER 3. SUPERSTRUCTURE INSTRUMENTATION

3.1 Instrumentation Objectives

The objective of the study of the northbound IH-35/northbound US 183 flyover ramp, henceforth referred to as Ramp P, was to determine the moments, torques, and thermal gradient-induced actions that occur during construction and long-term service of a curved, precast, prestressed concrete segmental box girder bridge erected in balanced cantilever. In order to determine those moments, torques, and actions, it was necessary to satisfy the following instrumentation objectives:

1. Determine the longitudinal strain distribution across the box at several sections along the ramp.
2. Determine the torsional shear strains at several sections along the ramp.
3. Determine the strains in the external post-tensioning strands.
4. Determine the temperature distribution across the box so that the thermally induced strains could be determined.

In addition to these instrumentation objectives, the behavior of an anchor diaphragm, anchor blister, and deviator block in the ramp were also to be studied. These bridge components were instrumented, but the results of their instrumentation and the objectives relating to their instrumentation will be reported by Davis (7). Furthermore, figures and discussion relating to instrument location in this report will not refer to the diaphragm, blister, or deviator instrumentation.

3.2 Span Selection

The portion of Ramp P constructed by the balanced-cantilever method consisted of a five-span continuous unit with span lengths of 38.1 m, 54.9 m, 43.4 m, 54.9 m, and 38.1 m (125, 180, 142.36, 180, and 125 ft). Instrumentation of the entire structure would have been expensive and time consuming. In addition, the resulting data would be too overwhelming to reduce. Thus, only one span of the structure was studied. It was decided that one of the 54.9 m (180 ft) spans should be chosen for instrumentation. Because pier P16 had been instrumented previously as an earlier part of the U.S 183 study (see Bonzon (6)), the upstation 54.9 m (180 ft) span between piers P16 and P17 was chosen.

3.3 Segment Selection

Three segments in the span between piers P16 and P17 were instrumented: P16-2, P16-10, and P16-17. Figure 3.1 shows a plan drawing of Ramp P and the locations of the instrumented segments. All three of these segments were located on the pier P16 upstation cantilever. Segment P16-2 was at the base of the cantilever where the maximum negative moment (tension in the top fiber of the section) and torque occurred during construction. Segment P16-10 is near the quarter point of the completed span where an inflection point in

the live load moment diagram of the span would occur. Segment P16-17 is near the midpoint of the completed span where the maximum positive moment from load will occur. It was decided that instrumentation of these locations within the span would provide an adequate picture of the most crucial points on the torque and moment diagrams of the span.

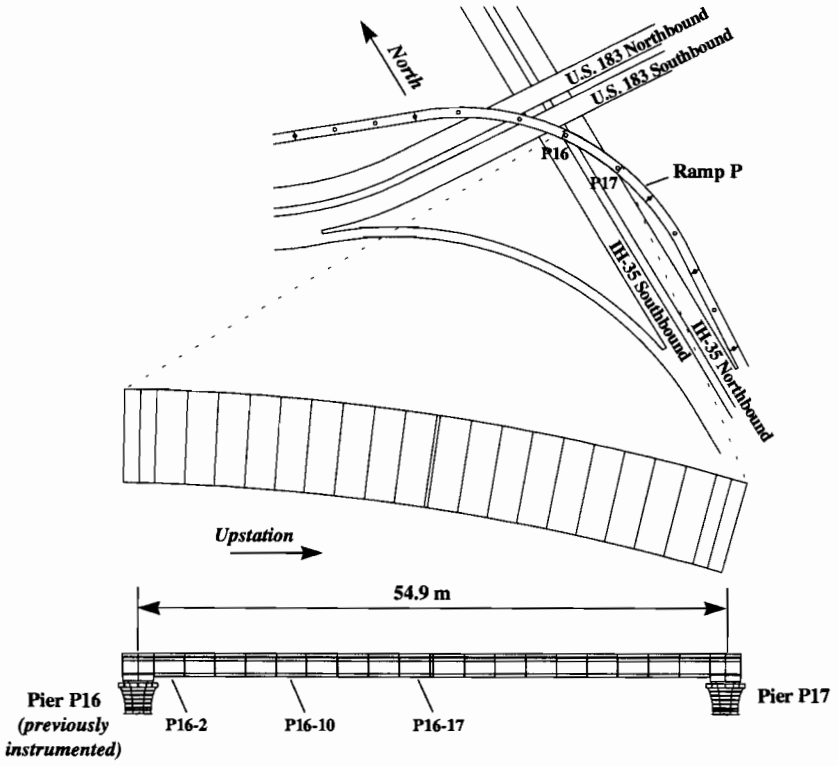

Figure 3.1 Instrumented sections in Ramp P

3.4 Gauge Types

Four different types of instruments were installed in the Ramp P superstructure: concrete strain gauges, steel strain gauges, Demec points, and thermocouples. In addition, a companion program conducted by the Applied Research Laboratories, a division of The University of Texas at Austin, provided a Model 800P Portable Tiltmeter manufactured by Applied Geometrics to monitor the slope and twist of the pier P16 cantilevers during construction. This section describes these instruments.

3.4.1 Concrete Strain Gauges

Concrete strain gauges are capable of measuring the strain in the concrete in regions where cracking does not occur. The concrete strain gauges used on the US 183 study consisted of an electronic strain gauge mounted on a short length of small-diameter steel

round. These units were attached to the rebar cages of the segments just before casting. A detailed description of the development and workings of this gauge is provided by Arréllaga (5).

All of the concrete strain gauges used for the US 183 instrumentation were manufactured by the US 183 researchers at The University of Texas at Austin, Ferguson Structural Engineering Laboratory (FSEL). A 4.76 mm ($^3/_{16}$ in.) diameter steel round was cut to a length of about 235 mm ($9^1/_4$ in.) and 20 mm ($^3/_4$ in.) of each end was threaded. The middle of the round was carefully sanded and cleaned and a 350 Ω electronic strain gauge was glued to the steel. The gauge was coated with acrylic paint then covered with a protective shrink tubing to protect it from the harsh concrete environment. Nuts and washers were then screwed onto the threaded ends of the steel round to provide a positive anchorage with the concrete and ensure strain compatibility between the concrete and the steel. These gauges were installed in the segments by tying them to the rebar cages at the precasting yard just before placement of the concrete. In the early stages of the US 183 instrumentation, a series of tests was performed to determine the most reliable gauge possible. These tests and the results are described by Andres (4). The gauge used in the US 183 project has been found to be durable and accurate. Figure 3.2 illustrates the concrete strain gauge. Figure 3.3 shows a completed concrete strain gauge in place on a rebar cage, just before placement of the concrete.

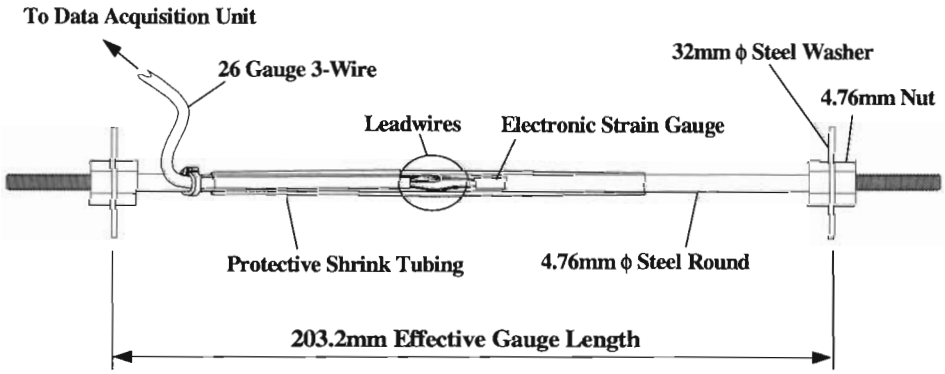

Figure 3.2 Diagram of concrete strain gauge

The electronic strain gauges used on the US 183 project were temperature compensated. The output of the gauge is calibrated not to shift with unrestrained thermal changes in steel for the temperature range of about 50°F to 100°F. Since the coefficient of steel is approximately the same as concrete, the output of the gauge should not vary for unrestrained thermal expansion or contraction of concrete. Thus, unrestrained expansion of the bridge from a linear thermal change that would not produce any stress in the bridge would not cause a change in the output of the gauge. On the other hand, restrained thermal changes in the bridge that do cause stresses would register in the output of the gauge. Thus, the output from the gauge is a true measure of the stress in the concrete and no calibration for

thermal volumetric changes needs to be done to interpret the gauge output. A series of tests to determine the output behavior of the concrete strain gauges from thermal changes in concrete specimens and in the data logging equipment was performed. The results of these tests are described by Davis (7).

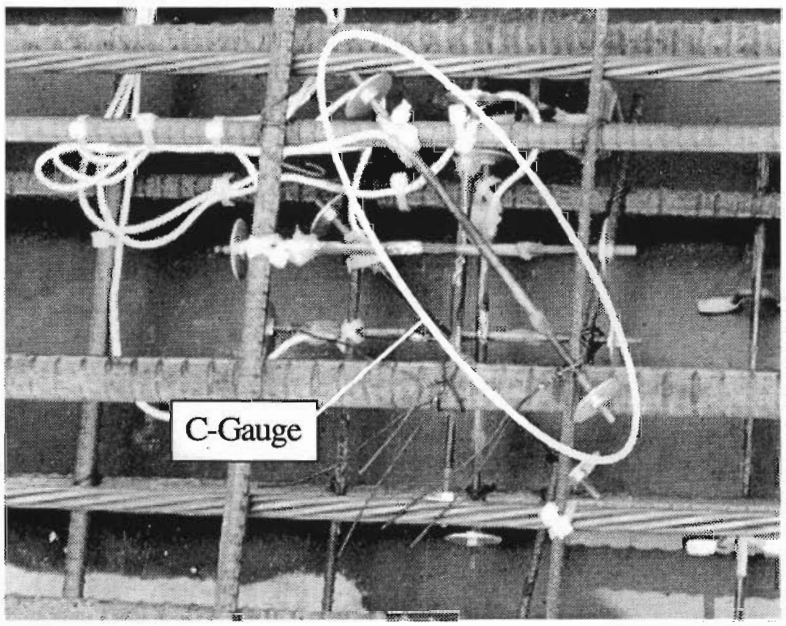

Figure 3.3 Concrete strain gauge tied in place on a rebar cage

3.4.2 Steel Strain Gauges

In areas where the concrete was expected to crack or where forces in the steel reinforcement were desired, a steel strain gauge was bonded directly to the steel reinforcement. The steel strain gauges discussed in this section were bonded onto the external post-tensioning strands.

Before the external tendons were stressed, electronic strain gauges were attached to the strands. The tendons were threaded into place inside protective polyethylene tubing. Small holes were cut into the tubing at desired locations, exposing the strands. A wire from a strand was lightly sanded and cleaned and a gauge was glued to the wire's surface. Then, acrylic paint and a fast drying-epoxy were placed on the gauge to protect it from rubbing against the polyethylene tubing during stressing and also from corrosion from the grout that was pumped inside the tubing afterward. The hole in the polyethylene tubing was patched just before grouting. Only one wire per 15.24 mm (0.6 in.) strand was gauged. Each external tendon contained nineteen strands. Three strands in each tendon were gauged at locations where information was desired. Arréllaga discusses the use of electronic strain gauges on prestressing strand in more detail (5).

3.4.3 Demec Points

Despite the reliability of the concrete strain gauges, very often a gauge will be damaged during casting. Sometimes the gauge wires will be broken and the electronic signal to the gauge is lost. The steel round that the electronic gauge is attached to can also become bent and the output from the gauge will be unreliable. The gauge might even debond from the steel round after a certain amount of time. If one of the two latter problems occurs, it will not be known until analysis of the data begins. It is sometimes difficult to make the judgment that a gauge has gone bad with only one's intuition about what the data should look like to go by. A simple and reliable backup to the concrete strain gauge is to use a Demec extensometer.

A Demec extensometer is a mechanical device that measures strain on the surface of the concrete. The device is simple. Two steel points are installed into the concrete after it has hardened. These points can be glued to the concrete surface. However, for the US 183 project, HILTI® brand Hit anchors were used to anchor the points into the concrete to a depth of about 32 mm ($1^1/_4$ in.). A second Hit anchor was placed a distance of 400 mm ($15^3/_4$ in.) away from the first point and in the direction that the strain is to be measured. As shown in Figure 3.4, the Demec extensometer has points on each of its ends that fit into the holes in the Hit anchors. One of the points can pivot to accommodate movement between the Hit anchors, and a dial gauge on the reader registers the amount of movement and is calibrated to give readings in terms of strain. The Demec extensometer used in the US 183 study had an accuracy of $4x10^{-6}$ m/m.

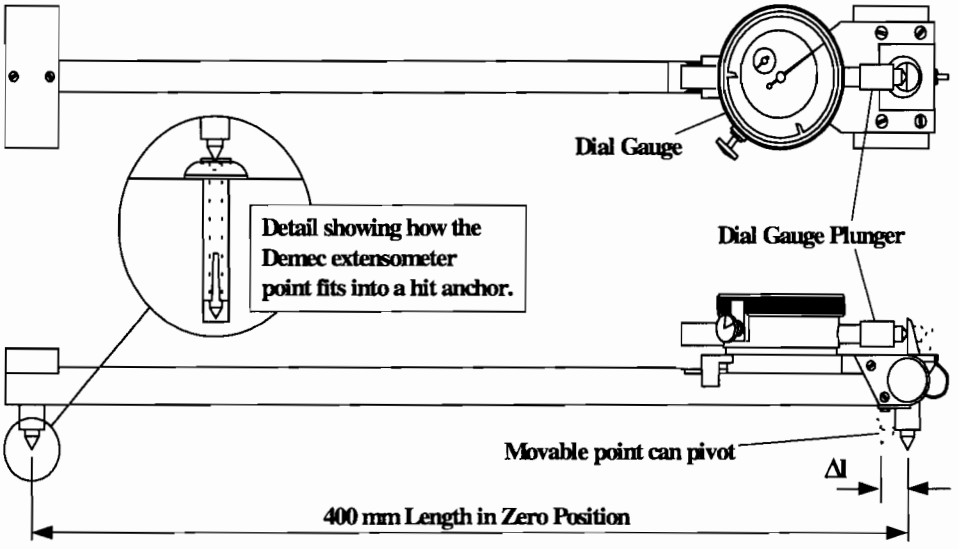

Figure 3.4 Diagram of the Demec extensometer

Demec points have the disadvantages that they are less accurate and more difficult to read data from than the electronic strain gauges. Because Demec readings are taken

manually, they can suffer from human error. Demec points give values of strains at the surface level of the concrete, whereas the concrete gauges are embedded a certain depth and provide strain readouts for concrete beneath the surface level. Therefore, there is not a direct comparison between strain values from the two instruments. Demec points are also not temperature compensated. Thermal strains that have no stress associated with them will appear in the data from the Demec points. Therefore, Demec points are most useful for reading short-term changes in concrete strain under controlled loading conditions where the temperature of the concrete does not vary significantly. Still, if read properly by a person who has experience with the Demec gauge, Demec points can provide a useful comparison to the electronic concrete strain gauge data. A detailed study of the use and accuracy of Demec points was performed by Arréllaga (5).

3.4.4 Thermocouples

Thermocouples were used to measure the concrete temperatures. The thermocouple is a simple electrical connection between two wires of dissimilar metals. The resistance of the connection between the two wires varies within the temperature of the connection. Thus, the temperature can be determined electronically. The thermocouples used in the US 183 study were fabricated from type T wire, which uses copper and constantan for the two dissimilar metals. Copper and constantan both perform well in the corrosive concrete environment.

3.4.5 Tiltmeter

The tiltmeter used to measure slope and twist of the pier P16 cantilevers during construction was a Model 800P Portable Tiltmeter manufactured by Applied Geometrics. Use of the tiltmeter came through the cooperation of the Applied Research Laboratories of The University of Texas at Austin. The 800P tiltmeter uses electrolytic resistance cells to measure angles from the baseline gravity vector (a straight line towards the center of the Earth, or in other words, a very precise plumb line). The precision of the 800P is smaller than 1 microradian (1 mm in 1 km). Ceramic tiltplates (also manufactured by Applied Geometrics) were cemented to the deck of the bridge. The tiltplates are mounts for the tiltmeter that allow precise placement and orientation of the tiltmeter for every measurement. The 800P tiltmeter has indexing bars attached to its bottom surface so that it can be precisely fitted to the tiltmeter plates every time measurements are taken. Four measurements are made with the tiltmeter at each tiltplate and these measurements are used to calculate a magnitude and direction of tilt. The data is read using a voltmeter. A Model 800 tiltmeter is shown in Figure 3.5. Further study of the use of tiltmeters for bridge instrumentation has been conducted by Hyzak (8).

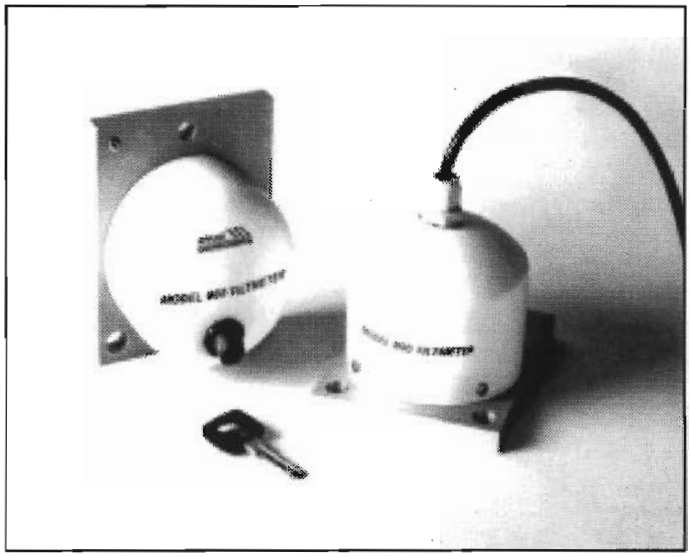

Figure 3.5 Picture of a Applied Geometrics Model 800 Tiltmeter

3.5 Data Logging Equipment

All of the electrical instrumentation systems used in the US 183 study required some form of automated data logging device. The data logging device used was a 21X Micrologger produced by Campbell Scientific, Inc. The electronic strain gauges were connected to the 21X Microloggers in Wheatstone bridge circuits. The 21X Microloggers are capable of recording eight channels connected in full Wheatstone bridge circuits. The capacity of these devices was increased by using AM416 Relay Multiplexers (also produced by Campbell Scientific, Inc.) for channel switchers. A 21X Micrologger coupled with four AM416 Multiplexers is capable of receiving 128 channels of data. Three 21X Microloggers were required to record the data in the superstructure of Ramp P. Data was usually recorded every one or two minutes for important events in the life of the bridge and hourly the rest of the time to track the thermal behavior of the bridge. To download the data, a portable notebook computer was carried into the bridge and connected directly to the 21X Micrologger devices through a parallel port connection. Then, software supplied by Campbell Scientific, Inc. (named PC208) was used to retrieve the data and store it in text files. More information on the 21X Micrologger and AM416 Multiplexor units can be found in Arréllaga (5).

3.6 Overall Instrumentation Scheme

This section will describe in detail the locations of the various gauges used to instrument the Ramp P superstructure and the reasons for selecting those locations. The

organization of this section is divided into sections by instrumentation objective: longitudinal strains, torsional shear strains, post-tensioning strains, and finally, thermal behavior.

3.6.1 Longitudinal Strains

Concrete strain gauges and Demec points were placed across three cross sections in the P16/P17 span in Ramp P: A, next to pier P16; B, at the quarter point of the span; and C and D, near the midpoint. Figure 3.6 shows the locations of the instrumented cross sections and their dimensions from the centerline of pier P16. All of these gauges were oriented to measure longitudinal strains and they were distributed across the cross section so as to provide a complete picture of the longitudinal strain distribution.

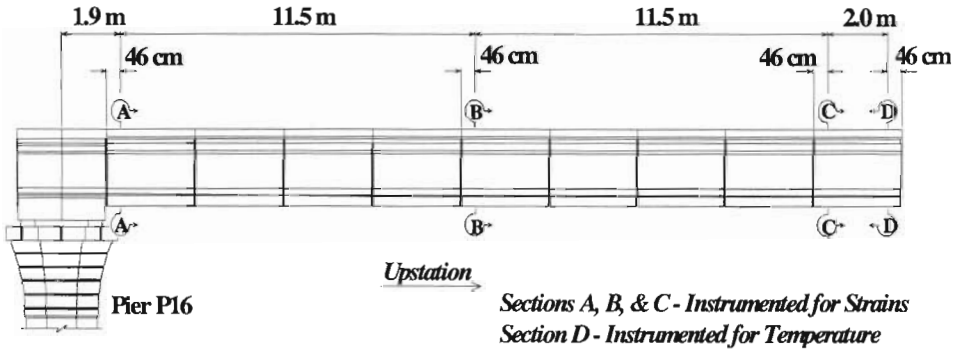

Figure 3.6 Locations of the instrumented sections in Ramp P

Longitudinally Oriented Concrete Strain Gauges

All concrete strain gauge designations used in the US 183 study begin with the letter "C" for "Concrete strain gauge." Figure 3.7 shows the locations of the longitudinally oriented concrete strain gauges in segment P16-2. A total of forty-eight concrete strain gauges were placed in segment P16-2; thirty-two of those gauges were oriented longitudinally. Gauges were placed throughout the entire cross section. More gauges were placed at the intersection of the webs and the top flange because peaks in the strain due to shear lag and diffusion of the cantilever post-tensioning forces were expected in these regions. The instrumented cross section was located at a distance of 460 mm (18 in.) from the segment face to avoid edge effects from the joint. Distribution of concrete strain gages is the same used in segments P16-10 and P16-17. Concrete strain gauges in segment P16-2 were numbered in the 600s. Similarly, corresponding gauges in segments P16-10 and P16-17 were numbered in the 700s and 800s, respectively.

One can notice from the reported dimensions for each segment that the placement of the gauges can vary by several centimeters from segment to segment (22). Placement of the gauges could not be a precise operation because they were tied to the rebar cage and the rebar

cage was always shifted about quite a bit during the casting operations. For this reason, the placement of the gauges cannot be known exactly. However, at least two inches of cover was provided for every gauge, and the locations shown are reasonably correct.

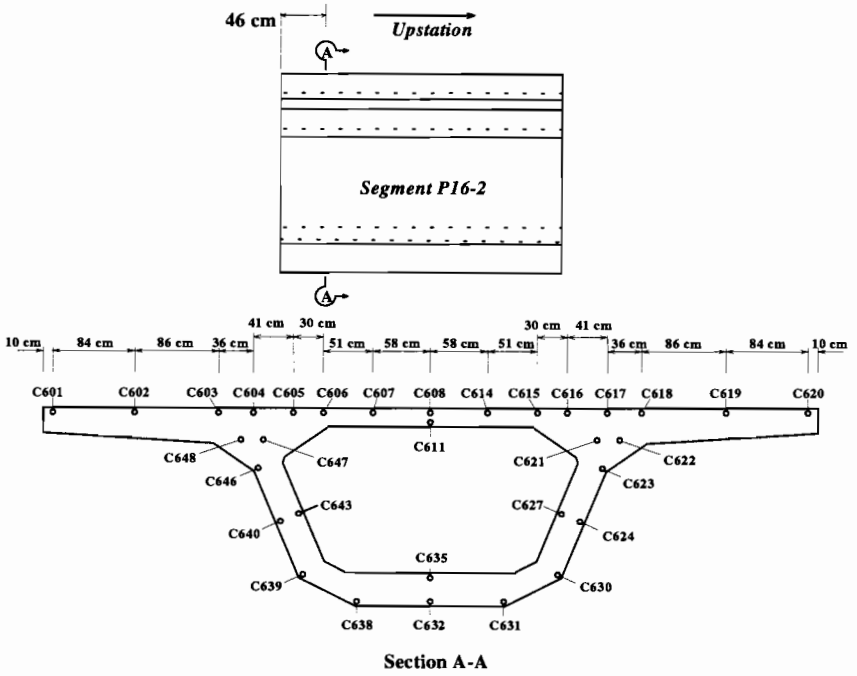

Figure 3.7 Longitudinal concrete strain gauges in segment P16-2

Longitudinally Oriented Demec Points

All Demec point designations used in the US 183 study begin with the letter "D" for "Demec point." Figure 3.8 shows the locations of the longitudinally oriented Demec points on segment P16-2. Demec points are only useful if they are located where they are accessible to humans. Therefore, the Demec points were only placed inside the box and on the deck of the bridge. A total of thirty-three sets of Demec points was placed on segment P16-2; twenty-one of these sets were oriented longitudinally. The same distribution of Demec points was used in segments P16-10 and P16-17. Demec points on segment P16-2 were numbered in the 600s as were the concrete strain gauges in that segment. Similarly, Demec points on segments P16-10 and P16-17 were numbered in the 700s and 800s. Use of the Demec points on the deck of the bridge was forfeited when the asphalt-wearing surface was applied. Fortunately, a live load test of Ramp P was performed before that time.

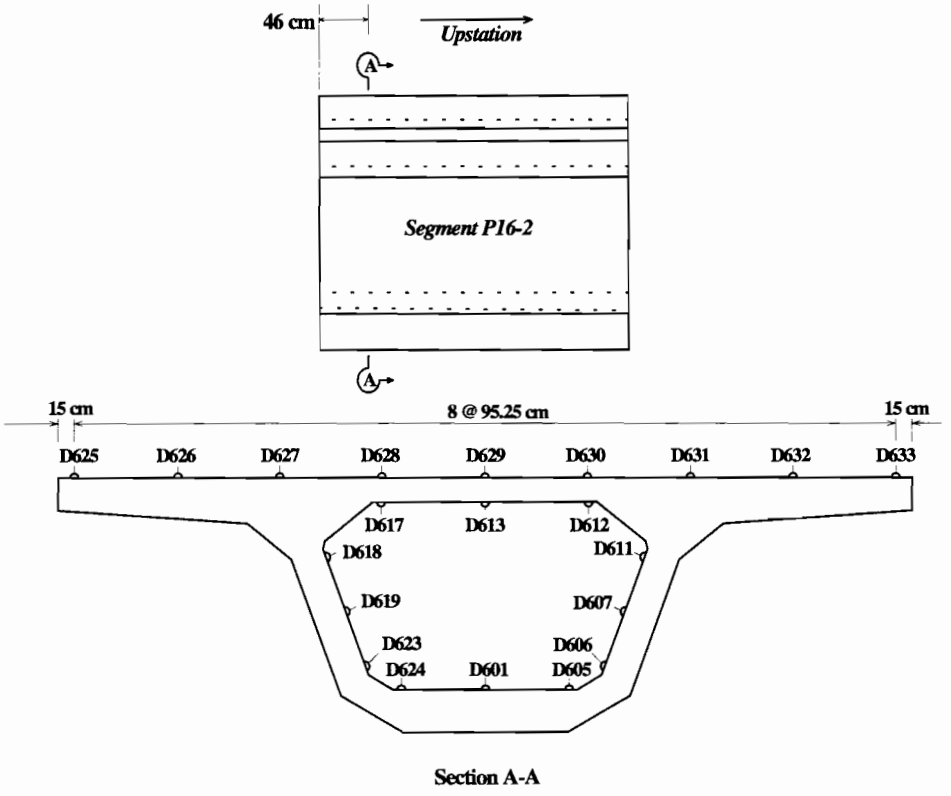

Figure 3.8 Longitudinal sets of Demec points in segment P16-2

3.6.2 Principal Strains from Shear and Torsion

At the same locations that were instrumented for longitudinal strains (see Figure 3.6), concrete strain gauges and Demec points were placed in the webs and on the top and bottom slabs of the segments in rosette arrangements so that principal strains in those areas could be determined.

Concrete Strain Gauge Rosettes

Figure 3.9 shows a rosette arrangement of concrete gauges. The locations and designations of the concrete strain gauges that were arranged into rosette patterns are shown

in Figure 3.10 for segment P16-2. Segments P16-10 and P-16-17 used similar arrangements with the rosettes numbered in the 700 and 800 series, respectively.

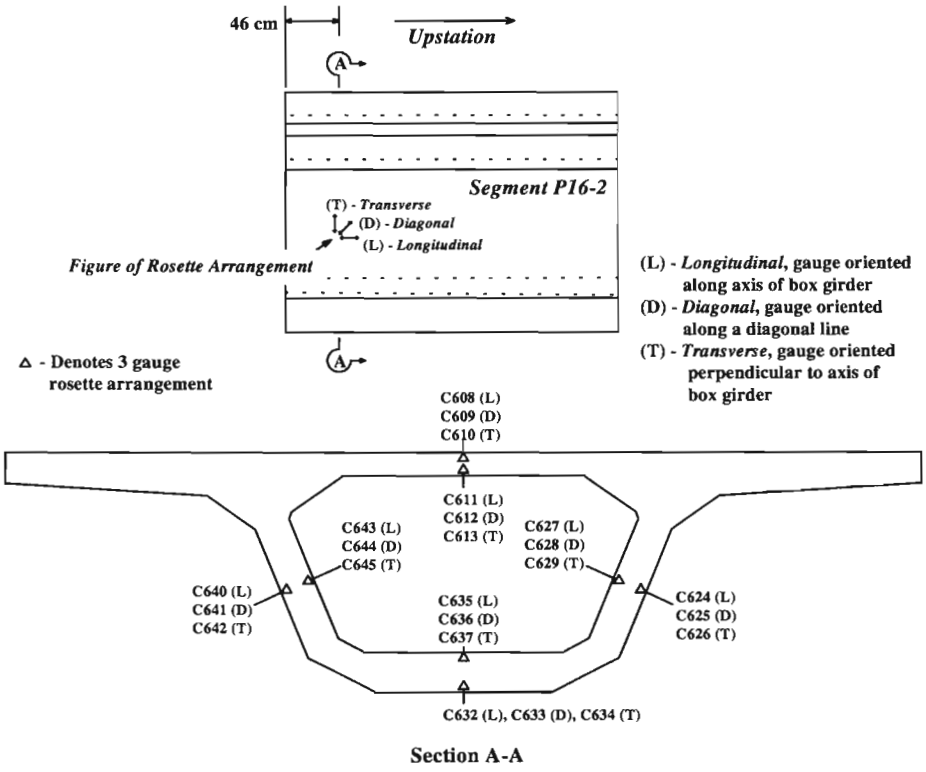

Figure 3.9 Concrete strain gauge rosettes in segment P16-2

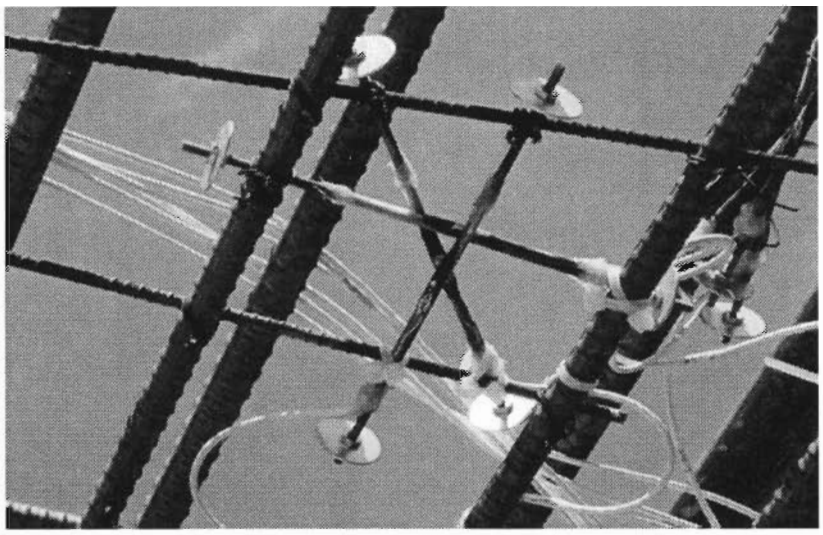

Figure 3.10 Concrete strain gauges arranged in a rosette pattern

Demec Point Rosettes

Demec points were also installed into the concrete surface on the interior of the segments in order to back up the electronic strain gauge data. The Demec point rosettes were made by installing four sets of points in a circular arrangement with each set of points at a 45° angle from the next set. A typical Demec rosette wheel is shown in Figure 3.11.

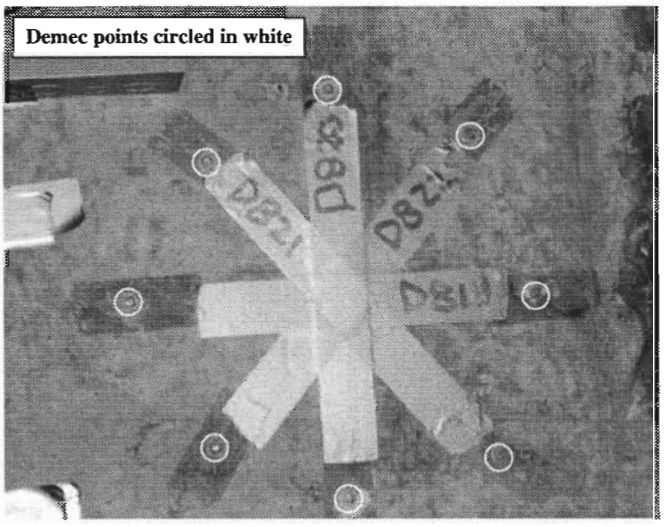

Figure 3.11 Picture of a Demec rosette wheel from segment P16-17

The locations of the Demec rosette wheels are shown in Figure 3.12 for segment P16-2. Similar layouts were used for segments P16-10 and P16-17.

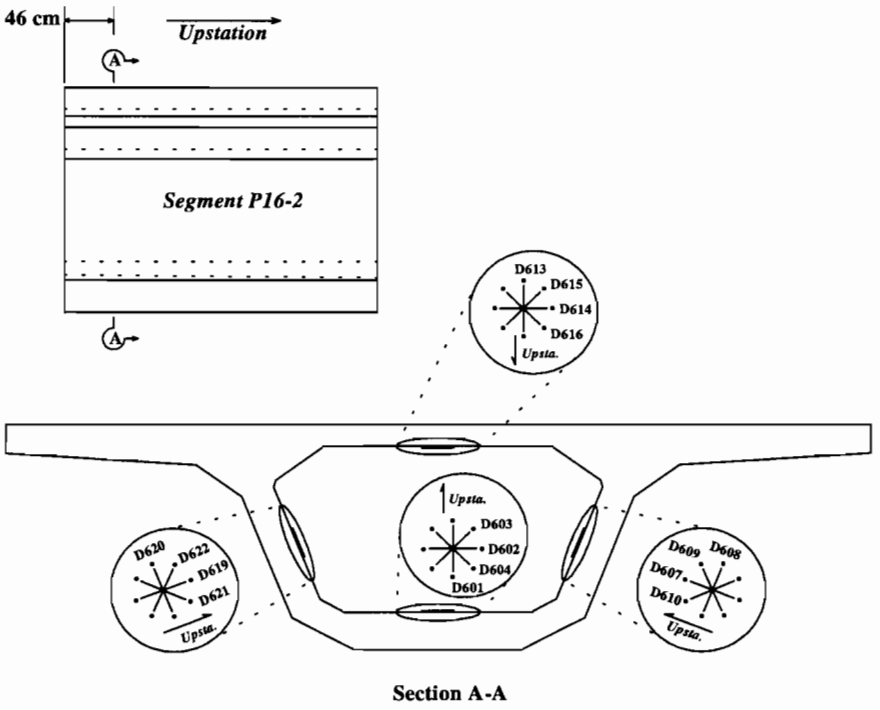

Figure 3.12 Demec rosette wheels in segment P16-2

3.6.3 Strains in the External Post-Tensioning Strands

The external post-tensioning strands are debonded from the bridge structure except for a few points at the deviators and anchorages. Therefore, their interaction with the structure is difficult to predict. Furthermore, friction losses across the deviators need to be known for an accurate construction analysis of the structure. Strain gauges were placed on the external tendons at three positions to give friction losses at two locations for each tendon in the instrumented span of Ramp P. These gauges were designated after the tendons upon which they were placed ("T1," "T2," or "T3") and upon which side of the girder the tendon was located ("L" for "Left looking upstation" or "R" for "Right looking upstation"). Thus, a typical external tendon gauge might be designated as T1La to indicate that it was placed on the left T1 tendon. Friction losses were measured across the vertical deviator in segment P16-10. Figure 3.13 shows the external tendon layout in the instrumented span and the locations where gauges were placed on the tendons.

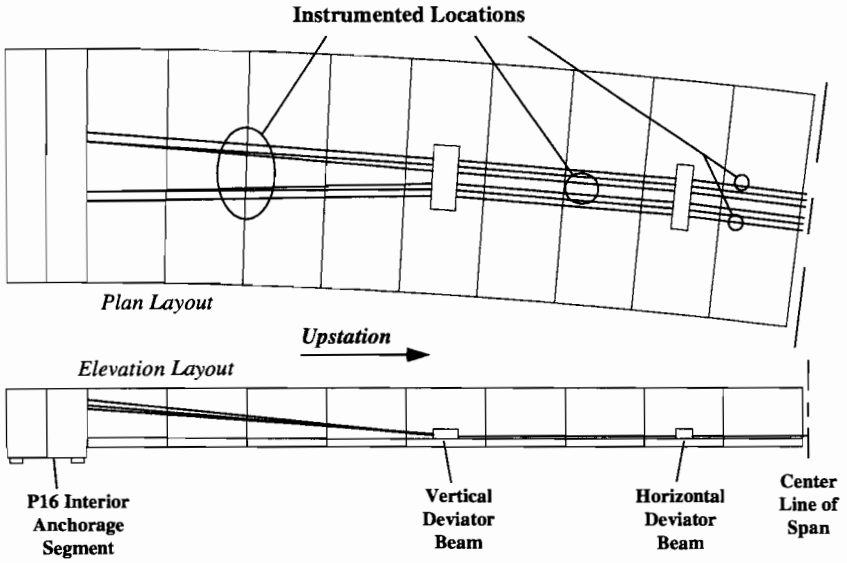

Figure 3.13 ***Instrumented locations on the external tendons in span 16***

3.6.4 Temperatures in the Ramp

All thermocouple designations used in the US 183 study begin with the letter "T" for "Thermocouple." It was decided for economy that one section instrumented for temperatures would suffice to determine the temperature distribution thoughout the superstructure since the sunlight hits all parts of the deck evenly. Thermocouples were placed on the upstation side of segment P16-17 near the midspan. These thermocouples were given number designations in the 800s to match the numbers of the other gauges in segment P16-17. Figure 3.14 shows the instrumented cross section.

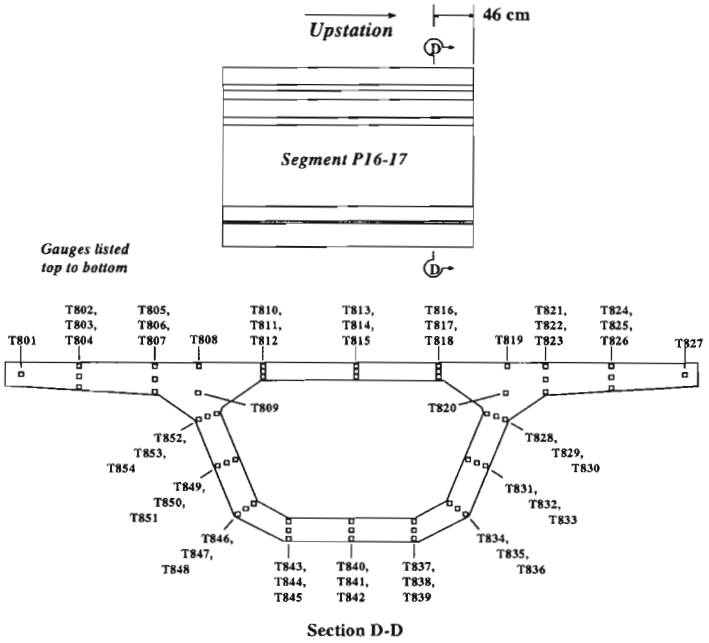

Figure 3.14 Thermocouple gauges in segment P16-17

3.6.5 Slope and Twist of the Ramp

Tiltmeter plates were cemented at intervals along the centerline of the bridge deck on each of the cantilever arms expanding off of pier P16 as construction occurred. After completion of the bridge structure, the tiltplates were removed and reinstalled inside the bridge for a live load test of the structure. Figures 3.15 and 3.16 show the locations of the tiltmeter plates for each of these phases of measurement.

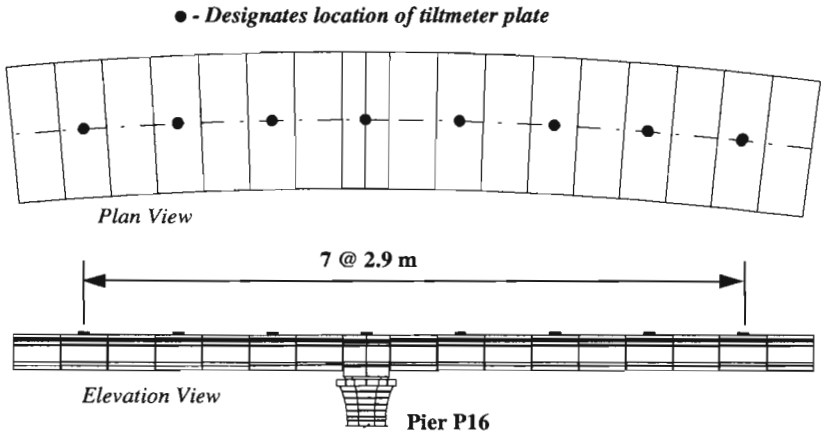

Figure 3.15 Locations of tiltmeter plates during the Ramp P cantilever construction

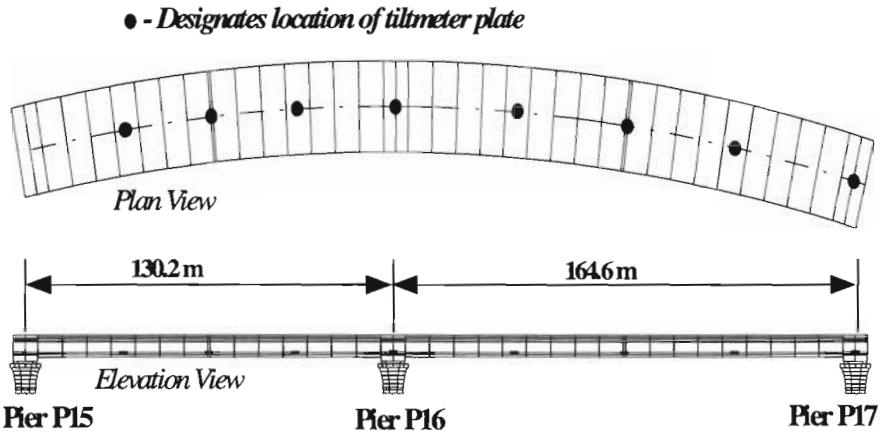

Figure 3.16 Locations of tiltmeter plates during the Ramp P live load test

3.7 Material Tests and Properties

Material properties for the concrete were determined from specimens taken at the time of precasting. Precasting of a segment required three truckloads of concrete (Section 4.2.1 of Chapter 4 discusses the precasting procedure). Three specimens of concrete from the second truckload were taken when each instrumented segment was cast. These specimens consisted of 15.2 cm x 15.2 cm x 53.3 cm (6 in. x 6 in. x 21 in.) plain concrete prisms. After the prisms had hardened, pairs of Demec points were installed on each of the four long-axis faces of the prism. Figure 3.17 shows the details of a typical prism. These specimens were used to determine modulus of elasticity and coefficient of thermal expansion values for the concrete.

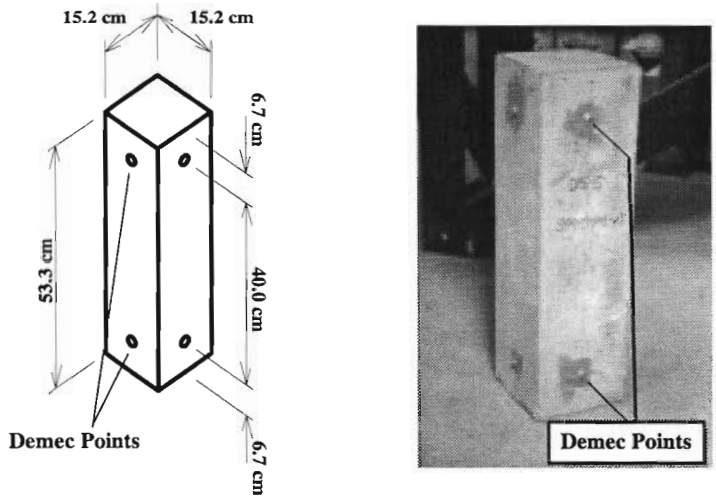

Figure 3.17 Typical concrete prism used for material tests

3.7.1 Modulus of Elasticity

The modulus of elasticity was determined twice for the specimens: once during September of 1996 and a second time during June of 1997. The specimens were placed in a hydraulic load frame and loaded up to 22,240 kN (5000 kips) in 4,448 kN (1000 kip) intervals. At each load interval, Demec readings were taken for each face of the specimen. The modulus of elasticity was then determined from the average strain across the four faces of the prism. Table 3.1 gives the results from both modulus of elasticity tests for the three instrumented segments in Ramp P. The average values that are given represent the averages from the three specimens for each segment.

Table 3.1 Modulus of elasticity values for selected Ramp P segments

Test Date	P16-2 (Cast 5/24/96)	P16-10 (Cast 6/4/96)	P16-17 (Cast 6/10/96)
9/24/96	43800 MPa (6350 ksi)	40900 MPa (5940 ksi)	41000 MPa (5950 ksi)
6/17/97	41900 MPa (6080 ksi)	37700 MPa (5470 ksi)	38400 MPa (5570 ksi)

Table 3.1 shows that the modulus of elasticity decreased with time for all of the segments. This is most likely due to hydration losses within the specimens. This behavior may not be typical of the concrete in the actual Ramp P structure. Curing conditions for the specimens and the concrete in the segments were not the same. The webs and the flanges of the segments were thicker than the width of the specimens. Thus, the concrete in the segments was more confined and better protected from hydration losses than the concrete in the specimens. Also, because more mass of concrete was present in the segments, the curing temperatures that occurred in the segments were probably higher than those in the specimens. For these reasons, it was felt that the measured moduli were probably lower than the actual moduli of the segments. The first set of measured moduli was chosen for conversion of the measured strains into stresses and for calculation models for all of the data analysis.

3.7.2 Coefficient of Thermal Expansion

Coefficient of thermal expansion tests were performed on single specimens for segments P16-2, P16-10, and P16-17. These tests were performed in July of 1997. The specimens were placed in a refrigerated climate at 5°C (41°F) for two nights until they reached a uniform temperature throughout their volume. Demec readings were taken immediately after removal of the specimens from the cold. The specimens were then placed in a warm environment at 33°C (92°F) for two nights until they again reached a uniform temperature throughout their volume. Demec readings were taken at the end of this period. The coefficient of thermal expansion was calculated as the change in the strain of the specimens divided by the change in temperature. Table 3.2 summarizes the results for the three specimens.

Table 3.2 Coefficient of thermal expansion values for selected Ramp P segments

	P16-2	P16-10	P16-17	Average
Coefficient of Thermal Expansion, α	$9.0(10^{-6})$ /°C	$9.7(10^{-6})$ /°C	$9.4(10^{-6})$ /°C	**$9.4(10^{-6})$ /°C**

3.8 *Interpretation of the Electronic Output*

After the instrumentation was in place inside the finished Ramp P structure, the first task of the data analysis from the electronic gauges was to examine the output for broken or debonded gauges. Broken gauges typically have a bad connection somewhere along their circuit and provide no output. Debonded gauges typically give erratic output that is apparent when output from all of the gauges is plotted over time. Figure 3.18 shows the output from the concrete gauges in segment P16-10 plotted over a period of three days.

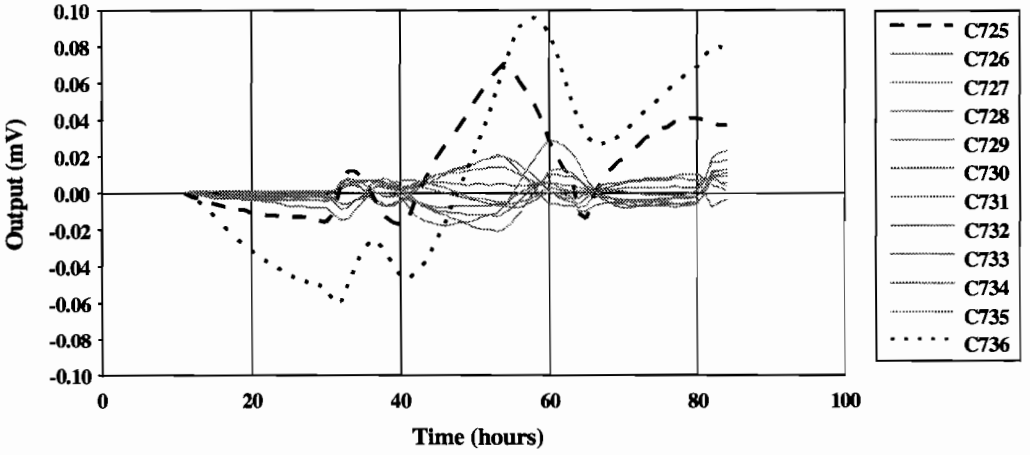

Figure 3.18 Sample of output from some concrete strain gauges in P16-10

The plot in Figure 3.18 makes it apparent that gauges C725 and C736 exhibit very odd behavior. Thus, those gauges were excluded from the database. Eighteen concrete gauges were excluded out of 144 total giving a success rate of 88%. The success rate for the external tendon steel gauges was much lower however. Fourteen out of thirty-six gauges were excluded from the measured results (a success rate of only 61%). Installation of the external tendon gauges took place under less than ideal conditions within the box girder, and the stressing process was very hard on the gauges, so it is not surprising that so many of these gauges had to be discarded.

Data from the gauges were recorded in units of millivolts (mV). These values were converted to strains by multiplication of a gauge factor number (1902 με/mV). Longitudinal stresses were then determined using measured values of the modulus of elasticity from the concrete prism specimens. Shear stresses involved more work. The shear stress could only be determined from a complete knowledge of the Mohr's circle of strain at a given point on the concrete for this reason, shear stresses could only be determined if all three concrete gauges were undamaged within a strain gauge rosette. First, the center of the circle was determined from the strains given by the longitudinal and transverse gauges. Then, the shear strain could be determined from the transverse strain gauge. The shear stress was then calculated by multiplication of the shear modulus. Figure 3.19 shows the orientation of the gauges within a concrete strain gauge rosette, the corresponding Mohr's, circle and the equations used to calculate the shear stress.

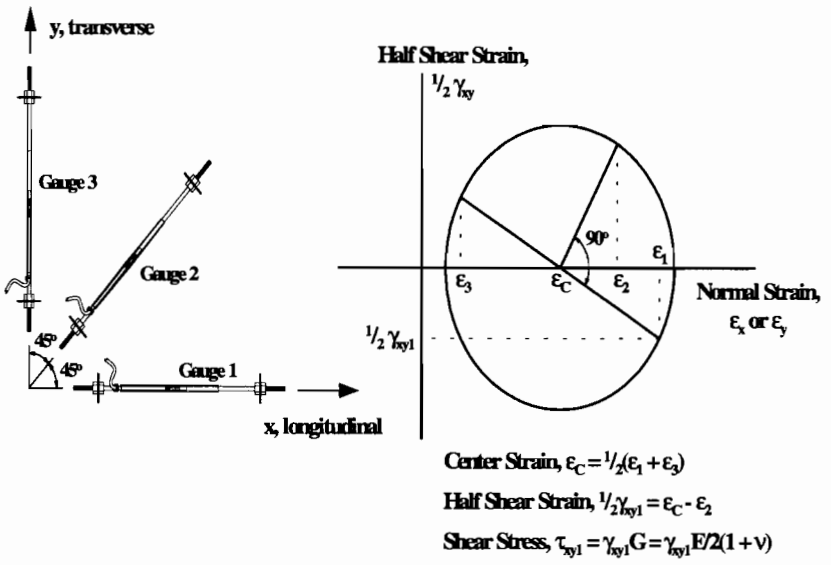

Figure 3.19 Mohr's circle for concrete strain gauge rosette

3.9 Comments on the Demec Point Data

While the general stress trends recorded by the Demec point data matched the trends of the electronic concrete gauges, the final stress plots through the section from the Demec points did not match the stresses from the electronic concrete gauges very well. Because most of the concrete gauges survived the casting process, the data from the Demec points were not necessary for the most part and are not presented in this report. Data from the Demec rosette wheels were particularly bad for determining the principal stresses. The area circumscribed by the Demec rosette wheels was simply too large to act as a suitable stress block in the concrete. The size of the concrete member would have to be much larger in relation to the Demec rosette wheel for the data to be of much use.

CHAPTER 4. SUPERSTRUCTURE CONSTRUCTION PROCESS

4.1 Introduction

Typically for segmental bridges, the largest stresses that the bridge must withstand occur during the construction process. The sequence of construction greatly affects the final distribution of dead load and prestressing moments and torques. Furthermore, the events of the construction process greatly effect the economy and durability of the final structure. This chapter will describe the construction sequence for the northbound IH-35 to northbound US 183 flyover ramp, called Ramp P for short. The precasting and erection processes for the superstructure will be outlined, and the various problems that were encountered during these processes will be discussed. Further details and photos are given in the MSE? thesis of the senior author (22).

4.2 Precasting Operations

The precasting yard for the US 183 elevated bridge was located in south Austin about forty kilometers (twenty-four miles) from the construction site. All of the precast components of the project, except for precast straddle bents, were precast at the yard and stored there until the time of erection. At the peak of precasting, eleven beds were used in the production of superstructure segments. Typical production rate for the beds was one segment per day. In addition to the beds used to precast superstructure segments, one bed precast segments for thirteen segmental piers. Twelve of these piers constituted the substructure for the Ramp P flyover. One of these segmental piers was instrumented and studied by the US 183 research team. The precasting and construction procedures for the segmental piers are discussed in detail by Bonzon (6).

The Ramp P superstructure segments were precast in three beds. One bed precast all of the typical segments for the ramp, another precast the two end anchorage segments of the five-span continuous unit, and a special bed was constructed to precast the interior anchorage segments so that they could be match-cast on both faces. Figure 4.1 shows the completed superstructure of the bridge with the different components of the structure labeled. Precasting of the interior anchorage segments did not occur until late in the precasting yard's life. Precasting of these segments was delayed until erection of the Ramp P substructure was completed so that the final alignment of the ramp piers could be determined and accounted for in the geometry of these segments.

4.2.1 Precasting of the Typical Segments

The segments of the Ramp P superstructure were cast in a short-line precasting bed. Figure 4.2 shows the set-up for the bed and the basic precasting steps. The fabrication of a segment occurred in two stages: the assembly of the rebar cage and the placement of the concrete. Each morning at the start of the work day, about 5:00 A.M., the ironworkers would

begin to assemble a new rebar cage for the segment to be cast on the next day. Meanwhile, the precasting inspectors would break cylinders for all of the previous day's segments. If the concrete had reached the necessary strength of 27.6 MPa (4000 psi), then the forms would be pulled off and transverse pretensioning in the top flange of the segment would be released. A final survey was performed to determine the as-cast alignment of the segment that was cast the day before. The previous segment that had been used for the match-cast face was pulled away and moved to a finishing rack where any surface flaws such as broken shear keys were repaired. Thereafter that segment would be moved to the storage area. The forms were pulled away from the fresh segment, and it was moved forward to become the match-cast face for the next segment to be cast in the bed. A bond breaker was applied to the face of the match-cast segment.

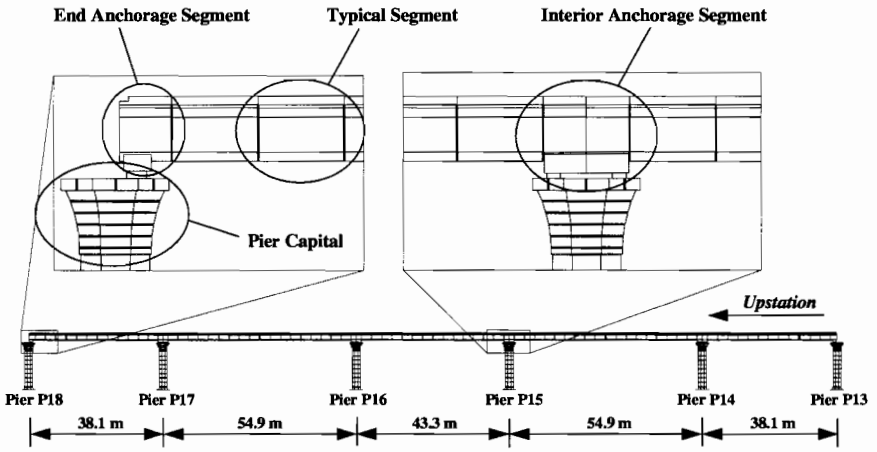

Figure 4.1 Various components of the ramp

The forms were quickly cleaned and sprayed with form oil, and then the new cage was lifted and placed inside the forms. After dropping the cage in the form, post-tensioning ducts and anchorages were tied into the top flange, and then additional steel was added to the webs. The inner core form was then inserted. Next, transverse pretensioning tendons in the top flange were placed and stressed. The cage was finished by placing the last layer of steel in the top flange, a simple rectangular grid of bars that was tied on the ground and then lifted into place by crane. Before casting the concrete, a surveyor checked the alignment of the match-cast segment, and the rebar was checked by an inspector who would oversee the casting of the segment. Placement of the concrete usually began by 5:00 P.M.

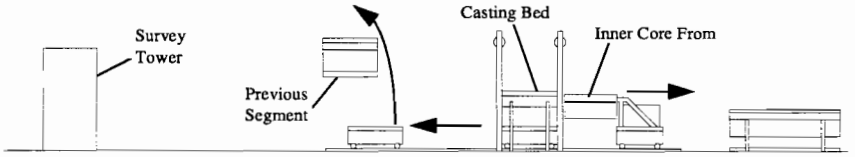

1. The previous match-cast segment is pulled away and moved to a finishing rack. The core form is removed.

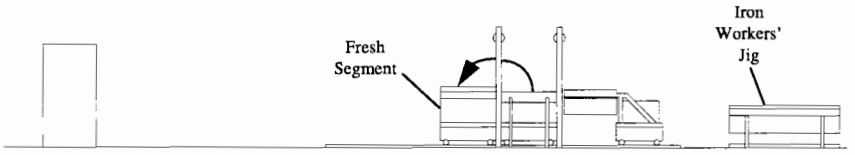

2. The fresh segment is moved forward to be utilized as a match-cast face.

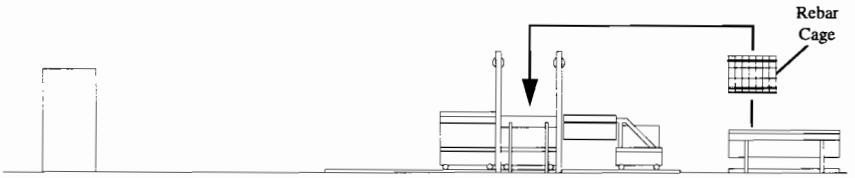

3. A new rebar cage is moved from the iron workers' jig and placed inside the casting bed forms.

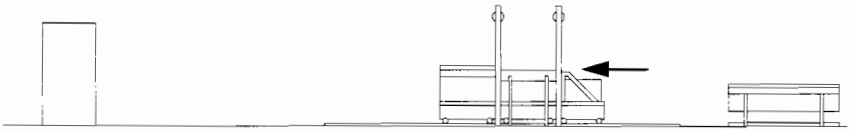

4. Additional work is done on the cage. The core form is inserted. Prestressing in the top flange is stressed.

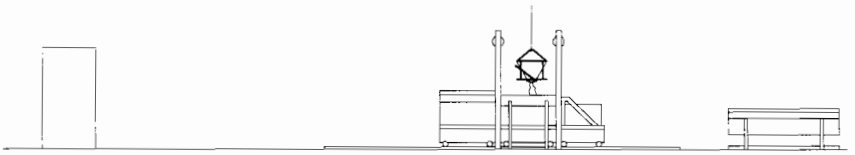

5. A final survey of the alignment is performed. Concrete is placed.

Figure 4.2 Steps in the precasting process

The concrete batch plant was located at the precasting yard. Three truckloads of concrete were necessary for the casting of one Ramp P superstructure segment (about twelve cubic meters of concrete or sixteen cubic yards in customary units). Concrete was first placed in the webs of the segment where congestion of steel usually made proper placement difficult. In addition to the congestion of steel, the first load of concrete was usually mixed with less slump than the next two loads. This was to keep the concrete placed in the webs from running out into the bottom flange. Proper vibration of the concrete was essential to

eliminate voids. Concrete was vibrated through the webs until it just began to flow into the lower flange of the segment. Additional concrete was then dropped through a hole in the top of the core form directly to the lower flange until it was filled. The remaining concrete was placed in the top flange. The casting of the concrete generally took about an hour to complete. Figure 4.3 shows the basic steps in the placement of the concrete. Afterwards the deck surface was finished and brushed, a curing compound was sprayed on the concrete, and the exposed surfaces were covered to keep the concrete moist. The concrete would usually reach the necessary strength for prestress transfer within twelve hours, allowing the casting cycle to begin again the next day.

Precasting operations for the end anchorage segments followed the same procedures as the typical segments, except that different formwork was used.

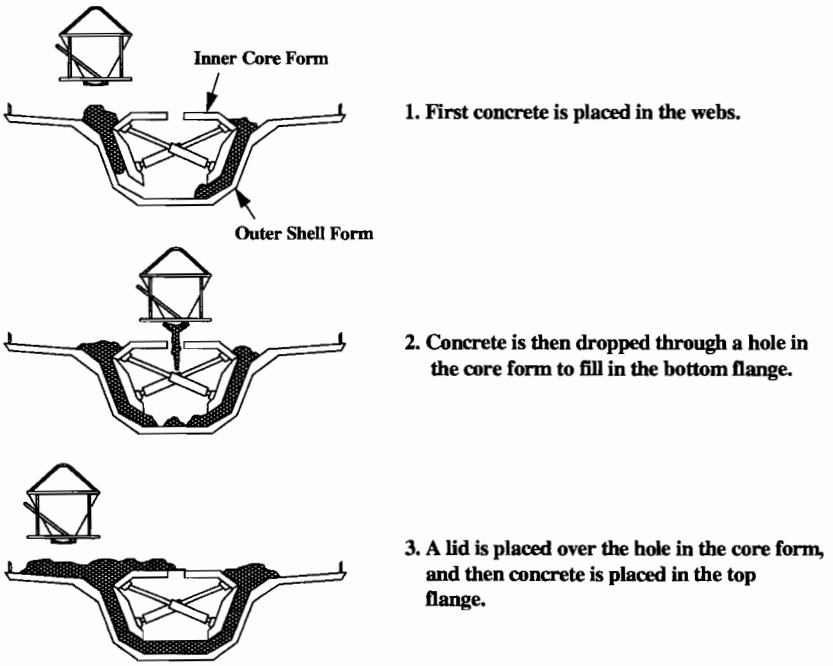

Figure 4.3 Procedure for placement of the concrete

4.2.2 Precasting of the Interior Anchorage Segments

Precasting of the interior anchorage segments involved a special bed because of the necessity to match-cast against both faces at the same time. Precasting of an interior anchorage segment began by placing the two typical match-cast segments on either end of the bed. Figure 4.4 shows the layout of the bed. The anchorage segment was cast in two half-segment pieces because of lifting weight restraints. An intermediate form was placed in the center of the bed where the joint would be between the two halves of the segment. The rebar cage was tied together inside the form for one of the two halves. Next, the core form was placed. Final geometry was checked and inspection was performed on the cage before the

concrete was placed for the first half segment. After curing, the intermediate form was removed, and a bond breaker was placed on the face of the new half-segment. The cage was assembled for the second half. The geometry was surveyed and the cage inspected before casting of the second half began. After curing, the segments were separated from each other and moved to storage. The forms were cleaned, and the process began all over again.

Precasting of the four interior anchorage segments did not begin until after all of the typical Ramp P segments had been precast. These four segments had, by far, the slowest production rate for any of the segments produced at the precasting yard. The reasons for the slow production rate of these segments are simple. The segments were cast in two halves so that they could be erected one half at a time, reducing the weight, and allowing for a smaller crane at the construction site. The bed had to allow for match-cast segments on both ends that made the layout of the bed complicated and unlike the other casting operations that had occurred at the yard. The steel layout for these segments was complex because of the high number of anchorage zones present in these segments. The rebar cages for these segments were assembled directly in the forms because of the complex steel layouts. Thus, the smooth operational cycle that had been established with the other beds was not maintained at this bed. These precasting operations occurred in the final stages of the precasting yard's life as the yard was being shut down and dismantled. The experienced workers had already moved on to other construction projects. Only a skeletal, inexperienced crew remained to work the interior anchorage segment bed. Because only four of these segments were produced the crew assigned to the bed never had time to develop a good experience base for their production. Also, the steel layout was not the same for every interior anchorage segment; unique reinforcing details were required in each anchorage segment to meet the number and placement of the saddles and anchorages necessitated by geometry of the external tendons. The bed that was set up for the production of these segments was rather makeshift because it only had to be used four times, and it was not set up with the emphasis on rapid turnaround that had gone into the design of the other beds in the yard.

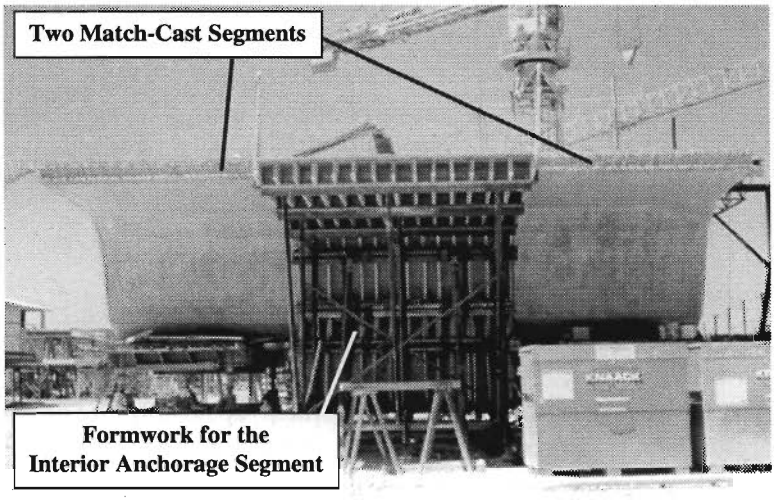

Figure 4.4 The layout of the interior anchorage segment bed

In the contractor's favor, the precasting yard had consistently maintained a heavy lead in their production of segments over the ability of the crews at the construction site to erect the segments. Therefore, there had been no time pressure on the production of the interior anchorage segments for Ramp P. Their fabrication was slow, but in no way impaired the pace of the entire construction project. The complications that occurred were most likely anticipated by the contractor and did not raise a great amount of concern because they did not interfere with the critical paths in the construction plan.

4.2.3 Storage of the Segments

Segments were stored at the precasting yard until the night they were to be erected. They were given no protection from the external climate during the storage time and no special curing provisions were provided for the concrete after the forms were removed. Additional finishing work was often performed in the storage area. Just before the segments were to be transported to the erection site, they were power sprayed to remove dust and other dirt that accumulated on the surfaces of the segments. Figure 4.5 shows the storage area.

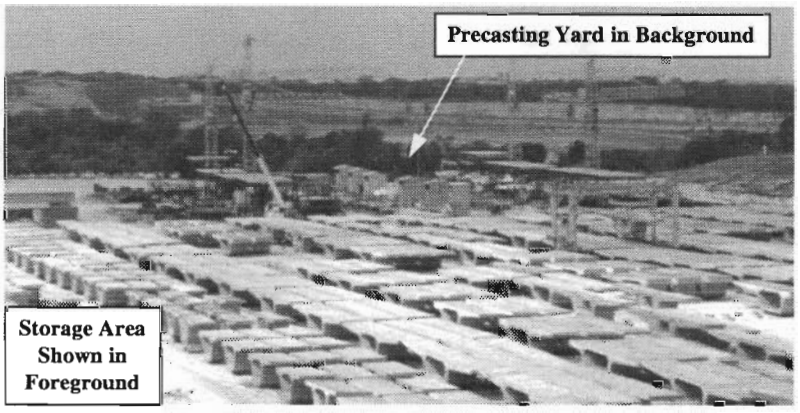

Figure 4.5 View of the storage area

Precasting of the Ramp P substructure occurred in the summer of 1995 and erection of the substructure occurred in the spring of 1996. Precasting of the superstructure occurred in the summer of 1996 and erection occurred in the fall of 1996. Ramp P opened to traffic in March of 1997.

4.3 Superstructure Erection

The central five spans of the superstructure of Ramp P were erected in balanced cantilever and then made continuous. Additional spans upstation and downstation from this five span unit were constructed span-by-span with a pair of traveling erection trusses. Most of the erection occurred at night. This section deals only with the construction of the five-span continuous unit that was constructed in balanced cantilever. The construction process has been broken into seven phases for discussion in this section. These phases are depicted

in Figure 4.6. Problems that occurred during the construction will be discussed in Section 4.4.

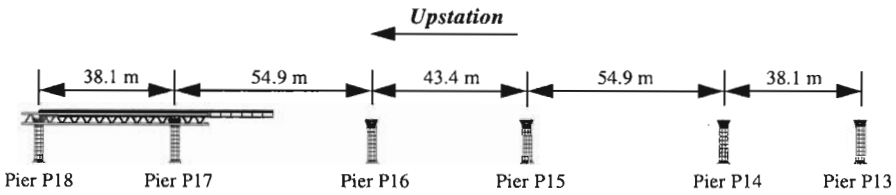

Phase I: Construction of the P17 cantilever unit and the completion of the upstation endspan.

Phase II: Construction of the P16 cantilever unit.

Phase III: Construction of the P14 cantilever unit. Construction begins on the P15 unit.

Phase IV: Completion of the downstation endspan and the P15 cantilever unit.

Phase V: The central span is completed. The free cantilever wings of the P15 and P16 units are extended by one segment.

Phase VI: Final bearing adjustaments are made on P17. The upstation 54.9 m span is completed. The same process is repeated on the downstation half of the bridge.

Phase VII: The last external tendons are placed and stressed. The barriers are cast and a wearing surface is applied to the deck.

Figure 4.6 Construction Phases for Ramp P

4.3.1 Phase I

On the upstation side of the five-span unit at pier P17, trusses used to construct the span-by-span portion of the bridge were moved forward and used to help construct the first 38.1 m (125 ft) span of the balanced cantilever unit. The two halves of the interior anchorage segment for pier P17 (segments P17-1a and P17-1b) were lifted onto the erection trusses by crane, and then brought together to make a whole segment. The interior anchorage segment

was aligned and then dropped onto temporary bearings and tied down to the pier capital with Dywidag post-tensioning bars. Figure 4.7 shows the interior anchorage segment for P17 after this sequence of events.

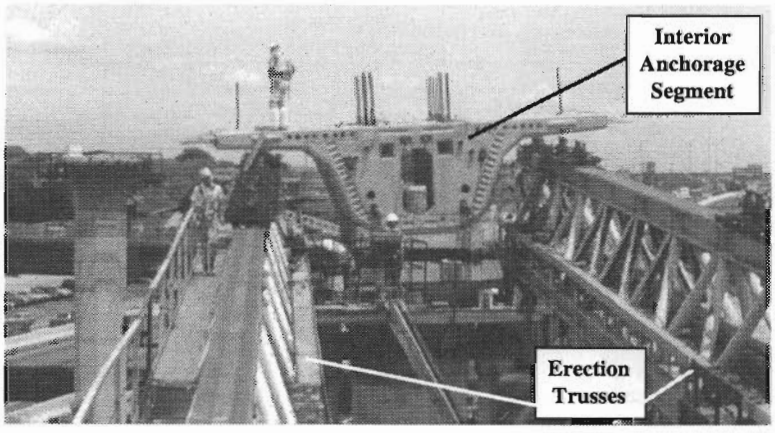

Figure 4.7 Interior anchorage segment for P17 after erection

With the interior anchorage segment in place, construction of the cantilever began. The steps involved for erecting the segments are described in detail in the section dealing with Phase II of the construction. Figure 4.8 shows the P17 cantilever during construction. After the cantilever was finished, the 38.1 m (125 ft) span was completed by adding the end anchorage segment and three typical segments onto the erection trusses. These segments were temporarily stressed together with Dywidag post-tensioning bars, and then a cast-in-place joint was placed to connect these segments to the cantilever, thus completing the span. After the joint had hardened, post-tensioned tendons running through the bottom flange of the girder provided full continuity of the span. Figure 4.9 shows the completed span. Figure 4.10 shows the locations of post-tensioning tendons for the construction of the first span.

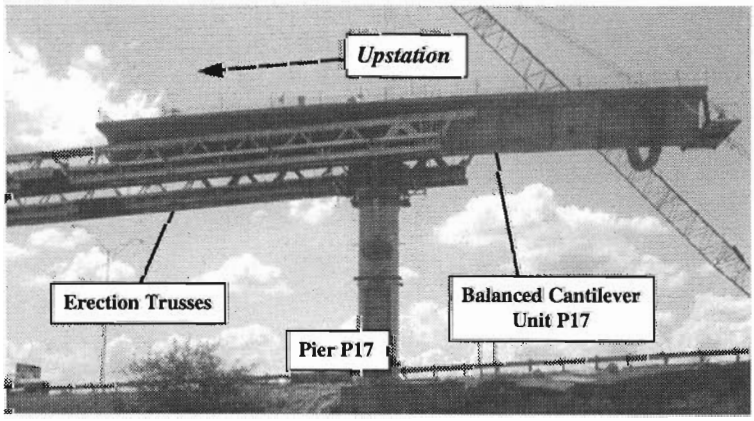

Figure 4.8 P17 cantilever unit during construction

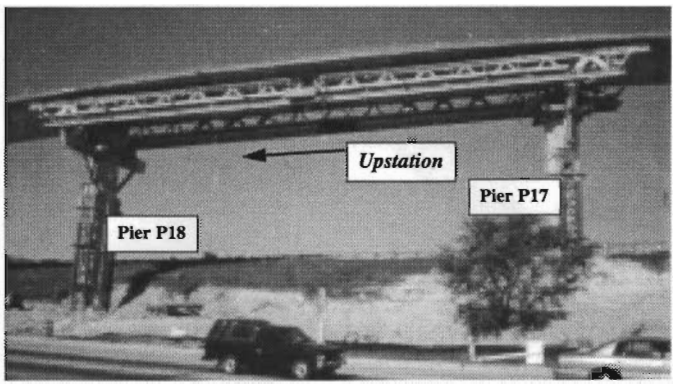

Figure 4.9 Completed endspan between piers P17 and P18

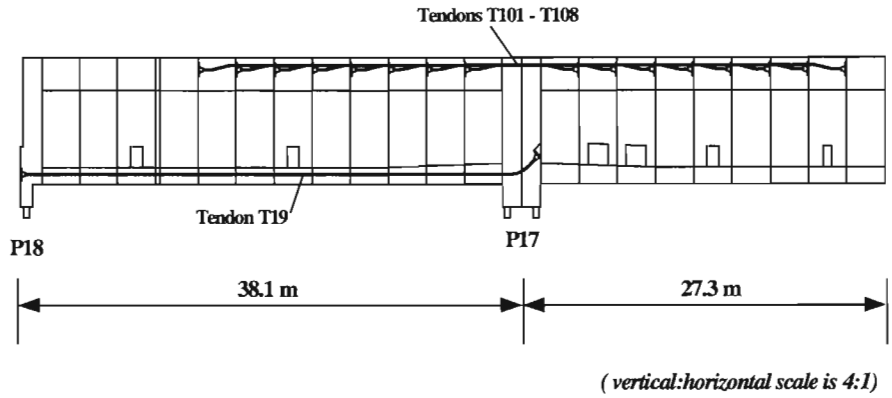

Figure 4.10 Post-tensioning layout at the end of Phase I

4.3.2 Phase II

Because no erection trusses were available at pier P16, the erection procedure for the interior anchorage segment was complex. Figures 4.11a and 4.11b show the steps involved in the erection of the interior anchorage segment. In Step 3, dry fitting of the joint was used. This was necessary so that the alignment of the two halves could be checked. If the two halves of the segment were pulled together with epoxy on the joint faces and it was then discovered that the two halves could not be brought together because they were slightly out of line with one another, then the epoxy would harden before the two halves could be pulled apart, re-aligned and brought back together. The hardened epoxy would compromise the match-cast fit of the joint.

After the two halves of the interior anchorage segment had been joined in Step 5, the whole segment was lifted with hydraulic rams so that reinforced grout bearings could be cast (Step 6). At this time, permanent tie-down bars were dropped through vertical ducts in the anchorage segment and coupled to threaded stubs projecting out of the top of the capital. These tie-down bars consisted of sixteen Dywidag 36 mm ($1^3/_8$ in.) diameter threaded bars.

The alignment of the segment was surveyed and checked. When the grout bearings reached a strength of 37.9 MPa (5500 psi), the segment was dropped into place and stressed to the pier capital (Step 7).

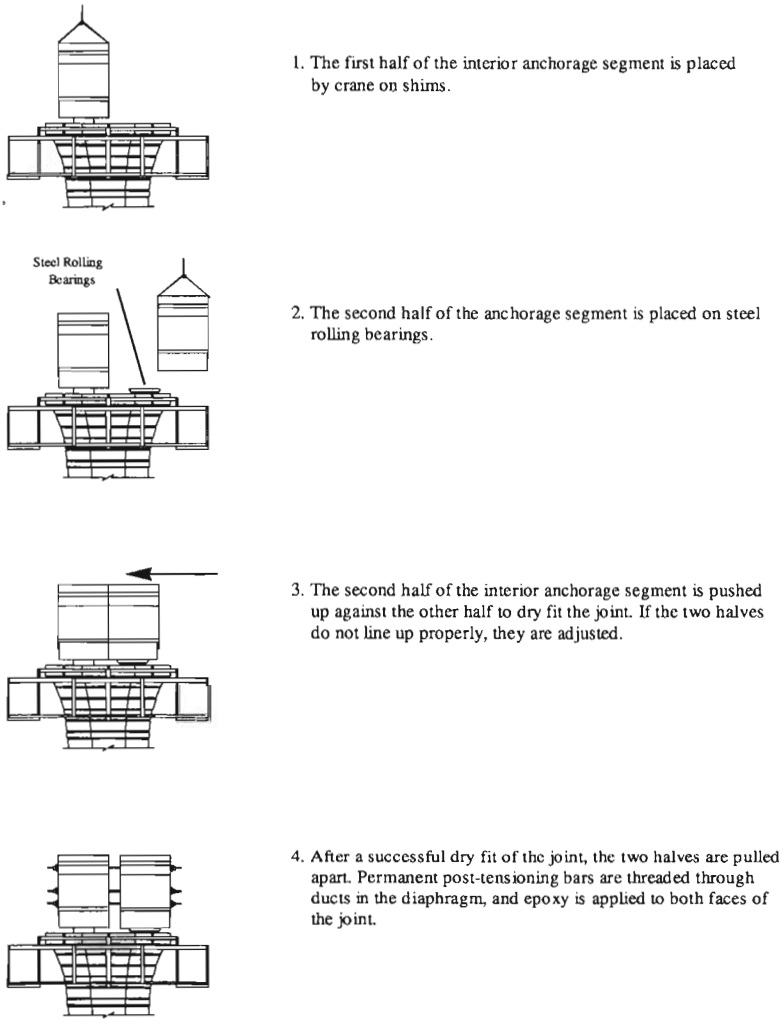

Figure 4.11a Steps in the erection of an interior anchorage segment

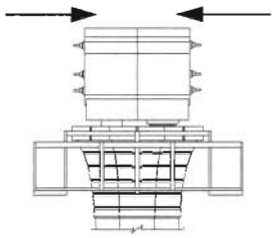

5. The two halves are stressed together.

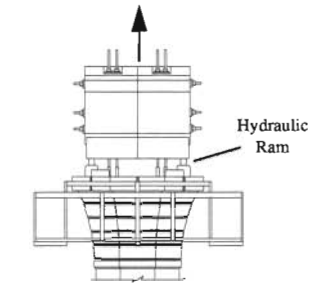

6. The whole segment is lifted with hydraulic rams. Post-tensioning bars are dropped through vertical ducts and coupled to stubs left sticking out of the top of the capital. Reinforced grout bearings are cast underneath the anchorage segment.

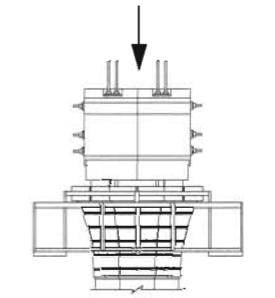

7. After the new grout bearings have reached strength, the vertical post-tensioning bars (tie-down bars) are stressed.

Figure 4.11b Steps in the erection of an interior anchorage segment (continued)

For the erection of the segments in cantilever, blisters for temporary Dywidag post-tensioning 36 mm ($1^3/_8$ in.) diameter-threaded bars were located in the top and bottom of the typical segments. Anchorages for negative moment post-tensioning tendons or cantilever tendons were located in the top flange just over the webs. Figure 4.12 shows the cross section of a typical segment and the locations of the blisters and anchorages required for the cantilevering process. Temporary post-tensioning bars were used to hold the segment in place and provide compression for the joint epoxy until the cantilever tendons could be placed and stressed through the top flange. For most of the cantilevering process the temporary post-tensioning bars were anchored in the blisters except for the first two segments erected on either side of the interior anchorage segment. The interior anchorage segment did not have blisters or ducts for the temporary post-tensioning bars because the saddles for the external tendons occupied the space where the bars would need to pass. Therefore, instead of stressing bars through the blisters, bars were inserted and stressed through some of the ducts for the as-yet-unused cantilever tendons. After these first segments were temporarily stressed

to the interior anchorage segment, cantilever tendons were threaded and stressed across the top flange. With the first set of cantilever tendons stressed, the temporary post-tensioning bars were then removed from the cantilever ducts. The single bar stressed across the bottom flange was left to provide compression until the epoxy had time to cure (one night). Figure 4.13 shows the erection steps for the first two segments erected in cantilever. Figure 4.14 shows the interior anchorage segment for P16 before those steps. Figure 4.15 shows the P16 cantilever unit after those steps.

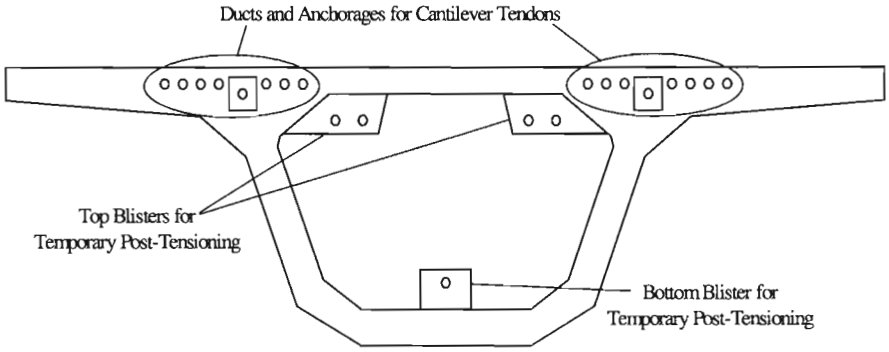

Figure 4.12 Cross section of segment showing locations of blisters

For all other segments that were erected in cantilever, blisters were used to anchor the temporary post-tensioning. The typical construction sequence for the addition of a new segment to the cantilever is illustrated in Figure 4.16. A segment was brought up to the end of the cantilever by crane. The temporary post-tensioning bars were put in place. After epoxy was applied, the bars were stressed and the segment was released from the crane. This process was repeated for a segment on the other cantilever wing, and then cantilever tendons were threaded through the top flange ducts and stressed. Afterwards, the top post-tensioning bars were detensioned. The bottom bar was left overnight until the joint epoxy had cured. A new segment was brought into place by crane and the process was repeated.

Seven segments were erected on each wing of the P16 cantilever unit. Six pairs of cantilever tendons were stressed (one pair for each of the first six cantilevered segments). The seventh segment in each cantilever wing was supported by the temporary post-tensioning bars until continuity could be made across the spans). Figure 4.17 shows the P16 cantilever unit during construction. Figure 4.18 shows the layout of the cantilever tendons for the P16 unit.

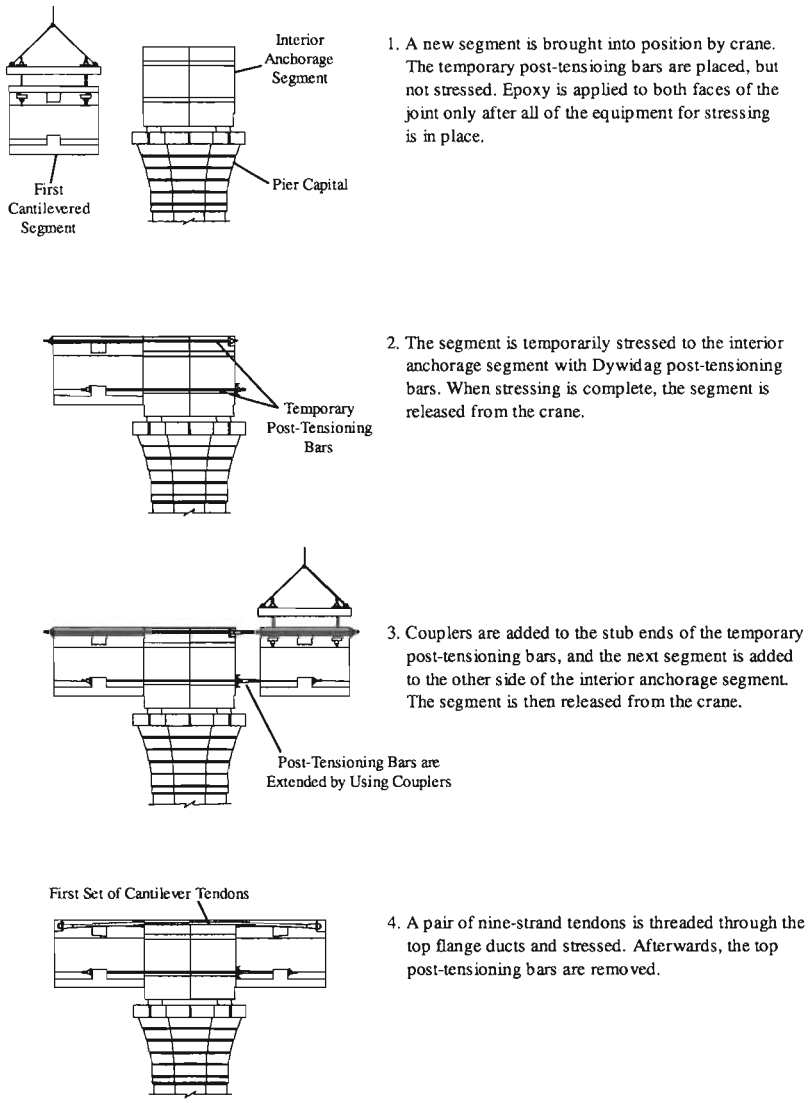

Figure 4.13 Steps in the erection of the first two cantilevered segments

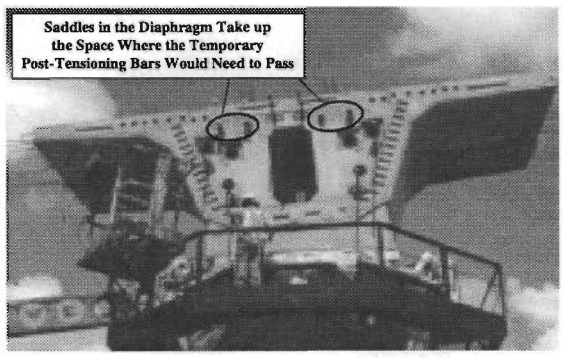

Figure 4.14 The P16 interior anchorage segment after erection

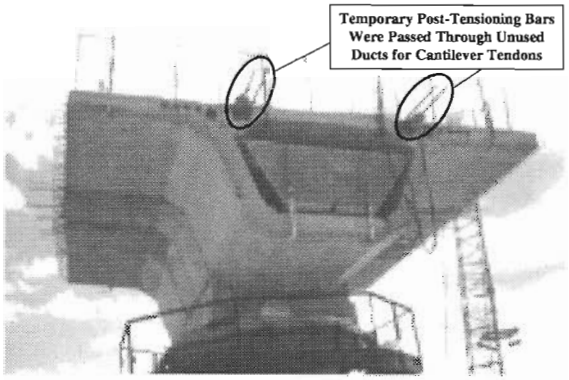

Figure 4.15 P16 with two cantilevered segments

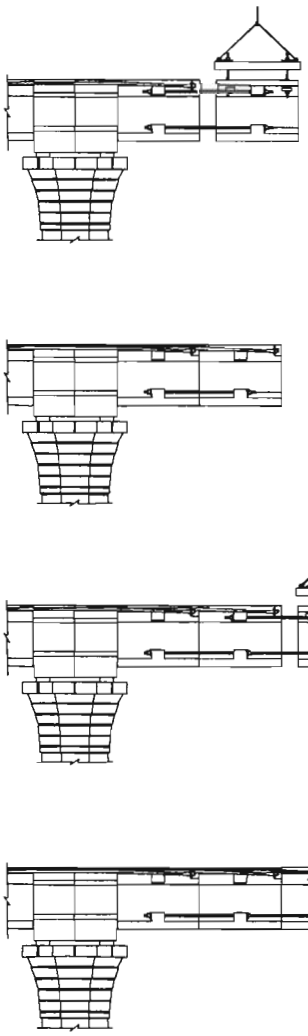

1. A new segment is brought into position by the crane. Temporary post-tensioning bars are threaded through the blisters. Epoxy is placed on both joint faces before stressing of the bars begins.

2. After the segment is secured with the post-tensioning bars, the cantilever tendons are pulled through the top flange ducts and stressed. The post-tensioning bars in the top blisters are detensioned, but the bottom bar is left to provide the minimum compression across the bottom flange for curing of the joint epoxy.

3. The next segment is brought into position. A coupler is added to the bottom bar so that it may be extended to the hanging segment. Otherwise, erection continues as described in Steps 1 and 2.

4. Temporary bars were required across the bottom for one night. This was to provide proper compression on the joint epoxy in the bottom flange while it cured.

Figure 4.16 Steps in the erection of the cantilever

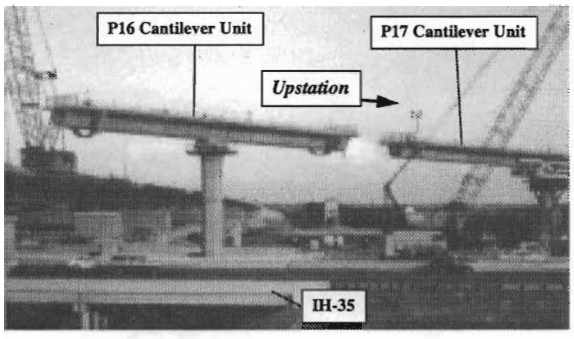

Figure 4.17 The P16 cantilever unit during construction

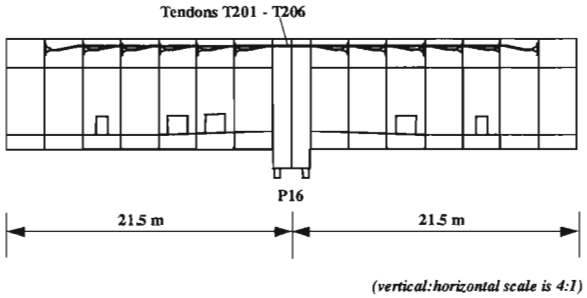

Figure 4.18 Layout of cantilever tendons for the P16 cantilever

4.3.3 Phase III

At the same time as the construction of the Ramp P superstructure, construction of the US 183 Northbound mainlane was underway. This necessitated that a certain amount of clearance be available underneath the Ramp P construction. For this reason, the contractor decided to place the interior anchorage segment and the first two cantilevered segments on pier P15 and then to move on to erection of the P14 cantilever unit before finishing the P15 unit. Thus, in Phase III, only a small part of the P15 cantilever unit was completed and all of the P14 cantilever unit was constructed. Figure 4.19 shows the P15 and P14 cantilever unit under construction during this phase as well as the work that was proceeding on the northbound mainlane below. The steps for erection of the interior anchorage segments as well the cantilevering process for the typical segments followed the steps outlined in the discussion for Phase II. The post-tensioning layout for the P14 cantilever unit was symmetric about the midspan between P16 and P15 to the layout for the P17 cantilever unit.

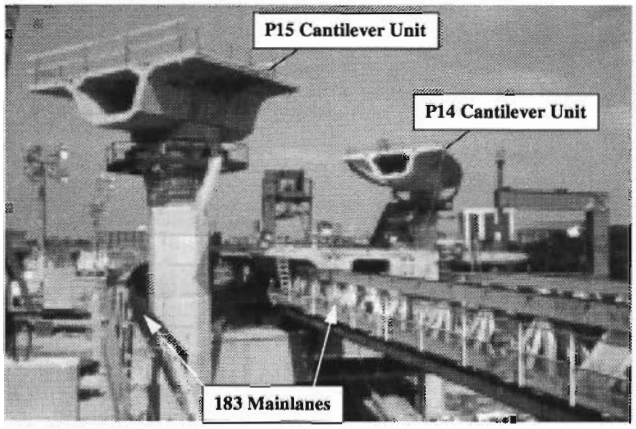

Figure 4.19 P14 and P15 cantilever units during Phase III construction

4.3.4 Phase IV

Falsework was erected next to pier P13 for the erection of the last four segments on the downstation 38.1 m (125 ft) span. The segments were lifted into place on the falsework, a closure joint was cast between the end of the P14 cantilever and the end segments, and continuity tendons were stressed. The process was the same as for the upstation endspan in Phase I. The P15 cantilever unit was finished in this phase as well.

4.3.5 Phase V

With the two central cantilevers completed, a closure joint was cast-in-place between the P15 and P16 cantilever units. Figure 4.20 shows the joint just before placement of the concrete.

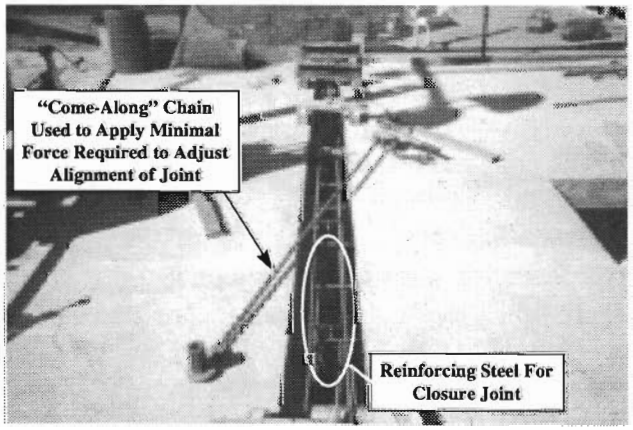

Figure 4.20 View of the closure joint before casting

After the closure joint had hardened, bottom flange continuity tendons were placed and stressed across the central 43.3 m (142 ft) span (tendon T20) and cantilever tendons were stressed across both of the newly joined cantilever units (tendon T301). Next, segments were erected on each of the free cantilevers and another pair of cantilever tendons was stressed across the entire unit (tendon 302). Figure 4.21 shows the arrangement of the tendons that were placed and stressed in Phase V.

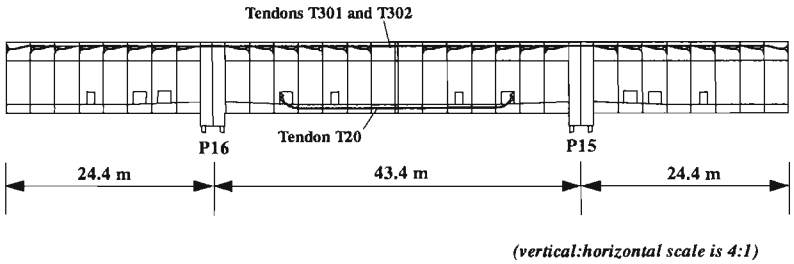

Figure 4.21 Layout of post-tensioning tendons for the end of Phase V

4.3.6 Phase VI

Segment P16-17 was added to the end of the free cantilever remaining on the P16 unit. The permanent bearings were placed at P17. At the same time, the alignment of the ramp was adjusted so the cantilevers from P17 and P16 lined up well. A closure joint was cast between the P16 and P17 cantilever units. Continuity tendons were placed in the bottom flange of the span and stressed (tendons T21 and T22). External tendons running from the end anchorage segment at pier P18 to the interior anchorage segment at pier P16 were also placed and stressed (tendons T1 and T2). The same process was repeated for the downstation 54.9 m (180 ft) span between piers P14 and P15. Figure 4.22 shows the layout of the post-tensioning tendons that were stressed in the upstation spans between P16 and P18. The downstation spans had the same geometry but were symmetric about the midline of the five-span structure.

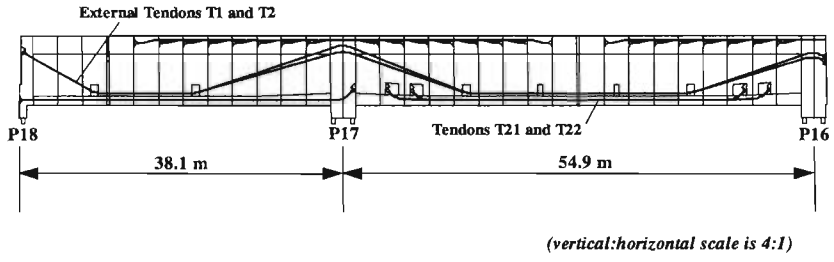

Figure 4.22 Layout of the post-tensioning tendons stressed in Phase VI

4.3.7 *Phase VII*

With the erection of the superstructure segments complete, the final stage of the construction process was the placement and stressing of the remaining external tendons in the structure (tendons T3 and T4). Figure 4.23 shows the layout of these tendons. Tendon T3 runs through all three of the spans shown. Tendon T4 only runs through the central span.

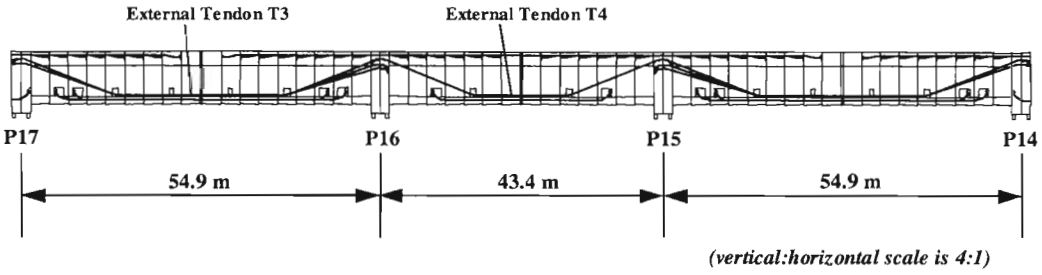

Figure 4.23 Layout of the last external tendons placed and stressed in Ramp P

After the external tendons were stressed, they were grouted. Barriers were cast on the top deck, and an asphalt overlay was applied. The bridge opened to traffic shortly thereafter. Table 4.1 summarizes the events in the construction of Ramp P with the dates of occurrence.

Table 4.1 Events and dates for the construction of Ramp P

Date	Event
4/96 — 7/96	Ramp P superstructure segments are precast
8/15/96 — 9/5/96	P17 cantilever erected
9/6/96 — 9/9/96	Remaining segments and CIP closure for span P17 placed
9/9/96 — 9/22/96	P16 cantilever erected, continuity tendon T19 stressed in span P17
9/23/96 — 9/24/96	Segments P15-1a, 1b, 2 and 3 erected for P15 cantilever
9/27/96 — 10/9/96	P14 cantilever erected
10/10/96 — 10/14/96	Remaining segments and CIP closure for span P13 placed
10/15/96 — 10/16/96	Remaining segments for P15 cantilever erected
10/17/96	Continuity tendon T19 stressed in span P13
10/21/96 — 10/24/96	CIP closure and continuity tendon T20 stressed for span P15
10/24/96 — 10/29/96	Tendons T301 and T302 stressed, P15-16, P16-16, and P16-17 erected
11/5/96 — 11/7/96	Alignment at P17 adjusted, CIP closure for span P16
11/11/96 — 11/12/96	Continuity tendons T21 and T22 stressed for span P16, permanent bearings set at P17
11/13/96	P15-17 erected
11/15/96 — 11/19/96	External tendons T1 and T2 stressed in upstation spans
11/19/96 — 11/22/96	CIP closure for span P14, continuity tendons T21 and T22 stressed, permanent bearings set at P14
11/23/96 — 12/7/96	Remaining external tendons T1, T2, T3, and T4 stressed
2/13/97	Live load test performed on Ramp P
2/97 — 3/97	Barriers cast on Ramp P, wearing surface applied
4/97	Ramp P opens to traffic

4.4 *Construction Problems*

Several problems were encountered during the construction process for Ramp P. This section lists the problems that occurred and how they affected the construction process.

4.4.1 Erection of the Interior Anchorage Segments

Two major problems occurred during the erection of the interior anchorage segments. First, it was difficult to place and join the two separate halves of the segment on top of the pier capitals. Second, the tie-down bars were difficult to stress on pier P16.

Joining the Two Halves of the Segment

The scheme devised for bringing together the two halves of the interior anchorage segment was poorly devised (see Figures 4.11a and 4.11b). Rather than devising a scheme to lower the two halves into line with each other using the crane, the contractor relied on his ability to push one of the segment halves laterally if the two halves did not line up with one another. This was done using a small hydraulic ram that was fixed to the top of the pier capital with anchor bolts. This ram barely supplied enough force to shove one of the segment halves sideways, and the resulting effort damaged the top of the capital. Figure 4.24 shows the scheme and what occurred. The top of the capital was not detailed for the type of load the ram placed on it, and the concrete was severely split.

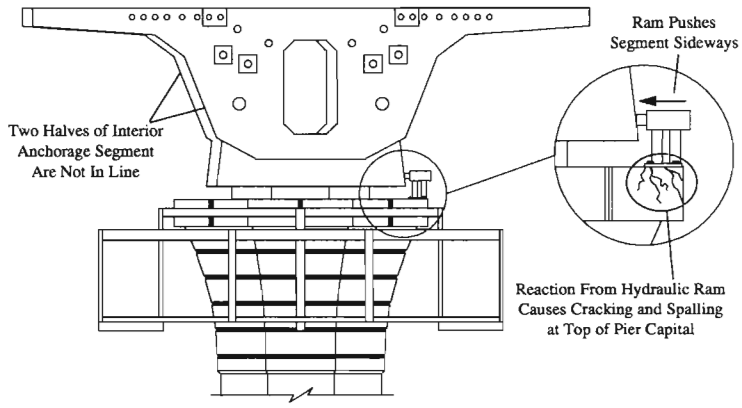

Figure 4.24 Scheme for moving the two halves of the interior anchorage segment into line

Furthermore, the steel roller bearings that were intended to allow the second half of the anchorage segment to be easily pushed up against the first half had a coefficient of friction that was too high. The contractor found it extremely difficult to move the segment half after it was placed on the capital. Three nights were required to erect the interior anchorage segment for Pier P16 because of these difficulties.

Stressing the Tie-Down Bars

After the interior segment was in place on Pier P16, problems were encountered with the stressing of the tie-down bars. The tie-down bars on Piers P15 and P16 were permanent. Therefore, the anchorage plates in the deck for these bars were recessed into blockouts that could be filled with grout after completion of the structure. Unfortunately, these blockouts were too constrictive for the original hydraulic ram the contractor intended to use for stressing the bars. A special long-necked ram was required to fit down into the blockout. As a result, only a few of the tie-down bars could be stressed before construction of the P16 cantilever unit began. Thus, the contractor could not rely on the pier to carry an unbalanced moment from the cantilever. When segments were erected on that unit, two cranes had to be used simultaneously to support segments at both wing tips. Only when both segments were properly attached to the ends of the cantilevers and the unit was in balance could the cranes be released. Fortunately, the contractor already had two cranes at the job site for the erection of Ramp P. Figure 4.25 shows the special long-necked ram required to stress the tie-down bars on Piers P15 and P16. This ram was acquired before erection of the P15 anchorage segment, so the problem was avoided at that unit.

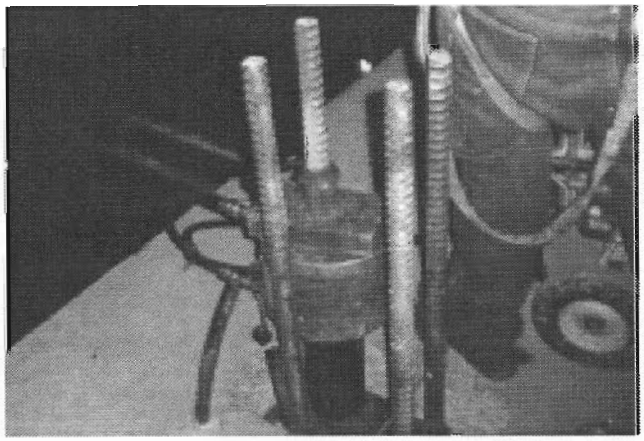

Figure 4.25 Ram necessary for stressing the tie-down bars on P15 and P16

The interior anchorage segment had been split into halves so that a smaller crane could be used on the job site. The weight of a whole segment would have necessitated a much larger crane than the one used. The extra volume of the anchorage diaphragms in the interior anchorage segments made its weight much greater than the other superstructure segments. No problems occurred with the erection of the P17 interior anchorage segment because the erection trusses simplified the manipulation of the two segment halves.

4.4.2 Erection of the First Two Cantilevered Segments

Problems occurred during the erection of the first two cantilevered segments because the scheme to pass the temporary post-tensioning bars through the ducts for the cantilever tendons was deficient (reference Figure 4.13 for the steps involved in this sequence). The ducts for the cantilever tendons had too small of a diameter to properly accommodate the coupler used for the bars. The Dywidag couplers had a diameter of 67 mm ($2^5/_8$ in.) and the cantilever tendon ducts had a diameter of 76 mm (3 in.) that left almost no spare room for the coupler to fit through the duct. Furthermore, the cantilever tendon ducts were chorded between joint faces because of the horizontal curvature of the bridge. The small angle breaks in the duct forced a small bend in the temporary post-tensioning bars and wedged the coupler up against the side of the duct. When it was time to remove the bars from the tendon ducts, the workers found that the bars were almost impossible to get loose. In at least one instance (for the P16 cantilever unit), the bars had to be extracted from the ducts by using a hydraulic ram. The erection of the first two cantilevered segments on Pier P16 took two complete nights to finish. By comparison, the other segments on that cantilever unit were erected at a rate of six per night. Figure 4.26 shows a detail of how the temporary post-tensioning bars and couplers needed to fit through the top flange tendon ducts. The figure is to scale. It is obvious from the drawing that removing the coupler would be difficult. Furthermore, if the duct was indented even slightly at the time the segment was cast, removal of the coupler would have become impossible without damaging the concrete.

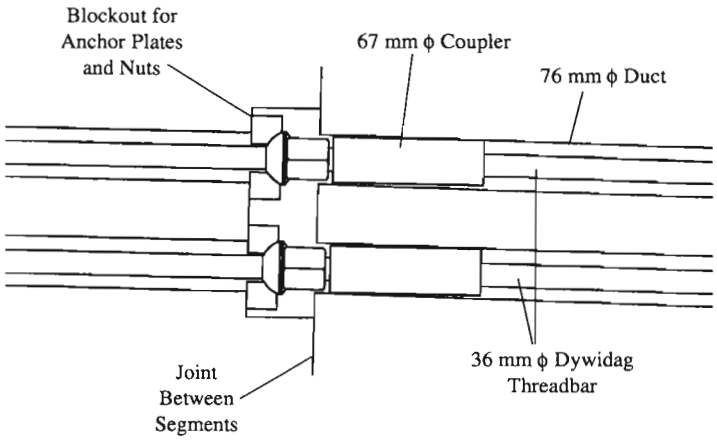

Figure 4.26 Detail for passing the temporary post-tensioning bars through the cantilever tendon ducts

In contrast to the problems that occurred with the erection of the first two cantilevered segments, the erection of the other segments on the cantilever went quite well. One of the

key reasons for this success was the use of external blisters for the temporary post-tensioning bars. These blisters allowed a loose fit for the bars and plenty of room to access the anchorage and coupling hardware. The ducts in the blisters were large enough to accommodate the 36 mm diameter ($1^3/_8$ in.) threaded bars, and the length of the blisters was so short that the bars had a large amount of play. The couplers were not required to pass through any ducts. Figure 4.27 illustrates how the loose fit of the temporary post-tensioning bars in the blisters helped in the erection of a segment. The worker on the right has to pass the bars between the blister on the foreground segment and the blister on the background segment that is hanging by a crane. It is not necessary for the crane operator to position the hanging segment very precisely because the worker has enough play in the post-tensioning bars to run them through the two blisters even when the segments are not completely in line. Once the bars and the rest of the stressing hardware were in place, the segment was easily drawn up to the end of the cantilever by stressing the temporary bars. When the bars needed to be removed, the workers had adequate access to the nuts and couplers to loosen them.

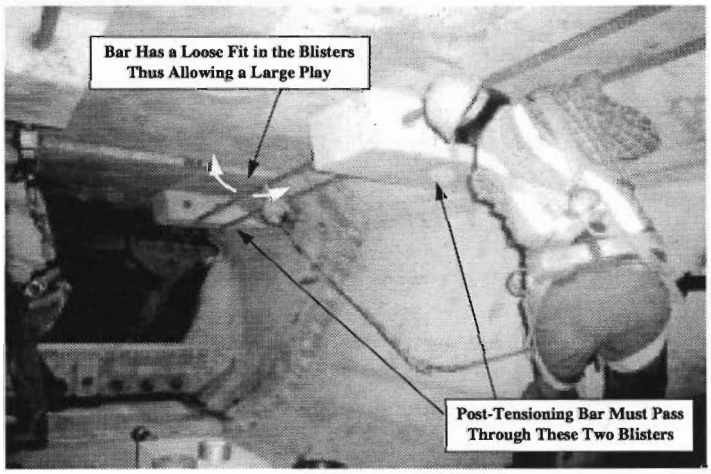

Figure 4.27 Demonstration of the typical temporary post-tensioning process

4.4.3 Transverse Post-Tensioning Duct

During the grouting of one of the transverse post-tensioning ducts in the top flange of the interior anchorage segment for P16, grout leaked out of the duct the concrete and into one of the ducts for a top flange cantilever tendon. The transverse duct passed directly over the longitudinal cantilever duct, and they were probably in contact with each other. Holes must have also been present in each of these ducts where they crossed. The grout had to be removed from the longitudinal duct because the tendon for that duct had not been placed yet, and the grout was creating a clog that would prevent any tendon from being threaded through the duct. The contractor was forced to chisel through the concrete deck to get to this duct and clean it out. Figure 4.28 shows the resulting damage. Many of the transverse prestressing strands in segments P16-1a and P16-2 were damaged during this process.

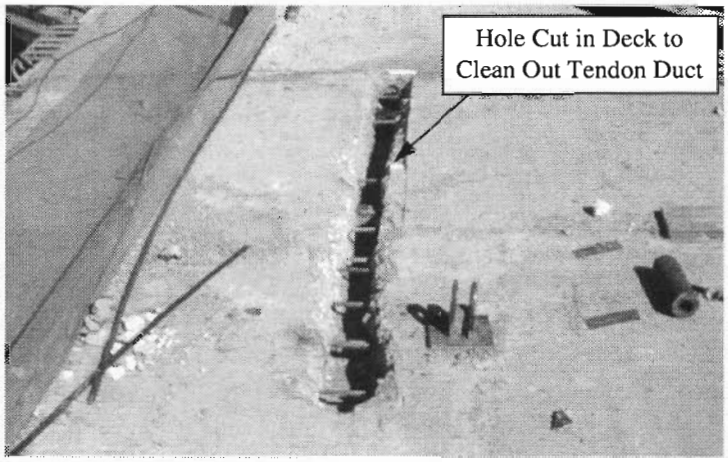

Figure 4.28 Damage done to the top deck because the cantilever tendon duct became obstructed

4.4.4 Squeeze Out of Joint Epoxy

When segment P17-3 was erected (the downstation segment adjacent to the interior anchorage segment on Pier P17), proper squeeze out of the joint epoxy was not achieved in the bottom flange. When two segments are stressed together, the epoxy applied to the faces of the joints should ooze out everywhere around the perimeter of the joint. This is known as squeeze out. Proper placement of the epoxy and a good seal of the joint faces should result in a uniform squeeze out. Squeeze out is checked by inspectors at the site. Epoxy had to be injected into the joint between P17-3 and P17-1 (the interior anchorage segment) to fill the voids between the segments. This error was most likely due to a poor match-casting of these segments during the time of precasting. The match-casting of these segments occurred in the special precasting bed discussed in Section 4.2.2 that had several problems during production.

A proper seal is required between segmental joints for durability of the structure. Voids in the joints could allow the intrusion of water around the internal tendons. Furthermore, voids in the joints could also result in stress concentrations. If a void exists at a joint, the stress will divert to the material around the void. Hardened joint epoxy is stronger than concrete. If a void occurs at a joint and causes overstress, the concrete will fail, not the joint epoxy. This phenomenon was seen in one of the spans of the mainlane construction. Voids present in the bottom flange of one of the joints have been attributed to spalling of concrete in span C47 of the US 183 mainlane.

4.4.5 Mislabeled Segment

During the erection of the P16 cantilever unit, two of the segments were incorrectly labeled. This error was not discovered until the segments were on the crane and epoxy had

already been applied to their faces. The error was discovered because the duct holes in the faces of the two segments did not match up with the duct holes at the ends of the cantilevers. The two segments had simply been switched with each other. Because the epoxy began to harden before the segments could be exchanged, work on the bridge had to cease until the epoxy could be ground off. The delay set back the construction schedule one night.

4.4.6 Alignment of the Cantilevers

When the two cantilevers for the upstation 54.9 m (180 ft) span were finally completed, it was discovered that they did not line up vertically by about 15 cm (6 in.). This flaw was easily corrected by jacking up the girder at Pier P17. Figure 4.29 shows the girder being jacked up off of its temporary bearings with hydraulic rams. The girder was jacked up until the alignment was corrected. In general, vertical and horizontal alignment problems are easily fixed in segmental bridges by jacking up the girder at some pier. Problems with twist can be particularly difficult for the closed cell girders because they are very torsionally stiff, but no problems of that nature occurred in this project.

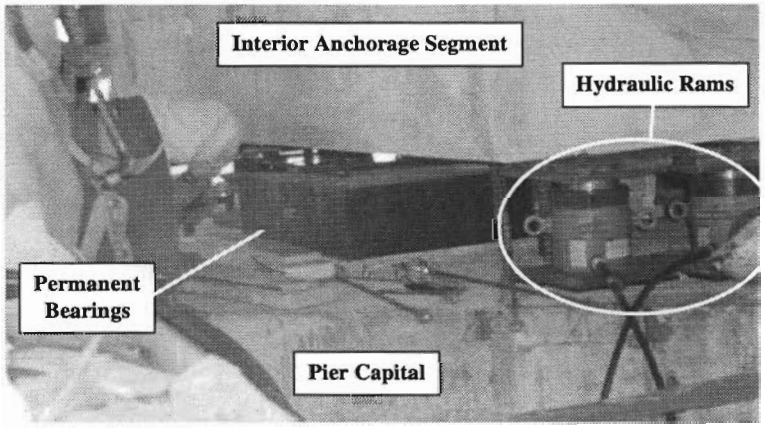

Figure 4.29 Picture of the hydraulic rams used to jack the girders at the bearings

4.4.7 Work Inside of the Girder

Access to the interior of the girder was a continuous problem during the erection of Ramp P. Access openings were located at midspan for each of the spans in the continuous unit. Therefore, the access opening did not become available until erection of the last segment on the cantilever. As a result, the only way to get from the top of the deck to inside the girder as the cantilevers were being erected was by riding in a manlift from the deck to the open end of the box girder. This presented a frustration to the workers during the cantilever stages of the construction because they could not easily move about the bridge to perform the erection tasks.

The poor choice of location for the access openings was also a hindrance during the stressing of the continuity tendons. All of the anchorages for continuity or external tendons

were located towards the ends of the spans in the interior of the box girder. The hydraulic rams necessary for stressing had to be dropped in at the midspan openings and moved to the ends of the girders over the piers. Movement of the rams within the girders was difficult because of the size and weight of the rams and because there were many obstacles that they had to be moved over, such as the deviator beams and the bottom blisters.

Once the ram had been moved through the girder, it was often difficult to get the ram into position against the anchor head. This task generally involved quite a bit of ingenuity on the contractor's part. The contractor was able to get the ram into position by a complicated series of maneuvers involving "come-along" chains (a heavy chain with an attached hand crank for pulling or lifting). Figure 4.30 shows a "come-along" chain being used to maneuver a ram into position against an anchorage blister for a continuity tendon. Foresight on the part of the designer to provide convenient access for stressing equipment would greatly facilitate construction.

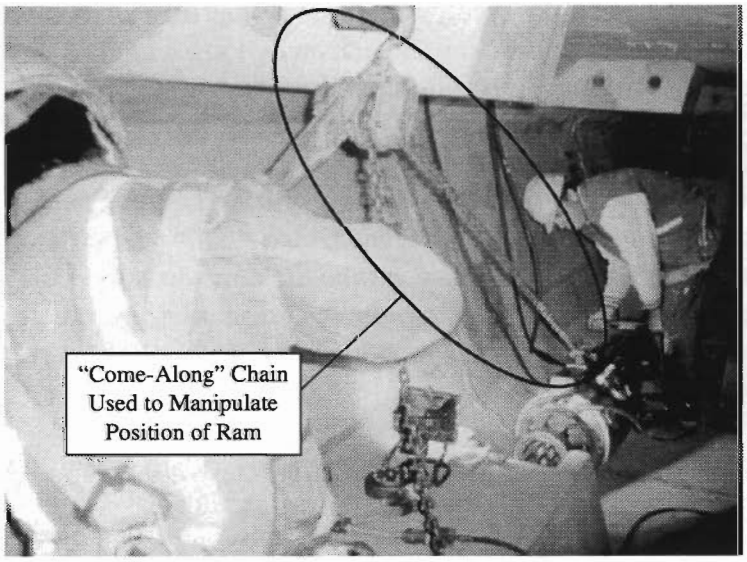

Figure 4.30 Workers manipulate the hydraulic ram inside of the box girder

Lighting was also a problem inside the girder. Much of the time, workers relied on flashlights for internal illumination. A permanent lighting system inside the girder would have made much of the interior work easier. After closure of the cantilevers, quite a bit of work is done inside the girders, including post-tensioning, grouting, and installation of utilities. Furthermore, over the long-term life of the bridge, inspection and maintenance must be performed inside the girder. A permanent lighting system would facilitate the performance of all of these tasks.

Finally, the locations of the drainpipes inside of the girders for both the mainline units and the ramps have proven to be an irritation during the performance of any task inside of the box girder since their installation. The drainpipes were centered across the interior space of the girder cross section. Thus, they occupy much of the space that is available for workers

and inspectors to walk through inside the girders. In the ramps, the space available to pass through the anchorage diaphragms is quite small, and the drainpipes make passage through the ramp girders difficult. Furthermore, access holes in the bottom flanges of all of the girders are also located along the midline of the cross section and the drainpipes prevent complete opening of the hatches of these access holes. A strong cooperative effort should have been made between the structural designers and the designers of the drainage details to prevent this problem. The drainpipes could have easily been located in the corners of the interior cross section, thus, placing them out of the way of individuals who must do work inside the completed bridge.

4.4.8 External Tendons

Failures during Stressing

Three of the twelve external tendons in Ramp P broke during stressing. The reasons for the failures have not been positively identified at the time of this writing, but the most likely reason for the problem stems from the unusually long length of these tendons and their complicated geometry. The longest of these tendons passed through three spans of the ramp and was over 153.1 m (502 ft) in length. This tendon also passed through four saddles and six vertical deviators. During stressing of these tendons (the T3 tendons in Figure 4.23), about 60 cm (2 ft) of slack had to be pulled out of the tendon plus an additional 60 cm (2 ft) of elongation before the final force was reached. Originally, the contractor was not power-seating the wedges into the wedge plate each time the ram was stroked. If the wedges are not power-seated, the strands will slip back into the duct a small amount before the wedges catch and hold the strand. It is likely that the wedges in the anchor head were not seating equally during this process.

The tendons were made up of nineteen Dywidag 15.2 mm (0.6 in.) diameter Grade 270 strands with multiplane anchorages (also from Dywidag). The wedge plate for these tendons is pictured in Figure 4.31. It is likely that the strands passing though the holes on the outside of the plate were slipping further than the strands in the center of the plate before the wedges would seat. This would allow for greater losses on some of the strands. The result would be that the total force in the tendon would not be distributed evenly among the strands. The strands experiencing less slip before the wedges caught would have a greater stress in them. The ram was stroked about eight times before the stressing was completed on these tendons. The cumulative effect of the wedges seating unequally after eight strokes of the ram may have been substantial enough to cause problems.

Post-tensioning of tendons is monitored in two ways: the force in the ram and the elongation of the tendon. The force in the ram is an indicator of the total force in the tendon, but does not tell if that force is distributed evenly among the strands. While the total force in the tendon may have been small, the majority of the force may have been distributed to only a few of the strands in the tendon because of the uneven seating. These strands would be overstressed as the final force for the tendon was approached, causing them to break. If this phenomenon occurred, the elongations would not be equal among all the strands. If the inspector measures the elongation of the tendon by just one strand, this effect would be

missed. Figure 4.31 shows the slip process that may have occurred during the stressing of these tendons. Problems of getting the ram into proper position against the wedge plate (mentioned in Section 4.4.7) probably contributed to this problem as well.

After two tendons had been broken, the contractor began power seating the wedges every time the ram was stroked, but problems still occurred in the longer external tendons. Again, the length of the tendons may have been the problem. When the tendons were placed, the strands within the tendon were not laid out in an orderly manner. The strands crossed over and around each other along the length of the tendon. They had a small amount of tangle. When stressing began, this tangle could have been pulled into a knot near the anchorage. The strands were also being cinched up against the bottom of the duct because the tendon had to pass through a saddle immediately after coming out of the anchor sleeve. This factor could have contributed to the formation of a knot. Such a knot could have resulted in an uneven distribution of force among the strands of the tendon. The same result from uneven seating of the wedges would occur. As the final force in the tendon was being applied, some of the strands would become overstressed and break. Figure 4.32 shows where a knot may have occurred.

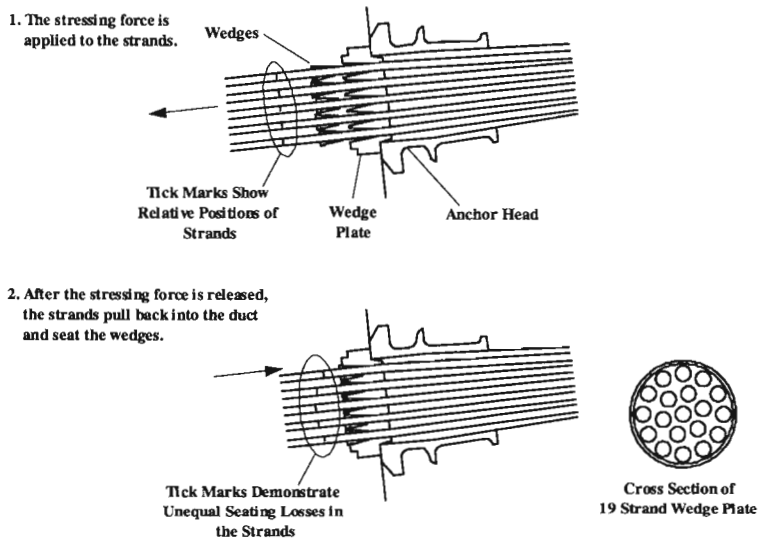

Figure 4.31 Potential unequal seating of the wedges into the wedge plate

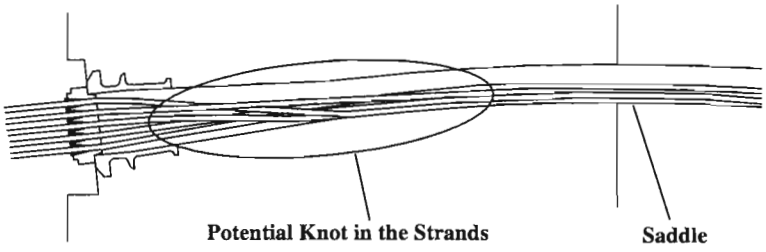

Figure 4.32 Knots may have occurred in the external tendons

A further problem that may have occurred that would have contributed to the failures could have been rubbing of the strands against the edges of the saddle and deviation pipes. These pipes had no trumpets (diabolos) at their ends. Because of this, precise alignment of the pipes is necessary to avoid problems with the tendon rubbing against the edges at the ends of the pipes. High friction losses can occur if the tendon does so. Proper control of the alignment of these pipes is difficult in a short-line casting bed. The horizontal curvature of the bridge probably contributed further to alignment problems. High friction losses caused by the rubbing of the strands against the deviation pipes would have concentrated most of the tendon force near the stressing end. Wear of the strands would also occur where they crossed through the pipes.

Tendons were rejected after two wires had broken. The three failures that occurred were more severe than three broken wires. Typically, several wires ruptured and even an entire strand may have ruptured completely. The breaks occurred just past the wedge plates that might point to knotting of the tendons as the main cause. The problems that occurred probably were not isolated to the three tendons that failed. The tendons currently in the bridge may have some problems with knotting and uneven force distribution across their strands though there have been no indications of broken wires in any of the in-place tendons.

Horizontal Geometry

The horizontal geometry of external tendons in horizontally curved box girders can be difficult to deal with because the tendon follows chords between deviators. Proper visualization of the three-dimensional geometry is important to avoid having the tendon scrape up against the sides of the webs or other components within the box. In Ramp P, the horizontal geometry of the external tendons made the stressing of the outside T3 tendon difficult ("outside" meaning the outside of the bridge's horizontal curve). The ram could barely be fit against the anchor head because it was bumping into an adjacent external tendon that was chording towards the center of the box. Proper allowance for the size of the ram had not been met because the horizontal geometry of the external tendons and the size of the ram with dial gauge and hose attachments were not properly visualized. Further evidence that the horizontal geometry of the external tendons was not fully visualized came from the temporary post-tensioning blisters in the bottom of the girder. The innermost external tendon on the outside of the bridge curve routinely bumped up against the bottom blisters in Ramp P, as shown in Figure 4.33. Possible problems with misalignment of the deviation and saddle pipes were already discussed in the previous section but would also be relevant to this topic.

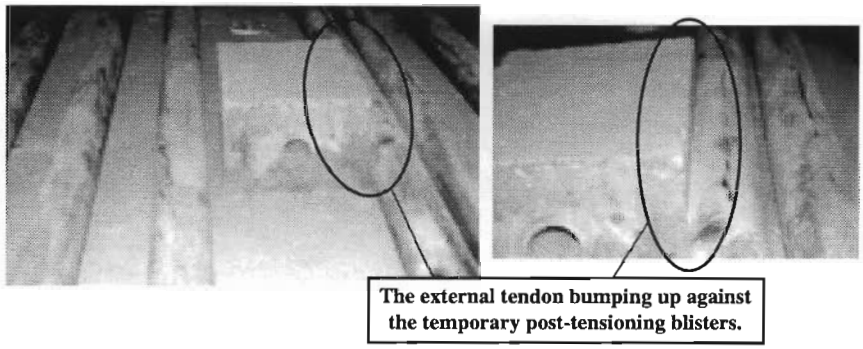

Figure 4.33 ***Horizontal alignment problems with the external tendons***

Grouting

Grouting of the external tendons proved to be difficult because of the long lengths of the ducts. The crew in charge of grouting found it difficult to eliminate voids in the duct. Very often, the workers had to punch holes in the duct to create vents to remove air pockets. External tendons have a great advantage over internal tendons in terms of grouting because voids can easily be detected by tapping against the side of the duct. The worker simply listens for a hollow sound to indicate an air pocket. The problem with the external tendons in Ramp P was their length. Over such long lengths, it becomes more difficult to maintain a uniform grout pressure that will push air bubbles out the vents. Often the grout in the ducts had to be compressed several times that inevitably lead to leaks occurring at the connections between the polyethylene pipe and the steel deviation or saddle pipes.

4.4.9 Temporary Grout Bearings

The original construction plan for Ramp P called for temporary bearings made of reinforced grout to be cast underneath the interior anchorage segments of the ramp. The contractor found these bearings difficult to remove (they had to be chipped out) when it was time to install the permanent bearings. Shortly into construction of the ramp, plastic bearings were allowed instead so that this problem could be eliminated.

4.4.10 Uplift of Superstructure off of Bearings

As of this writing, the Ramp P superstructure has partially lifted off of one neoprene bearing at Pier P18. There is about a 2 mm ($^{1}/_{16}$ in.) gap over one third of the area between the top of the neoprene and the mortar plinth on the bearing located on the outside of the superstructure's horizontal curve. Similar problems have also occurred on the curved spans constructed by the span-by-span method. The problem has not been diagnosed as of this time, but could be attributable to torsion created in the structure by the external tendons. Before the external tendons were stressed, the problem had not occurred. It was first noticed after the stressing of the external tendons. Figure 4.34 shows several views of the problematic bearing.

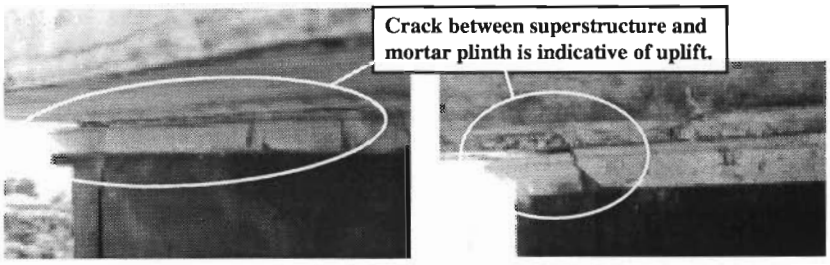

Frontal View (looking upstation)

Side View (looking towards the ouside of the horizontal curve)

Figure 4.34 Uplift off of one of the P18 bearing pads

4.5 Conclusions and Recommendations

The problems described in Section 4.4 can be divided into three categories: design related, construction related, and inspection related.

4.5.1 Design Issues

The problems that were considered pertinent to design topics included the unusually long lengths of the external tendons and the resulting stressing problems, specifications on temporary components such as the grout bearings, the working space inside the girder, access to the inside of the girder, space for placement of rams at anchorage areas, and the uplift of the superstructure from the bearing pad. Also mentioned is the correction to the alignment between the P16 and P17 cantilevers.

Conclusions

The poor positioning of the access holes at midspan, the inadequate space left for the stressing rams, and the overall difficulties presented by the working area inside the girder reflect a lack of sensitivity in the design and working drawing stages to the details of the construction process. Consideration of these details is important because they affect the workers' abilities to perform the required tasks of the construction process. Poor details will result in a slower construction pace and a decline in quality of the final product. The economy of the structure is affected on a short-term basis because of the slowed construction rate, and there is a danger of long-term durability or aesthetic problems because the quality of the structure may be impaired by a lower caliber of workmanship.

Special consideration was necessary for the external tendons because of their long length. Failures probably occurred because of a combination of several factors. The wedges were not power seated every time the ram was stroked leading to unequal seating of the

wedges and a nonuniform distribution of stress among the strands of the tendons. The long lengths of the tendons required over a meter of length to be stroked before the final force in a tendon was reached. This may have led to the formation of a knot in the strands between the anchorage and the nearby saddle. Friction loss measurements indicate that the strands of the tendon were most likely rubbing against the edges of the deviation and saddle pipes leading to excessive stresses in the strands. Difficulty in placing the ram against the wedge plate inside the girder probably contributed as well. Difficulty was also encountered in grouting the tendons because of the long length of duct and the multiple vertical rises the tendons passed through.

There are problems with uplift of the superstructure off of the bearing pads. This could be a torsional effect related to the horizontal curve of the superstructure and the prestress forces from the external tendons through this curve.

The ability of the contractor to correct vertical and horizontal alignment problems between cantilevers by adjusting the bearing plinths at the piers demonstrates an adaptability of the balanced cantilever system that is useful for construction. The more adaptable the system is to quick changes, the less bound the designer and constructor are to uncertain variables during the planning stages. Adaptability of the details to change can greatly facilitate construction.

Recommendations

Though the contractor and construction engineer will ultimately make the decisions on the details of the construction scheme, the designer's investigation of a potential construction scheme should encompass all of the details of the process. Crucial to this thought process should be a sensitivity for what workers need to do for a specific task, where they have to be, what tools and materials they will have to manipulate, and under what environmental pressures. On-site inspectors suggested that an interior lighting system would have facilitated construction tasks inside the girder and would be useful for long-term inspection and maintenance. Interior lighting has been a specified detail for many box-girder bridges. The location of drainage details or utility pipes should not be ignored by the structural designer. Space should be allocated for these details so that their final placement does not impede long-term inspection and maintenance tasks that have to be performed inside the box girder. Generous space should be allowed for hydraulic rams used for post-tensioning near the anchorages and in areas where the rams will have to be moved. Allowances should be made for dial pressure gauges and hydraulic hoses attached to the ram. Consideration of the three-dimensional geometry of the girder is important. The manipulation of these rams is often quite difficult because of their size and weight. The ram does not just have to fit next to the anchorage, it has to be transported to that location and supported in place. Ideally, detailed records of the methods used by contractors to perform post-tensioning and erection tasks on projects should be kept and made available for subsequent projects. Thus, a database could be established and referred to for design decisions and to make recommendations when problems are perceived by inspectors at job

sites. Inspector diaries and videotapes of construction details would be the principal means to this end.

The length of tendon next to the live end anchorage of long post-tensioning tendons should be left straight and free of deviation saddles. This will allow twist in the strands to disburse away from the anchorage over a greater length of tendon so that the twist will not concentrate into a knot. Deviation pipes for external tendons should have trumpeted ends (diabolos ends) to prevent rubbing of the strands against the edges of the pipe. On-site inspectors should measure tendon elongations across several strands protruding from the back end of the ram to verify that all strands elongate the same amount. Inspectors should also require power seating of the wedges every time the ram is stroked, especially for long tendons that require many strokes of the ram to reach the design force. This requirement should be part of the project documents.

Currently nothing can be recommended concerning the uplift of the superstructure off of the bearing pad until the problem is further observed and analyzed. Most likely, the solution lies in a better understanding of the effects of external tendons on horizontally curved bridges.

4.5.2 Construction Issues

Construction problems that have been classified as issues for the construction engineer include the difficulties in the erection of the two halves of the interior anchorage segment and the first two cantilevered segments. Details of the temporary post-tensioning blisters that were designed by the contractor are also discussed under this heading.

Conclusions

The problems that occurred in the erection of the interior anchorage segment and the first two cantilevered segments are the result of lax construction engineering. Similarly, the placement of the bottom flange temporary post-tensioning blisters so that they conflicted with the alignment of the external tendons demonstrates an insufficient visualization of the three-dimensional geometry of the bridge by the contractor.

Recommendations

The contractor had the space and time at the precasting yard to perform a trial, dry fit erection of some of the Ramp P segments and should have done so. This would have immediately made apparent any potential problems in the proposed scheme for the balanced cantilever erection. Opportunities to test proposed erection schemes in controlled situations should not be bypassed. The misfortune of discovering flaws in the system when a segment is hanging from a crane at the site can be costly. This type of a test would have demonstrated the problems involved in placing the two halves of the interior anchorage segment and bringing them together in proper alignment on top of the pier capital. A dry fit erection test also presents an opportunity to test the match cast of selected segments. Such dry fit trials should be required for unusual operations.

Erection schemes for segments should include consideration of measures to adjust and correct the alignment of the segments. The erection scheme for the two halves of the interior anchorage segment did not properly meet such a goal.

Temporary post-tensioning details using threaded bars for prestress should permit as much free movement of the bar as possible. They should also allow easy access to coupler and anchorage components. Two alternatives to the method used to erect the first two cantilever segments are suggested here. Additional ducts could have been placed in the segments just for the temporary prestress. Thus, the bars would not have had to be removed after their use in the temporary stressing. Possibly a better suggestion would be to use components that are temporarily attached to the top of the segments that act as blisters for post-tensioning bars. Such a detail was used in the mainlane erection and is pictured in Figure 4.35. Steel blisters were temporarily fitted onto the deck surface of the mainlane segments and post-tensioning bars were threaded through them. It is unknown why such a detail was not used on Ramp P, but the system would have removed much of the erection work from the cramped inside of the girder and put it up onto the deck where plenty of room existed for the workers to perform their tasks.

Contractor proposals for structural details should include structural drawings that fully demonstrate that no conflicts exist with the other components of the bridge structure. Particular attention should be given to the three-dimensional geometry of the bridge. For example, plan sheets for the temporary post-tensioning blisters should have been drawn showing the horizontal curvature of the bridge and the locations of the external tendons in relation to the bottom flange blisters. This would have prevented the conflict that occurred between these two bridge components. Sheets that demonstrated the specific details of the proposed erection procedure would also help to delineate flaws in the idealization.

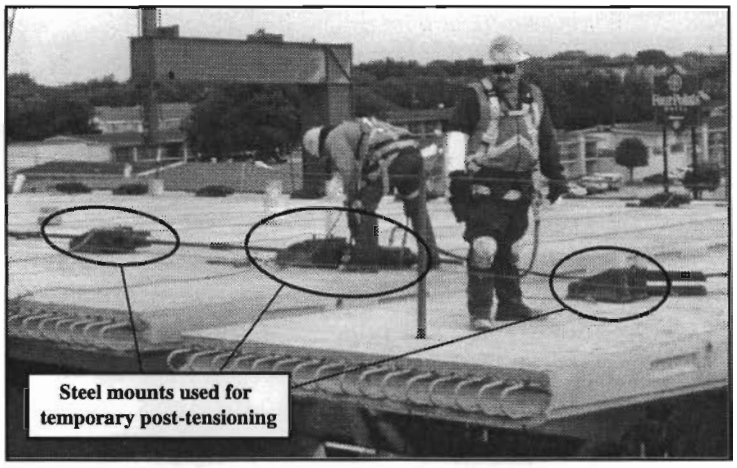

Figure 4.35 Alternative detail for temporary post-tensioning

4.5.3 Inspection Issues

The on-site inspector should thwart construction problems as they occur at the precasting yard. The mislabeling of the two segments and the grouting problem that occurred with the transverse post-tensioning duct is an example of such problems. Comprehensive quality assurance procedures coupled with thorough inspection at the time of erection can prevent long-term problems with structural performance.

Conclusions

Labeling of bridge segments at the US 183 precasting yard was performed by the contractor. It is unknown if an independent check procedure was used by the contractor's staff. Inspectors periodically walked through the storage area and looked over the segments for voids or other surface flaws. It is uncertain if the labeling of the segments was checked at such time.

The grouting problem that occurred with the transverse post-tensioning duct must have been the result of direct contact between the transverse duct and the longitudinal cantilever tendon duct and the presence of holes in these ducts at that junction. The quality assurance personnel could have noticed breaches in the surfaces of the ducts and directed them to be patched with caulk. Post-tensioning ducts should have sound surfaces free of dents or holes so that tendons can pass through them unimpeded once the concrete is cast and set. Pipes were placed through the ducts at the time of casting to help to strengthen the duct against damage when the concrete was placed for the precasting of the segments. These pipes prevent the ducts from becoming bent or from collapsing, but small damage can still be done to the surface of the duct especially by the concrete vibrator.

The poor squeeze out from the joint between P17-3 and P17-1b originated from actions at the precast site. Fortunately, the inspector present at the time of the erection of P17-3 paid careful attention to such details and recommended injection of epoxy into the joint.

Recommendations

Quality assurance personnel can easily verify segment labels prior to transport to the site by checking the details of post-tensioning duct locations or special features such as anchorage blisters or deviator beams. Construction and inspection records should be logged verifying the quality and identity of the segment prior to transport to the construction site.

Verification of the integrity of post-tensioning ducts should be a priority task before casting of the segment because correction of flaws after placement of the concrete can be difficult. Primarily, the presence of stiffening pipes in the ducts should be confirmed.

Full attention should be given to epoxy squeeze out between joints during erection. The cross section of the box girder should be as homogeneous as possible for complete and uniform transfer of stress, as well as integrity against environmental forces.

CHAPTER 5. CONSTRUCTION SEQUENCE DATA

5.1 Diffusion of Post-Tensioning

5.1.1 Temporary Post-Tensioning

Data demonstrating the diffusion of post-tensioning forces directly behind the anchorage zones was collected from the concrete gauges in segment P16-10 at the time the segment was erected. Figure 5.1 shows the stresses from the temporary post-tensioning bars and the dead load of the segment. These stresses are plotted next to the compressive stress required by the Proposed *AASHTO LRFD Segmental Guide Specifications* (17) during curing of the joint epoxy, 0.28 MPa (0.040 ksi). The plot of the measured stresses shows a very nonuniform distribution both horizontally and vertically. Horizontally, the stresses were particularly low near the wing tips of the top flange where the minimum compressive stress was not attained. This may be due to poor diffusion of the temporary post-tensioning force out to those portions of the cross section. Vertically, all sections along the webs had at least the required contact pressure. Additional fluctuations in the stress plot could be due to debris on the joint faces or problems with the match cast fit. Differential shrinkage in the segment or thermal effects during the curing process could have warped the segment face. It should be recalled that the gauges were placed 46 cm (18 in.) from the joint face. No problems were observed with the squeeze out of the joint epoxy between P16-10 and P16-8.

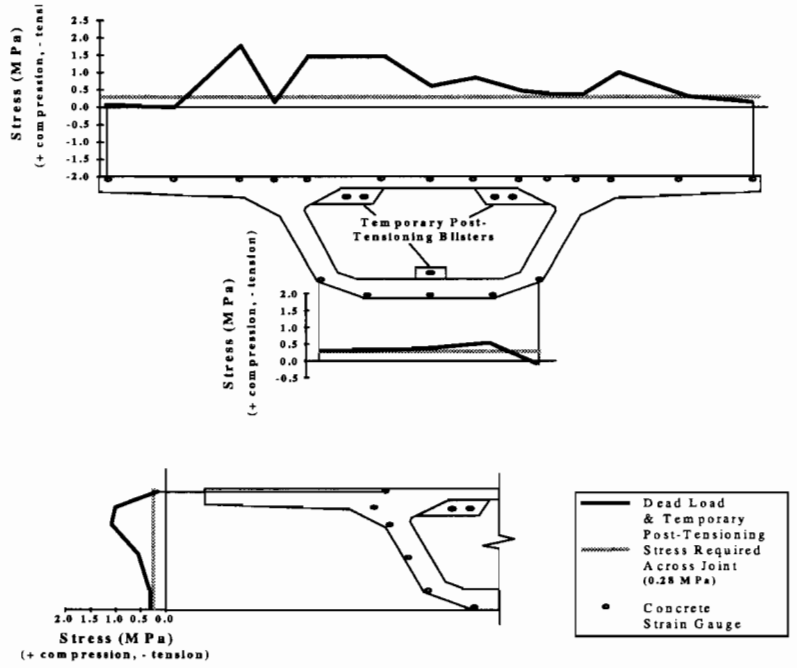

Figure 5.1 Diffusion of force from temporary post-tensioning in P16-10

5.1.2 Cantilever Post-Tensioning

The distribution of stress from the post-tensioning of cantilever tendon T205 in P16-10 was calculated in two ways: using the effective flange width method from Section 4.6.4.6.2 of the *AASHTO LRFD Bridge Design Specifications* (2) and using the full section properties under simple beam theory assumptions. These calculations are given in Appendix B (22). Directions in the commentary of the AASHTO code for the application of the specified effective flange method for normal forces are rather vague (see Section 2.3.3 of Chapter 2). Lines at 30° angles from the line of action of the concentrated forces are used to distinguish the limits of the effective flange width. However, Figure 4.6.4.6.2-4 in the AASHTO code does not clearly indicate that these lines should originate from the location of the concentrated normal load. In fact, the figure can easily be interpreted to show that the 30° lines originate from the edges of the webs. Also the AASHTO specifications do not clearly indicate how the horizontal prestressing loads distribute vertically through the webs and into the flanges. There are two considerations in this distribution. Application of strut-and-tie modeling shows the compressive force to spread into the webs and lower flanges following the 30° inclination from the tendon axis. However, this neglects the compatibility-induced zone of tension along the back face and bottom of the flange along the inclined compressive force distribution. Furthermore, if the loads are applied at the level of the top flange, how should the bottom flange be affected?

Figures 5.2 and 5.3 show how the AASHTO specifications were applied to the effective flange method calculation for this problem. The 30° lines were drawn so that they originated at the center of the applied concentrated loads. Figure 5.2 shows the dimensions of the effective flange widths. Because the compatibility requirements near the vertical edge and in the beginning portions of the bottom flange cannot be ignored in reality (even though they are ignored in strut-and-tie modeling), the area shown lightly shaded in the side view of Figure 5.2 was included in the calculation of stresses from post-tensioning. This is necessary as shown in the recommendations for post- tensioned anchorage zones discussed in Section 5.10.9.4 of the *AASHTO LRFD Bridge Design Specifications* (2) when treating edge tensile forces and spalling forces. This is accomplished by using normal and flexural actions (i.e. $P/A \pm Mc/I$) for these regions. Thus, no reduction of the bottom flange was made as is shown by the shaded area of the cross section in Figure 5.3. The distribution of measured stresses across the bottom of the cross section indicates full action of the bottom flange.

Measured stresses are presented for each of the two tendons (the right and left sides) as well as the sum of the two tendons. The right-side tendon was stressed first. There is a noticeable difference between the stress distribution caused by the left tendon when compared to the stress distribution caused by the right tendon. This should not be caused by the curvature of the cantilever because no actual horizontal curvature occurs over the length of one segment. The segments themselves have a trapezoidal shape, and the horizontal curvature of the bridge is accomplished by the angle breaks at the segmental joints. The cause of the difference is unknown.

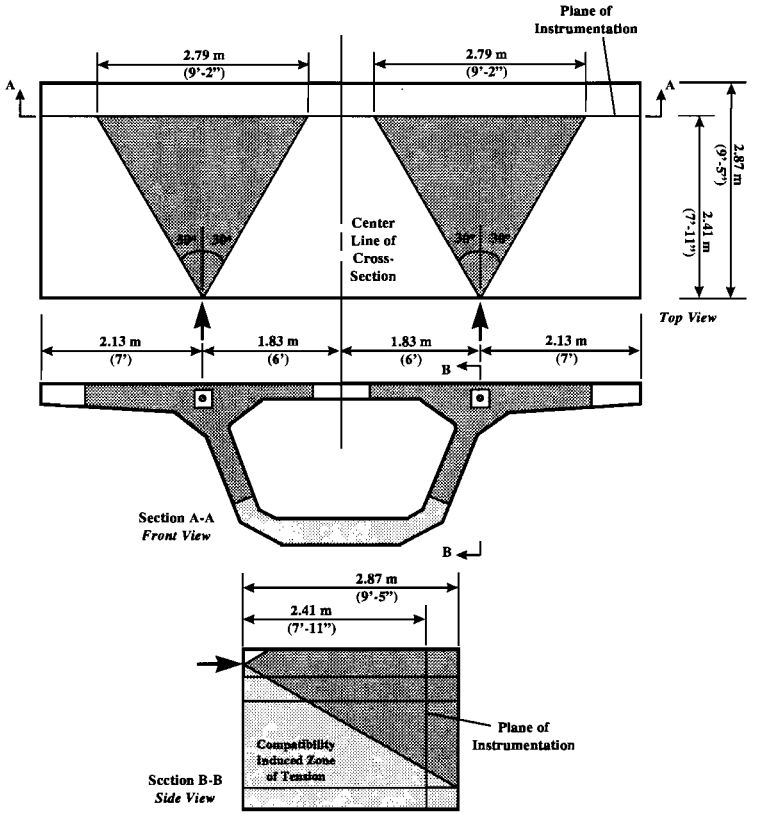

Figure 5.2 Effective area for calculation of stresses from cantilever post-tensioning

Along the vertical stress distribution shown in the lower part of Figure 5.3, it can be seen that the AASHTO method, which assumes plane sections will remain plane, failed to predict the actual shape of the stress distribution, though it did predict the top and bottom stresses fairly well. The effective flange width method specified by AASHTO may have been developed for correct prediction of stress at extreme fibers where most service level design is concerned. Horizontally, it appears that the beam theory calculation predicted the maximum stress better than the AASHTO method. However, the measured stresses might be too low because of potential error in the measured modulus of elasticity that was used to transform the strain gauge data to stress values as was discussed in Section 3.7.1 of Chapter 3. It should also be obvious that the AASHTO method is predicting the shape of the stress distribution better than the beam theory. The AASHTO method correctly predicted the drop in stress in the center of the top flange as well as the drops near the wing tips. Overall, the AASHTO method seems to work reasonably well. Table 5.1 compares predicted stresses from the AASHTO and beam theory methods with the measured values. Ratios of the measured stress to the calculated stress presented in the table that are greater than 1 indicate unconservative results.

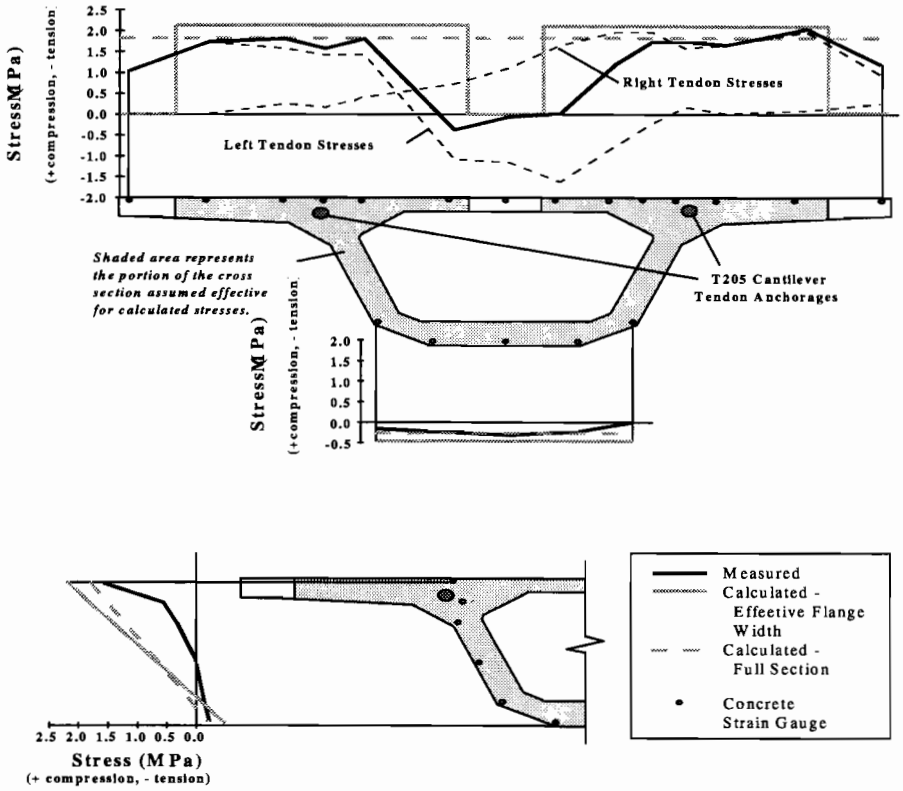

Figure 5.3 ***Diffusion of post-tensioning force from the cantilever tendons in P16-10***

Table 5.1 ***Comparison of measured and calculated stresses from diffusion of post-tensioning***

	Maximum Top Flange Compression (MPa)	Maximum Bottom Flange Tension (MPa)
Measured	2.01	0.31
AASHTO Effective Flange Width	2.21	0.45
Measured/Calculated	*0.910*	*0.689*
Full Section Properties	1.84	0.35
Measured/Calculated	*1.092*	*0.886*

Transverse stresses were also measured during the stressing of the cantilever tendons anchored in P16-10. These stresses are presented in Figure 5.4. When only the right-side tendon was stressed, some moment was present in the top flange that could be the result of warping. These stresses are very small however, and are only present in the structure for a small period of time. They pose no need for concern. After both sides were stressed, the transverse stresses were reduced to insignificant magnitudes.

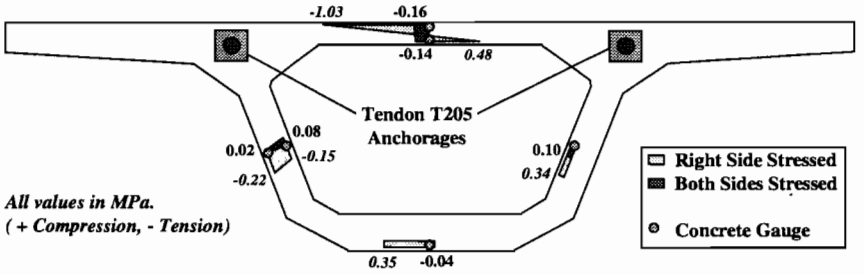

Figure 5.4 Transverse stresses from the stressing of the cantilever tendons in P16-10

5.2 Stresses During Cantilever Construction

The cantilever construction events for which data is presented in this section occurred during Phases II, V, and VI of the Ramp P construction process. Figure 5.5 shows the layout of the segments and cantilever tendons for the P16 upstation cantilever. Recording of the data from the Ramp P superstructure began just after P16-2 was temporarily post-tensioned to the P16 interior anchorage segment. The locations of the instrumentation and the construction process are discussed in greater detail in Chapters 3 and 4 respectively.

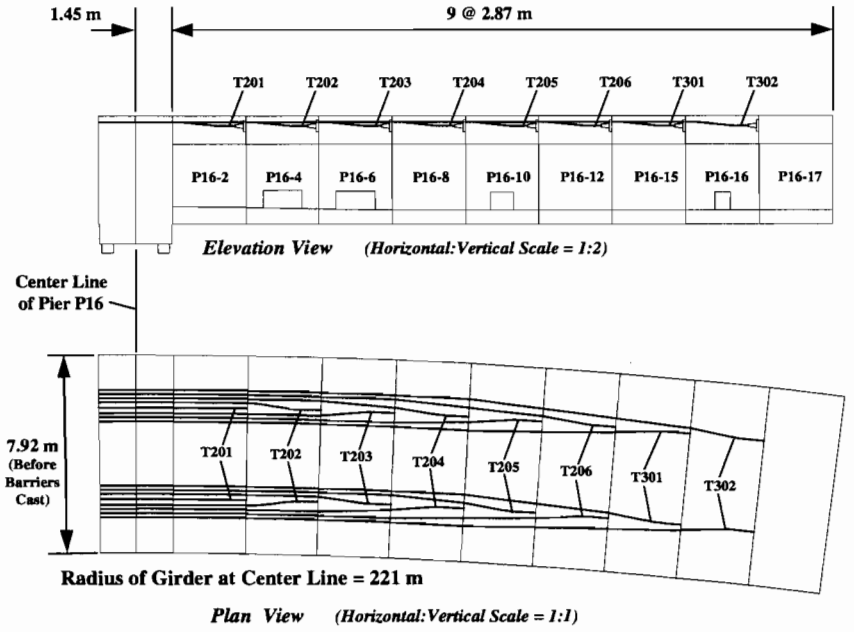

Figure 5.5 Layout of segments and cantilever tendons in the P16 upstation cantilever

5.2.1 Longitudinal Stresses

Measured and calculated longitudinal stresses for P16-2 after completion of the P16 cantilever are presented in Figure 5.6. The calculations were performed with the aid of a computer spreadsheet. Moments, torques, and shears were calculated at each joint face using the curved girder relations given in Equations 2-10 through 2-12 of Chapter 2 and assuming no forces occur at the free end of the cantilever. These calculations are given in Appendix B (22).

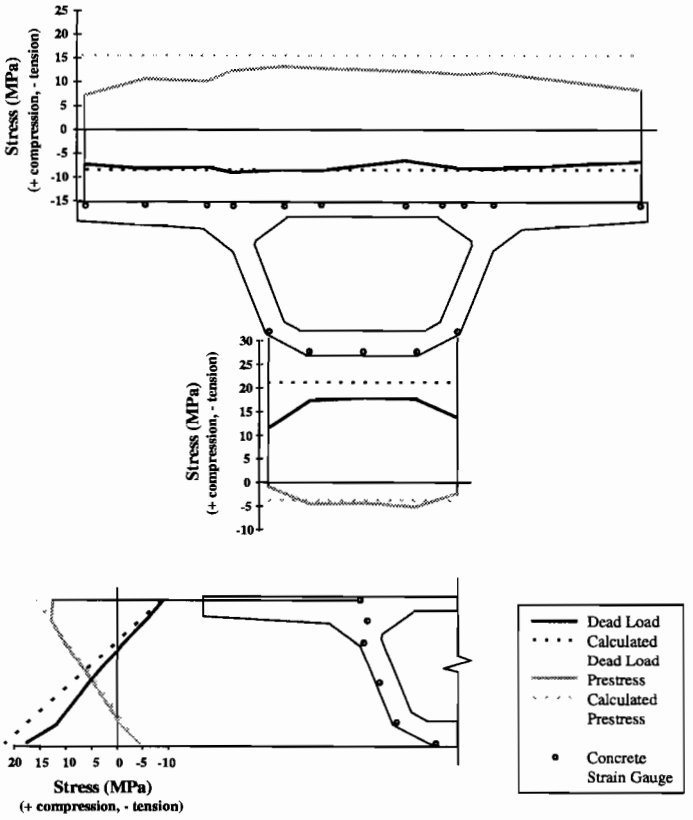

Figure 5.6 Measured and calculated longitudinal stresses in P16-2 after completion of the P16 cantilever

The measured plots indicate fairly smooth distributions of stress from dead load. According to Section 4.6.2.6.2 of the *AASHTO LRFD Bridge Design Specifications* (2), no shear lag was expected in the Ramp P cross section under the actions of loads applied on the full cantilever length. Furthermore, the P16 anchorage diaphragm that is in proximity to the plane of gauges in P16-2 should provide restraint against shear lag deformations. The calculated post-tensioning stresses agree well with most of the measured data except at the top of the cross section. The calculated dead load stresses agree very well with the measured

stresses at the top of the cross section, but deviate increasingly from the measured values as one looks down the vertical height of the web. The agreement between calculated and measured dead load stresses at the bottom of the cross section was very poor. It appears as if the neutral axis from the measured stresses is slightly lower than that calculated for the section. The properties of the concrete probably vary somewhat through the section because of the multiple batches of concrete required to cast a segment (see Section 4.2.1 of Chapter 4). Changes in the modulus of the concrete through the depth of the section could affect the location of the neutral axis. It is possible that the assumed weight of the concrete used in the calculations was higher than the actual weight. The difference in the vertical slopes of the calculated and measured slopes of the dead load stresses indicates that a lower moment than the calculated one is causing the measured stresses. Possibly, a combination of a downward shift in the neutral axis and a lower applied dead load moment account for the good agreement between the calculated and measured dead load stresses at the top of the cross section and the bad agreement at the bottom of the cross section. Average measured stresses through the top and bottom lines of concrete gauges are compared in P16-2 to calculated stresses in Table 5.2.

Table 5.2 Comparison of measured and calculated longitudinal stresses in P16-2 after completion of the P16 cantilever

	Cantilever Dead Load			Cantilever Post-Tensioning		
P16-2	**Average of Measured (MPa)**	**Calculated (MPa)**	**Measured / Calculated**	**Average of Measured (MPa)**	**Calculated (MPa)**	**Measured / Calculated**
Top	-7.84	-7.86	0.997	11.03	15.30	0.721
Bottom	17.64	20.97	0.841	-4.54	-3.92	1.158

Three concrete gauges were chosen out of the P16-2 cross section that were deemed to represent the behavior of the section fairly well: C604 (at the top of the left web), C607 (near the middle of the top flange), and C638 (at the bottom of the left web). Cumulative stresses in these gauges are plotted for the different stages of the cantilever construction process in 5.7. The trends of these gauges show that the dead load moment at P16-2 did not begin to exceed the post-tensioning moment until segment P16-15 was erected. This is indicated when the compressive stress in the bottom flange (gauge C638) becomes larger than the compressive stress in the top flange (gauges C604 and C607).

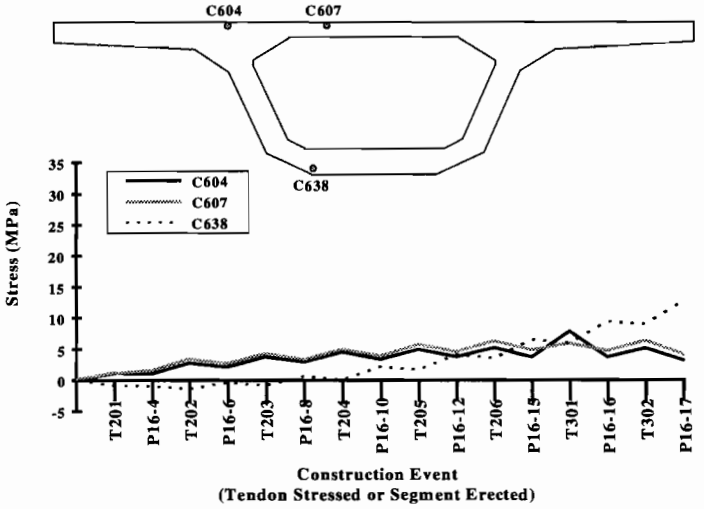

Figure 5.7 Stresses in selected concrete gauges from P16-2 over the course of the cantilever construction sequence

5.2.2 Shear Stresses

The calculations performed to determine longitudinal stresses in the P16 upstation cantilever also accounted for the torsion from the horizontal curvature of the ramp. Theoretical shear stresses in the webs and top and bottom flanges of the cross section were calculated and are plotted next to measured stresses in Figure 5.8. The calculated vertical shear stress did not compare at all well to the measured stresses. The proximity of this section of gauges to the support bearings and anchorage diaphragm may have affected the shear stress distribution at that location. Theoretically, no torsional or vertical shear stresses should have been produced by the internal post-tensioning in the cantilever. Only very low stresses were measured from the cantilever post-tensioning.

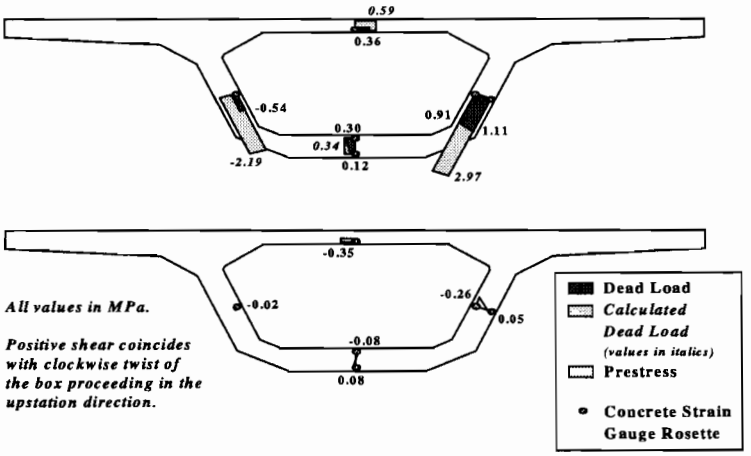

Figure 5.8 Measured and calculated shear stresses in P16-2 after completion of the cantilever

5.3 *Stresses During Continuity Post-Tensioning*

The stressing of the tendons for which data is presented in this section occurred during Phases VI and VII of the Ramp P construction process. Figure 5.9 shows the layout of the segments and continuity tendons for the downstation half of span P16.

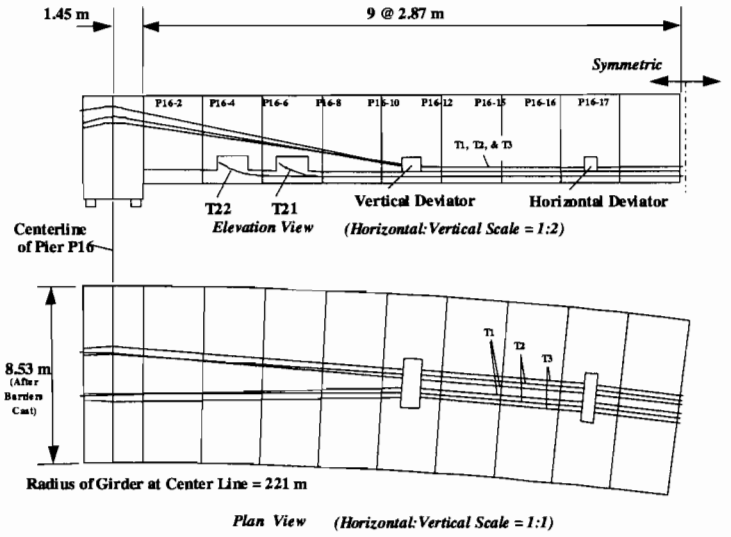

Figure 5.9 Layout of internal and external continuity tendons in span P16

5.3.1 *Longitudinal Stresses*

Longitudinal Stresses from the post-tensioning of the internal and external continuity tendons (T21, T22, T1, T2, and T3) are presented in Figures 5.10 through 5.12. Theoretical stresses were calculated using a two-dimensional frame solver, RISA2D (Rapid Interactive Structural Analysis 2-Dimensional) (18). Details of the calculation model are given in Appendix A (22). Equivalent loads were placed on the structure to simulate the post-tensioning. Friction losses across deviators were estimated for the external tendons based on Equation 5.9.5.2.2b-1 of Section 5.9.5.2.2 of the *AASHTO LRFD Bridge Design Specifications* (2): where f_{p2}/f_{p1} is the ratio of tendon force from the dead end to the live end of the deviator, μ is the coefficient of friction (0.25 radians^{-1}), and α is the angle break in radians across the deviator (0.04 radians or 0.08 radians were added to the angle breaks across the deviators and saddles, respectively, as an allowance for misalignment of the metal ducts). All other losses such as elastic shortening were ignored to simplify the analysis. These calculations are given in Appendix B (22).

The total stress presented in Figures 5.10 through 5.12 comes from all of the measured events in the construction sequence (erection of segments P16-4 through P16-17, the stressing of cantilever tendons T201 through T302, and the stressing of the continuity tendons T21, T22, T1, T2, and T3 in span P16). The total stresses do not include any creep

redistribution of dead load or thermal effects. The figures indicate that there was less moment at all of the sections than anticipated by the calculations. This is demonstrated by comparing the slope of the measured stresses through the web with the calculated stresses. The stress in P16-2 tends to drop off near the wing tips of the section. A slight reduction in the top flange width was required by Section 4.6.2.6.2 of the *AASHTO LRFD Bridge Design Specifications* (2) for P16-2 under the fully continuous structural configuration. Approximately 30 cm (1 ft) was removed on each wing tip of the cross section at P16-2. The reduction in the flange width made very little difference in the calculated location of the neutral axis or the moment of inertia for that section. Thus, the magnitudes of the calculated stresses were affected very little compared to a full section calculation, but the shape of the calculated top flange stress distribution was changed in such a way that it fit the shape of the measured top flange stress distribution better than a full section calculation would have. The effective flange specifications appear to have worked well. The large peak that occurs in the measured stresses over the right web of P16-10 is probably due to a local compressive strut in the concrete emanating from the vertical deviator beam.

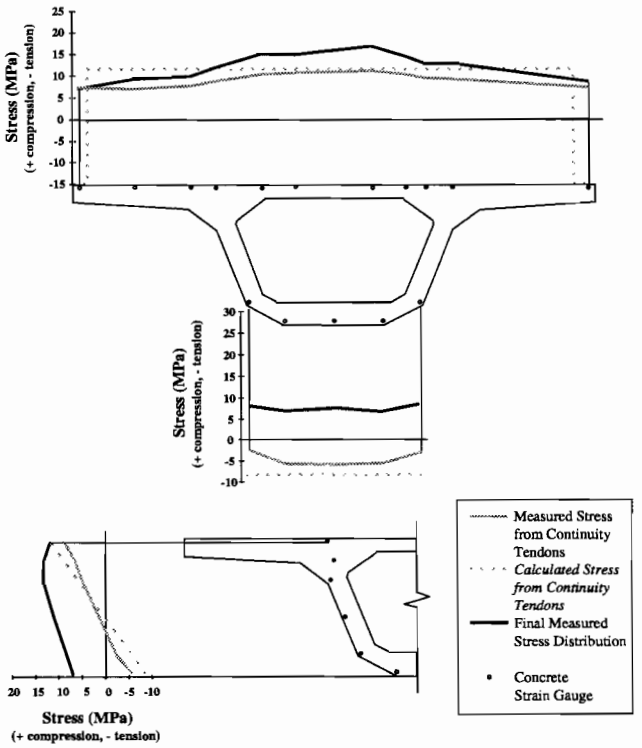

Figure 5.10 Measured and calculated stresses in P16-2 after stressing of the continuity tendons in Span P16

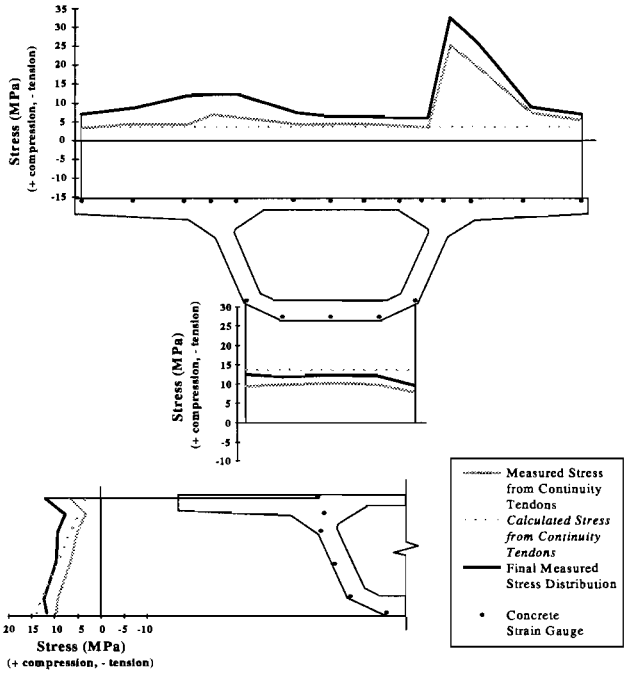

Figure 5.11 Measured and calculated stresses in P16-10 after stressing of the continuity tendons in Span P16

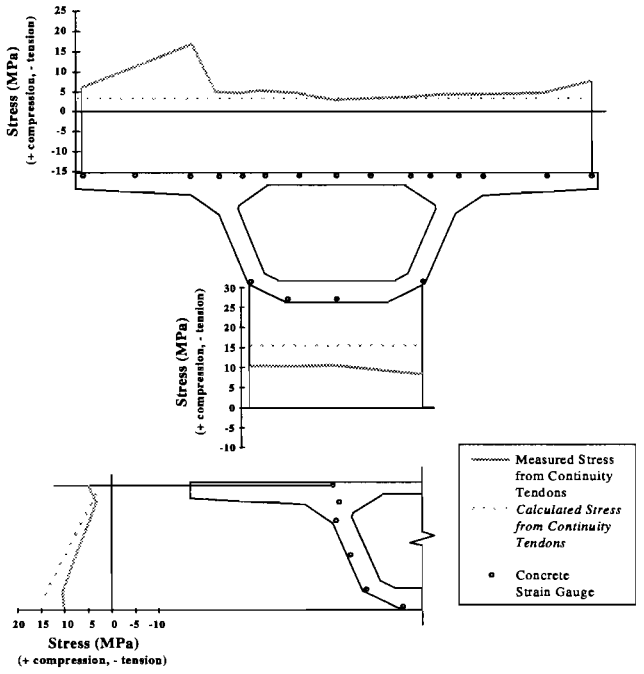

Figure 5.12 Measured and calculated stresses in P16-17 after stressing of the continuity tendons in P16-17

The averages of the measured stresses from the continuity stressing are compared to calculated values in Table 5.3. The most likely reason for the large differences between the measured and calculated stresses is that the true bearing and fixity conditions present between the piers and the superstructure were not represented in the calculation model that assumed either fixed or pinned connections.

Table 5.3 ***Comparison of measured and calculated stresses from the stressing of the continuity tendons in Span P16***

	Stressing of Continuity Tendons		
	Average of Measured (MPa)	**Calculated (MPa)**	**Measured / Calculated**
P16-2			
Top	8.97	11.65	0.770
Bottom	-5.75	-8.25	0.697
P16-10			
Top	7.09	3.61	1.964
Bottom	9.94	13.92	0.714
P16-17			
Top	6.22	2.93	2.123
Bottom	10.45	15.25	0.685

Cumulative stresses from selected gauges in each of the three instrumented segments during the continuity stressing operations are plotted in Figures 5.13 through 5.15. These plots demonstrate the changes that occur in the moment diagram during the continuity stressing process. Reversal of moment occurs in P16-2 as is indicated by the bottom flange stress becoming less than the top flange stresses (a switch from negative to positive moment). The opposite switch begins to occur in P16-2, but not quite as much because this section of gauges must be close to the inflection point of the moment diagram. No reversal of moment occurs in P16-17. The stresses start out at zero and a negative moment is applied to the section from the continuity tendons. The sharp but steady rise in stress measured by gauge C717 in P16-10 indicates that almost all of the continuity tendons are contributing to the sharp peak that occurs in the stress diagram over the right web of that segment.

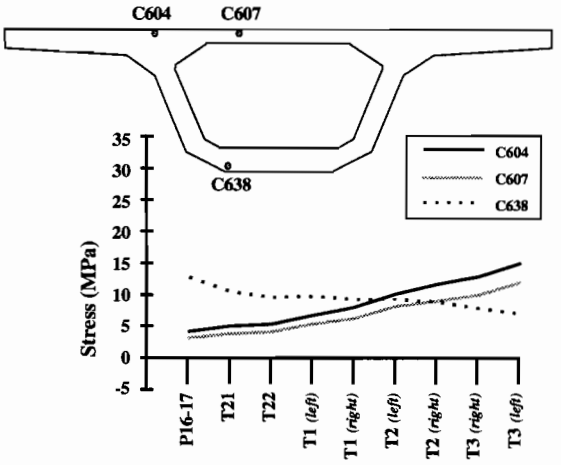

Figure 5.13 Stresses in selected concrete gauges from P16-2 over the course of the continuity stressing sequence

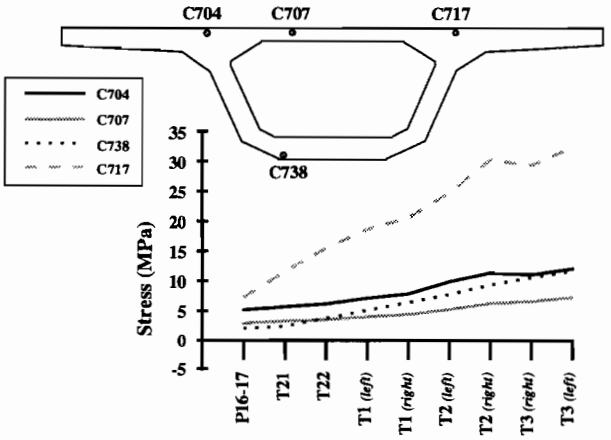

Figure 5.14 Stresses in selected concrete gauges from P16-10 over the course of the continuity stressing sequence

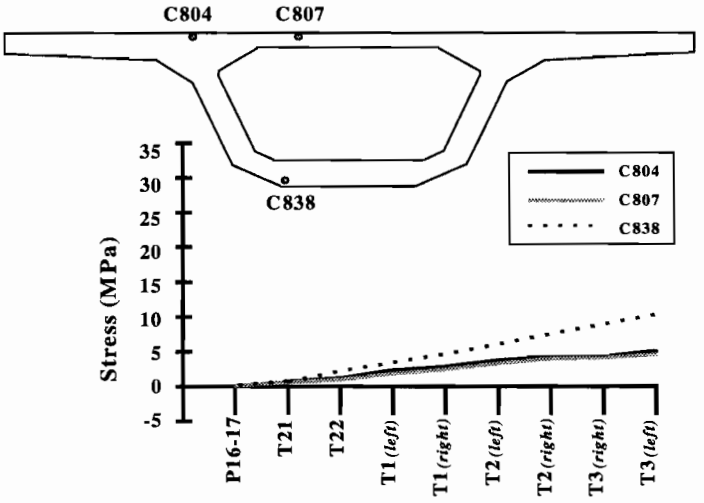

Figure 5.15 Stresses in selected concrete gauges from P16-17 over the course of the continuity stressing sequence

5.3.2 Shear Stresses

Shear stresses caused by the stressing of the external continuity tendons were determined from the concrete strain gauge rosettes. These results are presented in Figure 5.16. No calculations of theoretical stresses were attempted. The maximum final shear stress was 0.95 Mpa (0.14 ksi) that is $0.14\sqrt{f'c}$ (with f'_c in units of MPa). No problems due to shear should occur in the ramp.

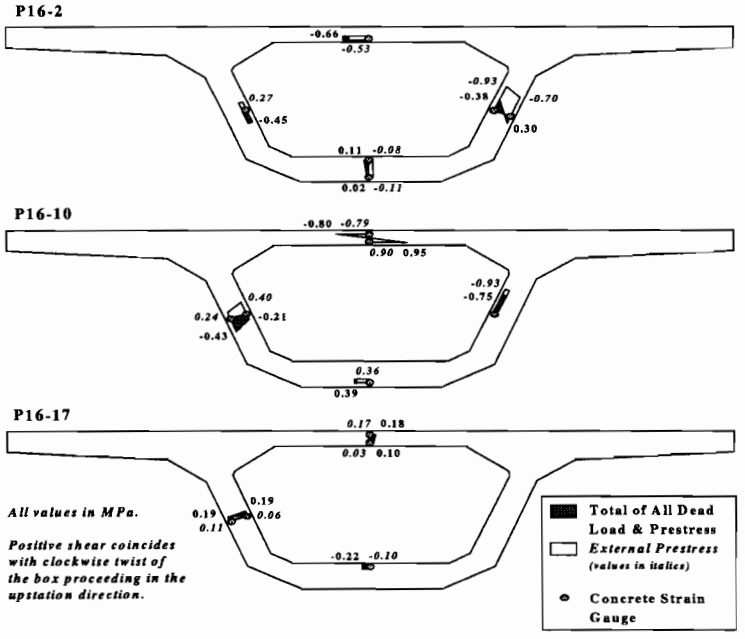

Figure 5.16 Shear stresses after completion of the continuity operations in Ramp P

5.4 Conclusions and Recommendations

5.4.1 Diffusion of Post-Tensioning

Conclusions

The AASHTO effective flange width method for normal forces over-estimated the maximum compression from the diffusion of post-tensioning, but only by 10% of the measured value. This error may be due to some uncertainty in the true value of the modulus of elasticity of the concrete. While the beam theory calculation gave a peak stress much closer to the measured, the AASHTO method was much better at predicting the distribution of the stress. Measurements of diffusion of post-tensioning from Roberts' study of the San Antonio Y indicated that the peak stresses were generally underestimated by the AASHTO method by as much as 30% (19). Roberts' measured stress data came from Demec point readings that may be less accurate than the concrete strain gauges used to measure the data presented in this chapter. Roberts concluded that the AASHTO method was acceptable within the tolerances given by allowable stresses because the peak stresses occurred over only a small portion of the cross section, and the $0.4f'_c$ compression limit under service loads is fairly conservative. Based on the results of the San Antonio Y and US 183 studies, no changes need to be made to the recommended AASHTO effective flange method for the actions of normal forces on cross sections except that directions for the application of the method should be clarified.

Measurements of transverse stresses during post-tensioning indicated that warping of the girder cross section occurs during the stressing process for pairs of tendons symmetrically placed on both sides of the cross section. Unless two rams are used simultaneously during the stressing process, one side must be stressed before the other. During the interval in which the ram is moved to the other tendon, the unsymmetrical loading from the first tendon causes transverse bending stresses in the section. However, the transverse stresses measured in Ramp P under these conditions were so small that they were negligible. After both sides were stressed, the transverse stresses were reduced to nearly zero. This behavior is interesting to note, but poses no need for concern.

Recommendations

The current AASHTO methods for analysis of the diffusion of post-tensioning were found to be satisfactory for design purposes. Figure 2.6.2.6.2-4 and the commentary for this section of the code should be changed to indicate that compatibility induced stresses and edge tensile stresses must still be considered near the end of the member just as in post-tensioned anchorage zones. The compressive force should be shown to spread out in a 30° cone into the bottom flange as shown in Figure 5.2. However, the end of the flange cannot be neglected where possible tensile effects occur. Further research to clarify this application is recommended.

5.4.2 Construction Analysis

Conclusions

The calculated and measured longitudinal stresses compared well for the free cantilever. However, the free cantilever is a completely determinate case making the structure easy to model. The analysis performed for the fully continuous structure failed to predict the measured longitudinal stresses within reasonable limits. Predicted stresses were off by as much as 50% from the measured stresses. Under the fully continuous case, many of the finer details of the structure become important for predicting the structural behavior. For example, the bearing conditions of the actual bridge can be very important to the distribution of the internal forces within the structure. Idealization of such details in the calculation model could account for some of the differences. In general, accurate modeling of the bridge structure during the design process is very difficult because of the uncertainties of variables that will depend entirely upon what happens during the construction process. Though the calculations performed were rudimentary, they might be representative of preliminary calculations that would be performed at the early stages of a design process.

There were some indications of shear lag in P16-2 under the fully continuous structural configuration. A slight reduction of the flange width at P16-2 was required for shear lag under the provisions of Section 4.6.2.6.2 of the *AASHTO LRFD Bridge Design Specifications* (2). The data does not suggest that changes in this section of the code need to be recommended.

Longitudinal stresses in P16-10 after the continuity stressing indicate a sharp peak in stress over the right web. This peak probably originates from the vertical deviator. High stresses were expected near the deviator due to the transfer of forces from the deviation of the external tendons into the rest of the structure. The plane of gauges in P16-10 is probably within the discontinuity zone of the vertical deviator where Bernoulli beam theory does not apply. None of the standard analysis programs that are used for bridge design and generally based on beam theory assumptions would predict such a peak. However, finite element or strut-and-tie modeling would predict compression struts projecting from the corners of the deviator towards the top flange. High stresses in top and bottom extreme fibers caused by local zones are typically not included in service state analysis of a bridge structure, nor are they checked against service load stress criteria from the AASHTO bridge design codes. This accepted omission indicates the serious logical flaw of basing design primarily on allowable stresses but ignoring local stress regions in calculations.

Torsional calculations for the free cantilever indicated very low stresses would occur. Measurements of shear stresses in P16-2 during construction indicated no excessive torsional stresses. Vertical shear stresses were not correctly predicted at P16-2 by beam theory calculations. The differences between the measured and calculated vertical shear stresses at this cross section may have been due to the proximity of the gauges to the support region and the heavy anchorage diaphragm. However, shear strains were not expected to be large in the webs of the box girder, and the concrete gauges may not be able to accurately measure the small changes in strain that are occurring.

Recommendations

No problems were indicated from the construction stresses. At this time, no recommendations are being made based solely on the stress data from the construction process.

CHAPTER 6. LIVE LOAD TEST

6.1 Test Description

On February 13, 1997, after completion of the structure, but before asphalt had been applied to the deck surface, a live load test was performed on Ramp P. Loading from two lanes of standard HS20 AASHTO live load vehicles were simulated with two pairs of back to back dump trucks. The exact axle loads of the HS20 vehicle could not be reproduced. Therefore, the dump trucks were placed back-to-back at a spacing that would closely simulate the moment produced by an HS20 truck. Data was recorded for five load cases.

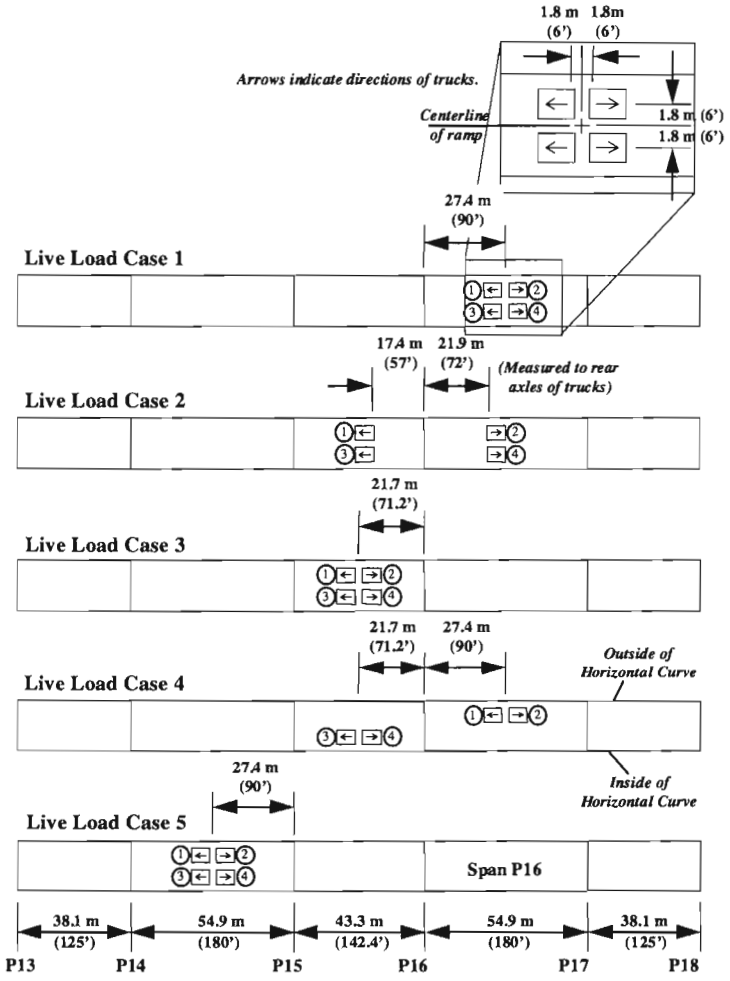

Figure 6.1 Live load test cases

Load case 1 was performed to produce a maximum positive moment at midspan in span P16. Load case 2 was performed to produce a maximum negative moment at the pier in span P16. Load case 3 was performed to test the carry-over moment to span P16 from load placed one span away. Load case 4 was performed to produce a maximum torque in the ramp. Load case 5 was performed to test the carry-over moment to span P16 from load placed two spans away. The locations of the dump trucks in these load cases are shown in Figure 6.1. The measured axle loads from the dump trucks used in the live load test are shown in Figure 6.2. Figure 6.3 shows some typical test procedures. The test took place from 8:30 A.M. until 1:30 P.M. Zero readings were taken before and after the test to subtract thermal effects away from the live load stresses.

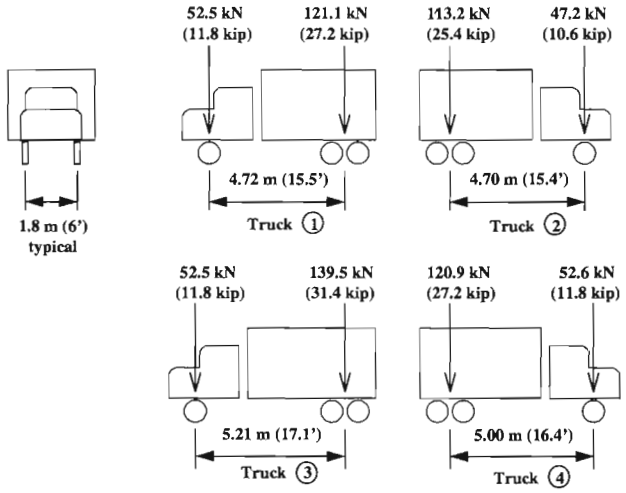

Figure 6.2 Live load truck axle weights

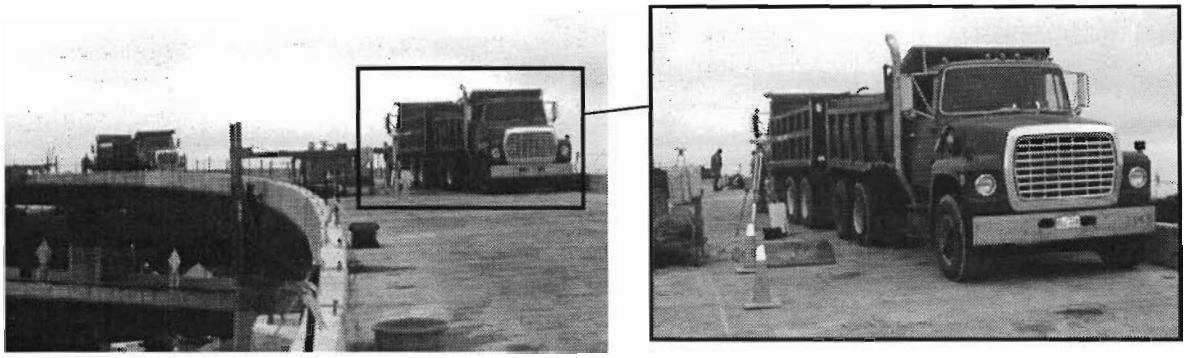

Figure 6.3 Pictures of the live load test (load case 4)

6.2 *Presentation of Results*

6.2.1 *Longitudinal Stresses*

Measured longitudinal concrete gauge stresses at P16-2 from each of the live load cases are plotted in Figure 6.4. The plots indicate that the highest negative moment stresses were produced by load case 1. Calculated stresses indicated the same result although the configuration of the live load in load case 2 is more consistent with a traditional design load for negative live load moment at the pier. However P16-2 instrumentation was 1.9 m from the pier centerline. Load cases 2 and 4 produced similar moments at the pier. The carry-over moment from a load two spans over was negligible. All of the live load stresses at P16-2 were significantly smaller than the stresses measured during construction.

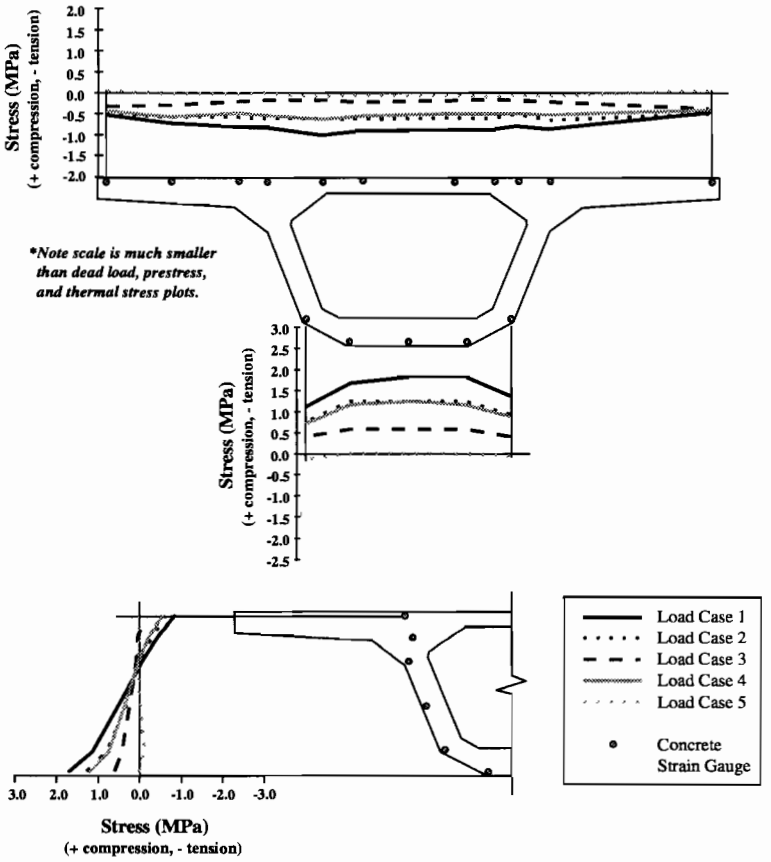

Figure 6.4 Measured live load longitudinal stresses in P16-2

Figures 6.5, 6.6, and 6.7 show the measured longitudinal concrete gauge stresses from load cases 1 and 2 for segments P16-2, P16-10, and P16-17, respectively. Calculated stresses at the levels of the strain gauges are also plotted in these figures. A slight reduction of the effective top flange width of P16-2 was required by Section 4.6.4.6.2 of the *AASHTO LRFD Bridge Design Specifications* (2). The internal forces at each section were calculated using a simple-two dimensional frame solver (RISA2D 18)). A description of the input file model is given in Appendix A (22). The model used for the calculated stresses employs several simplifications. The cross sections were modeled with their gross properties; no transformations of the prestressing steel were applied. The external tendons were not modeled, and the bearing pads were idealized as either fixed or free connections to the piers. A uniform modulus of elasticity was applied to the entire structure. Stress calculations for each section can be found in Appendix C (22). The plots of the longitudinal stresses indicate that the calculated results tended to overestimate the magnitudes of the stresses, particularly in the bottom flange. This may be due to errors in the presumed modulus of elasticity for the concrete in Ramp P. Results from the specimen tests most likely underestimated the modulus due to differences in the curing conditions between the concrete in the specimens and the concrete in the actual segments (as discussed in Section 3.7.1 in Chapter 3).

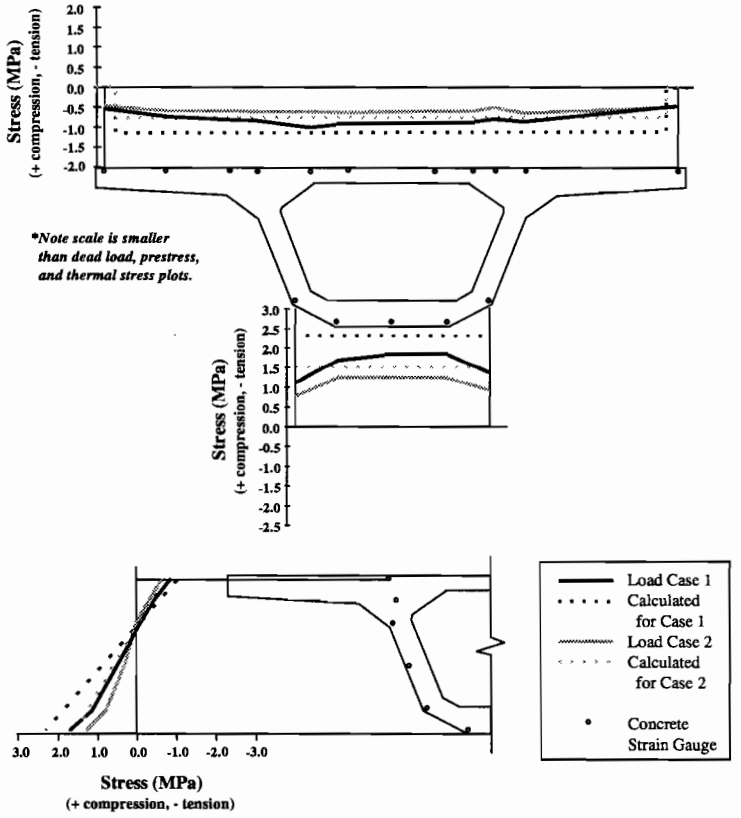

Figure 6.5 Measured and calculated live load longitudinal stresses in P16-2

Thus, when the measured data was converted from strains to stresses using the modulus measured from the specimens, the stresses were lower than what they might have been. Plots of the stresses for P16-10 in Figure 6.6 indicate that the calculated point of inflection for load case 1 was close to the actual point of inflection. All of the plots indicate that the neutral axis of the sections was close to that calculated from the untransformed section. Drops in the top flange stress near the wing tips for segment P16-2 indicate that some shear lag may be occurring. This would be consistent with the location of P16-2 near the support where shear forces are greatest. Some shear lag effect was predicted for the P16-2 cross section. The average measured stresses for the top and bottom flanges of P16-2 and P16-17 were calculated and compared to the frame solver results. The ratios of measured to calculated stresses are presented in Table 6.1. The measured stresses tend to be around 77% of the calculated stresses.

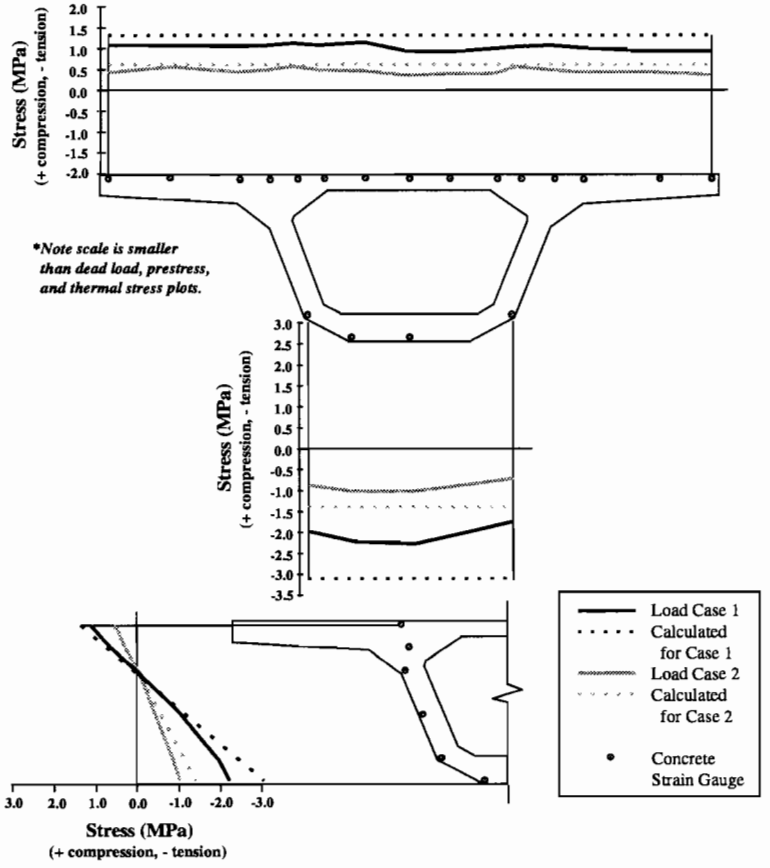

Figure 6.6 Measured and calculated live load longitudinal stresses in P16-17

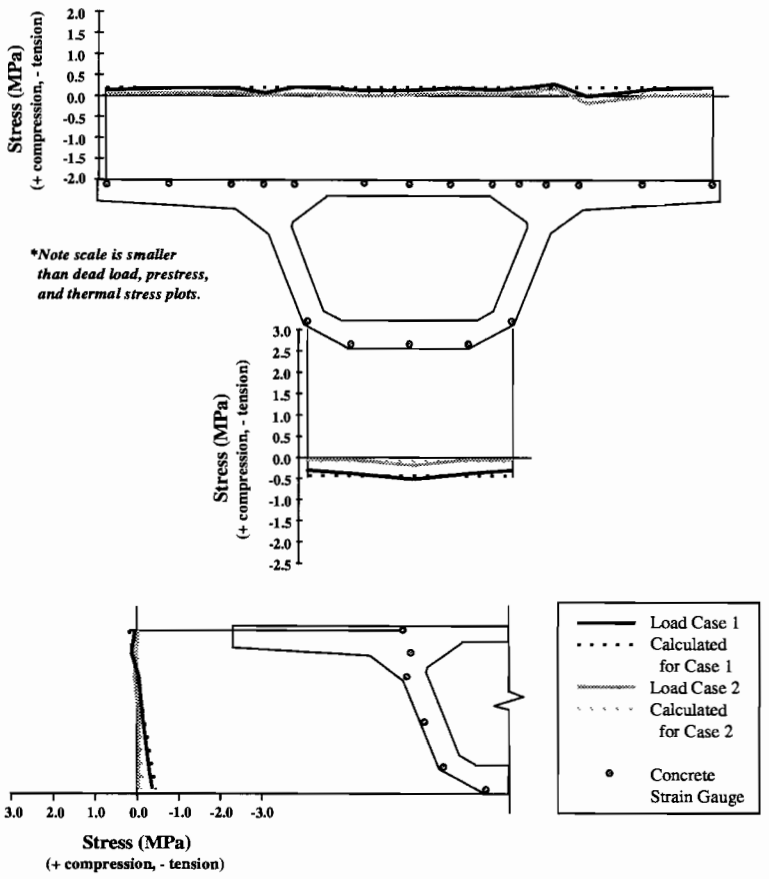

Figure 6.7 Measured and calculated live load longitudinal stresses in P16-10

Table 6.1 Comparisons of calculated and measured longitudinal stresses

	Load Case 1			Load Case 2		
	Average of Measured (MPa)	**Calculated (MPa)**	**Measured / Calculated**	**Average of Measured (MPa)**	**Calculated (MPa)**	**Measured / Calculated**
P16-2						
Top	-0.794	-1.153	0.689	-0.596	-0.751	0.794
Bottom	1.802	2.319	0.777	1.259	1.510	0.834
P16-17						
Top	1.054	1.349	0.781	0.475	0.605	0.785
Bottom	-2.264	-3.102	0.730	-1.012	-1.391	0.728

6.2.2 Shear Stresses

Shear stresses measured with the concrete gauge rosettes from live load cases 1 and 4 are plotted in Figures 6.8 through 6.9. Positive shear corresponds to clockwise twist of the girder progressing in the upstation direction of the ramp (into the page for all section figures). The measured shear stresses are plotted against calculated shear stresses. These calculations are given in Appendix B (22). The plots show that the approximate method over-estimated the shear stresses in the girder. The maximum shear stress of 0.16 MPa was measured in P16-17. This value was 29% of $\sqrt{f'_c}$. The low values of strain associated with these stresses may not have been high enough for the concrete strain gauges to measure properly. This could be the reason for the large disparity between the measured and calculated data.

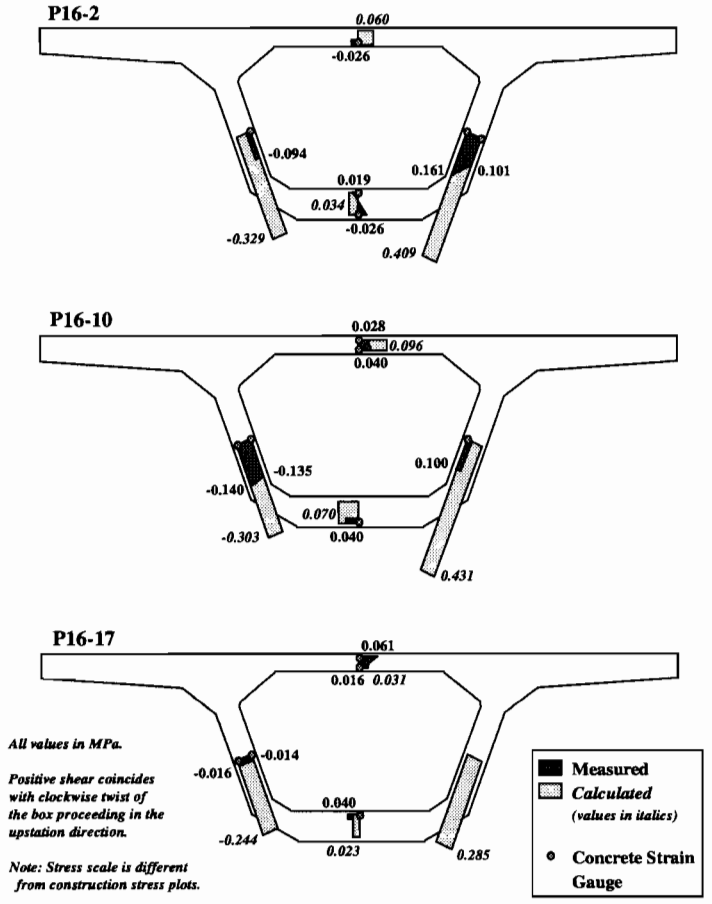

Figure 6.8 Measured and calculated shear stresses from live load case 1

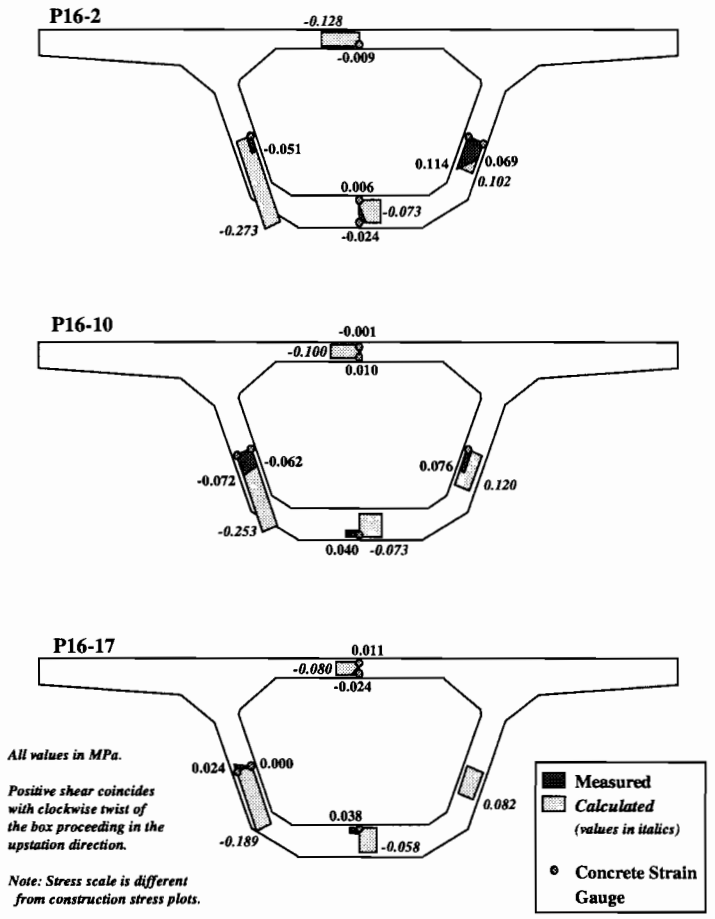

Figure 6.9 Measured and calculated shear stresses from live load case 4

6.2.3 External Tendon Stresses

Stresses measured in the external tendons from load cases 1, 2, and 3 are plotted in Figures 6.10 through 6.12, respectively. All of the load cases produced negligible stresses in the draped portions of the external tendons. The maximum stress increase was 8.4 MPa in the right T3 tendon that was produced by load case 1 with the trucks at the midspan of P16. The left tendon underwent a similar stress increase of 8.0 MPa tension. There seems to be no difference in the behavior between the right-side tendons and the left-side tendons. No data was available for the left side T1 and T2 tendons on the upstation side of the vertical deviator because of bad gauges. All of the external tendons in Ramp P were composed of nineteen 1.52 cm (0.6 in.) diameter low-relaxation strand. The area of each strand was 1.4 cm^2 (0.217 in^2) and the yield stress was 1860 MPa (270 ksi). Live load fatigue should not be a concern for the tendons. Ryals (20) recommends a fatigue limit of 69 MPa (10ksi) for external tendons.

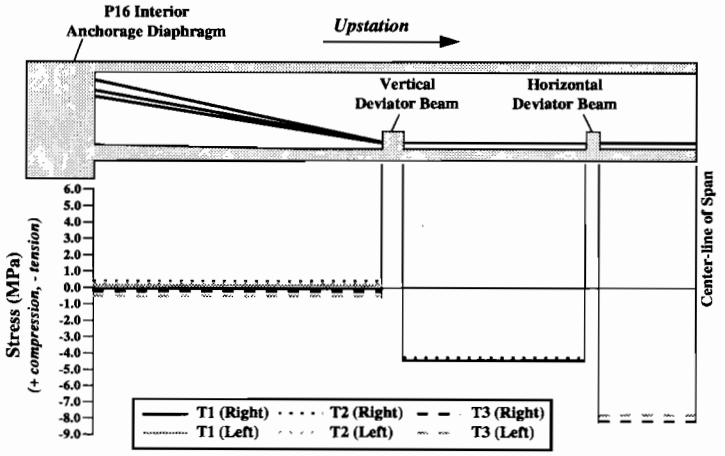

Figure 6.10 Stresses in the external tendons from live load case 1

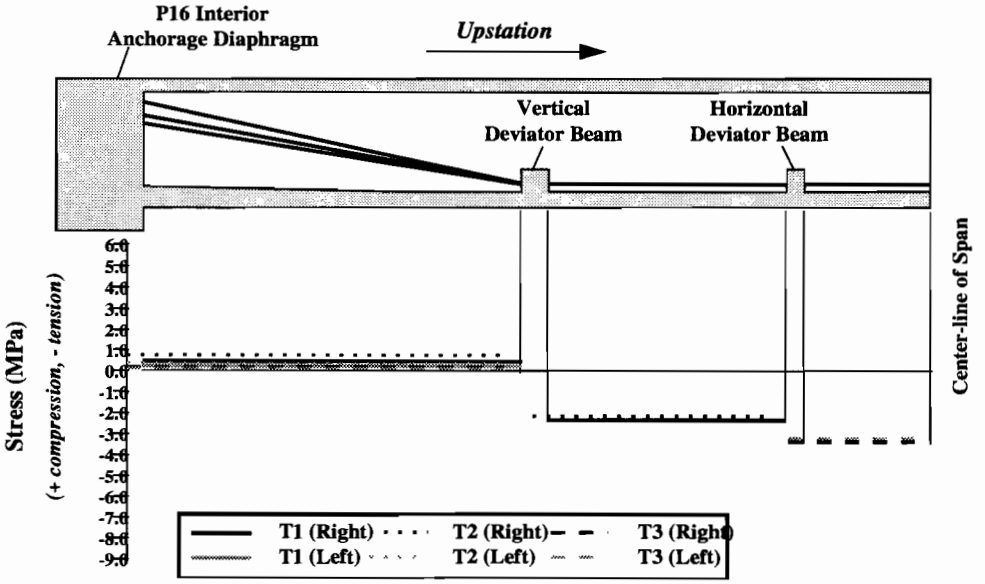

Figure 6.11 Stresses in the external tendons from live load case 2

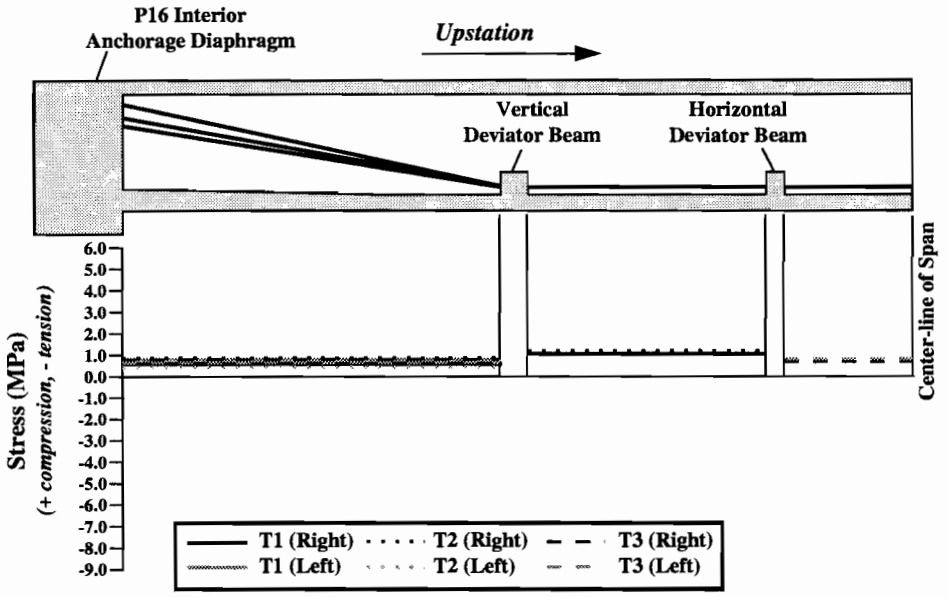

Figure 6.12 Stresses in the external tendons from live load case 3

6.2.4 Tilt Meter Data

The measured tilts and slopes of the ramp from load cases 1, 2, and 4 are plotted in Figures 6.13 through 6.15, respectively. Positive twist is clockwise as one proceeds in the upstation direction of the bridge. Deflections were calculated by integrating the tilt and slope values. The trapezoidal method was used for the integration. The integrated deflections were shifted so that boundary conditions of zero vertical deflections at piers P16 and P17 were met. Calculated slopes and deflections from a two-dimensional frame solver (RISA2D (18)) are also plotted. The model used for the calculated values was the same as that used to compare results in Section 6.2.1 for the longitudinal stresses. The same limiting assumptions discussed previously apply to these results. Table 6.2 lists the maximum slopes at the quarter points of span P16 from the measured and calculated results. Table 6.3 lists the maximum deflections at the P16 midspan from the measured and calculated results. The deflections are reported in absolute units as fractions of the span length, 59.4 m (180 ft). The slopes compared favorably despite ignoring the effects of the horizontal curve in the two-dimensional frame model. Some of the error may be attributable to the modulus of elasticity that was used to model the concrete in the two-dimensional frame model. As discussed in Section 6.2.1, the values for the modulus of elasticity used in the two-dimensional frame model may be lower than the actual modulus of elasticity in the concrete of Ramp P. The deflections compared less favorably. Ignoring the transformed tendon areas made the calculation model more flexible than the actual ramp. The modulus used in the calculation model was, again, probably a little low. On the other hand, the integrated values of deflection will be too small because area has been lost off of the measured slope curve where

straightline segments have been drawn between data points. The actual slope curve would be more rounded and enclose more area. The maximum calculated deflection was /5330, and the maximum integrated deflection was /7410. The true value is probably in between those two.

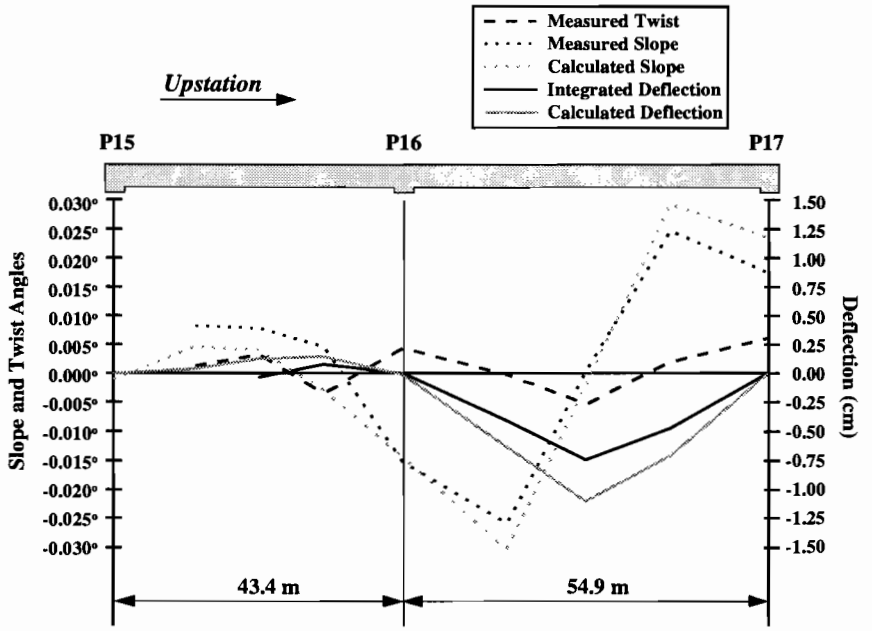

Figure 6.13 Tilts, slopes, and deflections from live load case 1

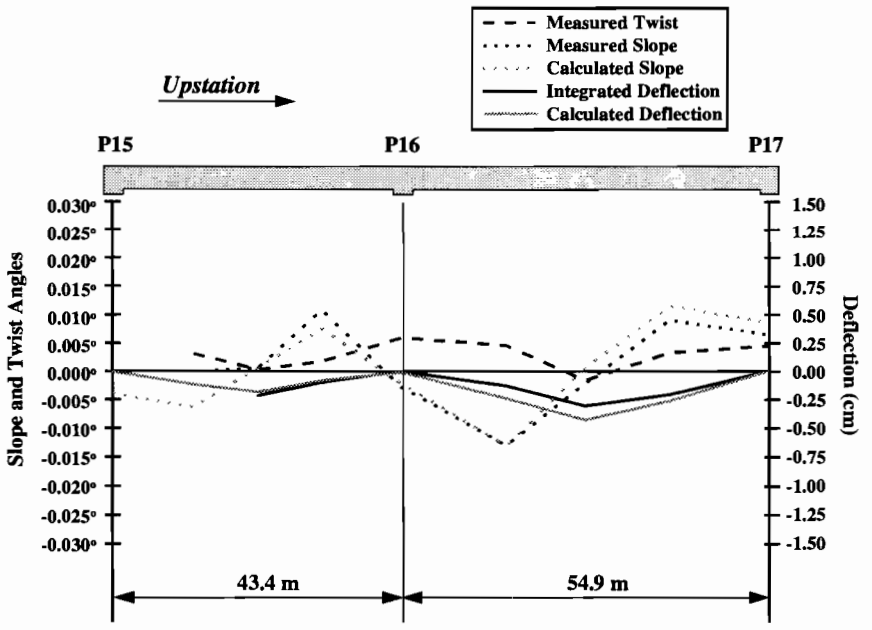

Figure 6.14 Tilts, slopes, and deflections from live load case 2

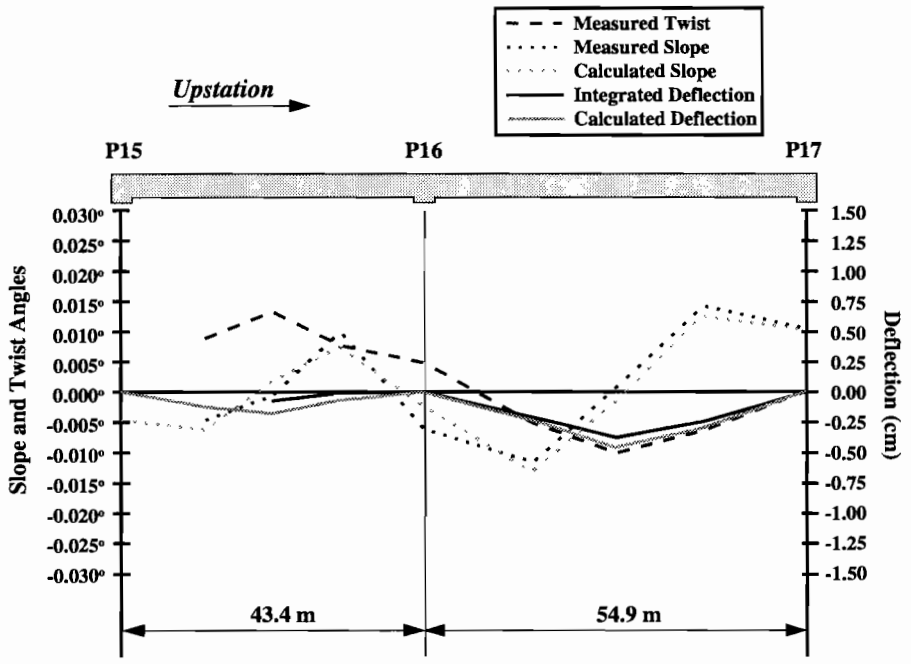

Figure 6.15 Tilts, slopes, and deflections from live load case 4

Table 6.2 Comparison of measured and calculated slopes

	Load Case 1	Load Case 2	Load Case 4
Downstation Quarter Point			
Measured	$-25.7(10^{-3})$ °	$-13.0(10^{-3})$ °	$-11.4(10^{-3})$ °
Calculated	$-30.9(10^{-3})$ °	$-13.2(10^{-3})$ °	$-13.2(10^{-3})$ °
Measured/Calculated	**0.832**	**0.985**	**0.864**
Upstation Quarter Point			
Measured	$24.6(10^{-3})$ °	$9.1(10^{-3})$ °	$14.2(10^{-3})$ °
Calculated	$29.8(10^{-3})$ °	$11.5(10^{-3})$ °	$12.6(10^{-3})$ °
Measured/Calculated	**0.826**	**0.791**	**1.127**

Table 6.3 Comparison of integrated and calculated deflections

	Load Case 1	Load Case 2	Load Case 4
Integrated	0.74 cm	0.30 cm	0.38 cm
Calculated	1.11 cm	0.43 cm	0.46 cm
Measured/Calculated	**0.667**	**0.698**	**0.826**
	As Fractions of the Span Length (59.4 m):		
Integrated	$/7410$	$/18290$	$/14440$
Calculated	$/5330$	$/13720$	$/12910$

6.3 Conclusions and Recommendations

6.3.1 Conclusions

Results from the live load test verify reliable service load behavior from the ramp. All of the measured stresses are probably slightly smaller than the true values because the modulus of elasticity used to convert the measured strains into measured stresses was most likely too small. Some shear lag is occurring in P16-2. Section 4.6.2.6.2 of the *AASHTO LRFD Bridge Design Specifications* (2) indicates that shear lag is most likely to occur near support regions, and a slight reduction of the effective top flange width was required at P16-2. The small drops in stress at the top flange wing tips in P16-2 are consistent with the AASHTO provisions.

Section 4.6.1.2 of the *AASHTO LRFD Bridge Design Specifications* refers to the analysis of structures curved in plan. Spans on bridges that subtend a central angle less than 12° may be analyzed as if straight. The angle subtended by span P16 of the US 183 Ramp P is 15.4°, thus consideration of the ramp's horizontal curve is necessary for its design. The standard practice of most engineers is to analyze the moments, axial forces, and vertical shears using a two-dimensional beam program that accounts for prestressing and time effects, and to analyze the torsional shears and transverse moments on the substructure using a three-dimensional frame solver that does not model the prestressing or time effects. The calculated results from the two-dimensional frame solver gave similar shapes for slopes and deflections as well as the longitudinal stress when compared to the measured results. Furthermore, there is little evidence that the horizontal curve of the bridge affected the distribution of live load to the external tendons from the inside of the horizontal curve to the outside. This indicates that the horizontal curve of the ramp had little effect on the distributions of the moment, axial forces, and vertical shears from the live load, and exclusion of consideration of the horizontal curve from calculations of these actions is acceptable for spans with central angles of up to 15.4° and probably higher.

All of the live load cases produced stresses that were much smaller than the dead load and prestress stresses. Furthermore, the live load deflections were minimal. This would indicate that the bridge probably has a large reserve for additional live load capacity under service conditions.

6.3.2 Recommendations

The effects of torsion on flexural behavior for horizontally curved bridges can be ignored for bridges with individual spans that subtend central arcs of up to 15°. No other recommendations are being made at this time.

CHAPTER 7. THERMAL BEHAVIOR

7.1 Temperature Trends

Daily temperature trends for the Ramp P structure are discussed in this section. Magnitudes for the maximum positive and negative temperature gradients measured through the cross section are presented. Statistical distributions of the occurrence of positive and negative gradients are tabulated and presented as well.

7.1.1 Daily Temperature Cycles

Measurements in other temperature studies have indicated that the thermal gradient shape shown in Figure 7.1 is generally applicable for concrete box girders (6, 16, 19, 21, 23). Studies of the thermal gradient shapes from the Ramp P data also indicated that the shape shown in Figure 7.1 was fairly typical for the Ramp P cross section. Figures 7.3 and 7.4 that show the maximum measured positive and negative thermal gradients confirm this. Based on the characteristics of this typical shape, the daily thermal gradients were evaluated based on adjusted top and bottom temperature magnitudes. To account for variations in ambient temperatures at different times, average thermocouple temperatures at any instant were calculated at the top of the box, the junction between the webs and the top flange, and the bottom of the box. The average temperature at the junction between the webs and the top flange was then used as a baseline reference temperature and deducted from the measured average top and bottom temperatures. The resulting corrected temperatures were taken as the basis for the determination of the thermal gradients. Figure 7.1 shows the locations of the thermocouples and the critical values of the thermal gradient that were calculated. The terms "top gradient" and "bottom gradient" are used throughout this report to refer to the magnitudes of the thermal gradient at the top and bottom fibers of the section.

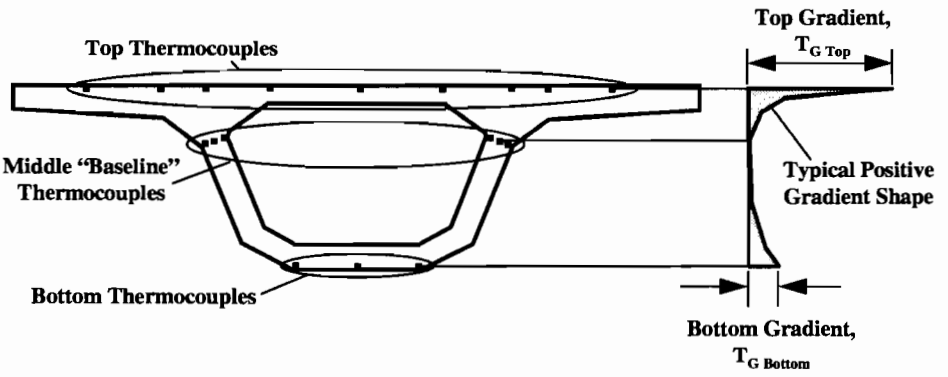

Figure 7.1 Thermocouples used to calculate thermal gradient magnitudes

A positive gradient is defined as the case where the top flange temperatures exceed the temperatures of the webs and bottom flanges. A negative gradient is defined as the case where the top flange temperatures are lower than the webs and usually the bottom flange temperatures. The maximum positive and negative gradients that were measured in the ramp occurred in March of 1997. Figure 7.2 shows the top and bottom gradient temperatures recorded in Ramp P, as well as the ambient air temperature from the month of March 1997. During this month, a large aberrant positive gradient occurred from the application of the asphalt wearing surface to the top deck of the bridge. This large gradient occurred when the 176°C (350°F) liquid asphalt was sprayed onto the surface of the deck temporarily heating the concrete. This event was excluded from the statistical counts of the data. Maximum positive gradients generally occurred in the afternoon around 3:00 P.M. Maximum negative gradients generally occurred in the early morning at about 7:00 A.M. Temperature trends for the ramp from the complete set of recorded data reported by Thompson are presented in Appendix D (22). Thermal monitoring is ongoing.

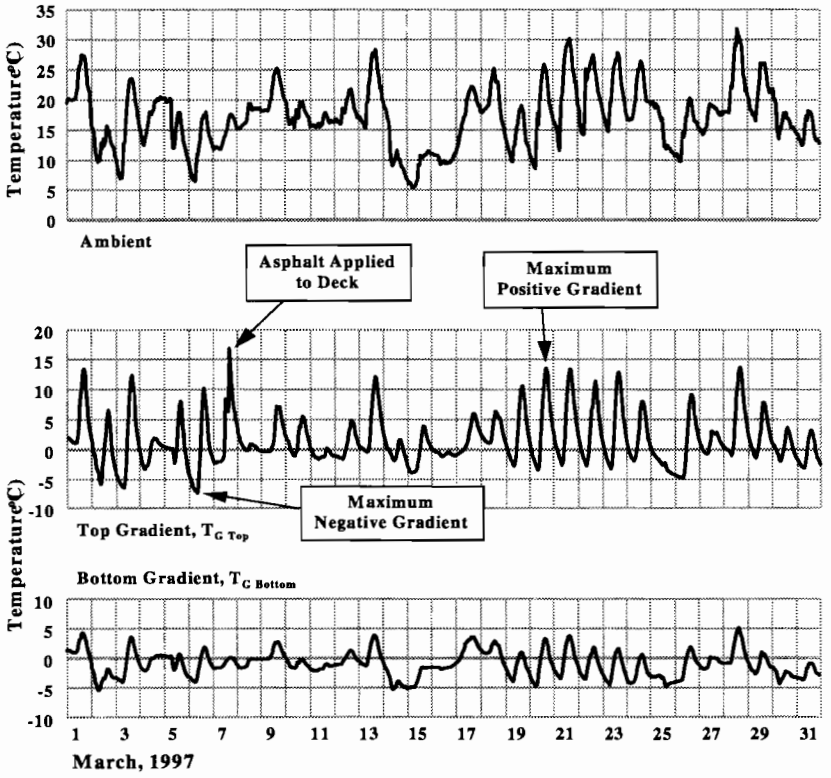

Figure 7.2 Measured thermal gradients for the month of March 1997

The maximum positive and negative thermal gradients that were measured in Ramp P are shown in Figures 7.3 and 7.4. Temperature values for the all of the thermocouple gauges are presented in a tabular form. Selected thermocouples have been plotted to show the shape of the temperature distribution. It is apparent from the data presented in these figures that the

actual gradients that occurred have complex, three-dimensional distributions that are influenced by the shape of the box cross section.

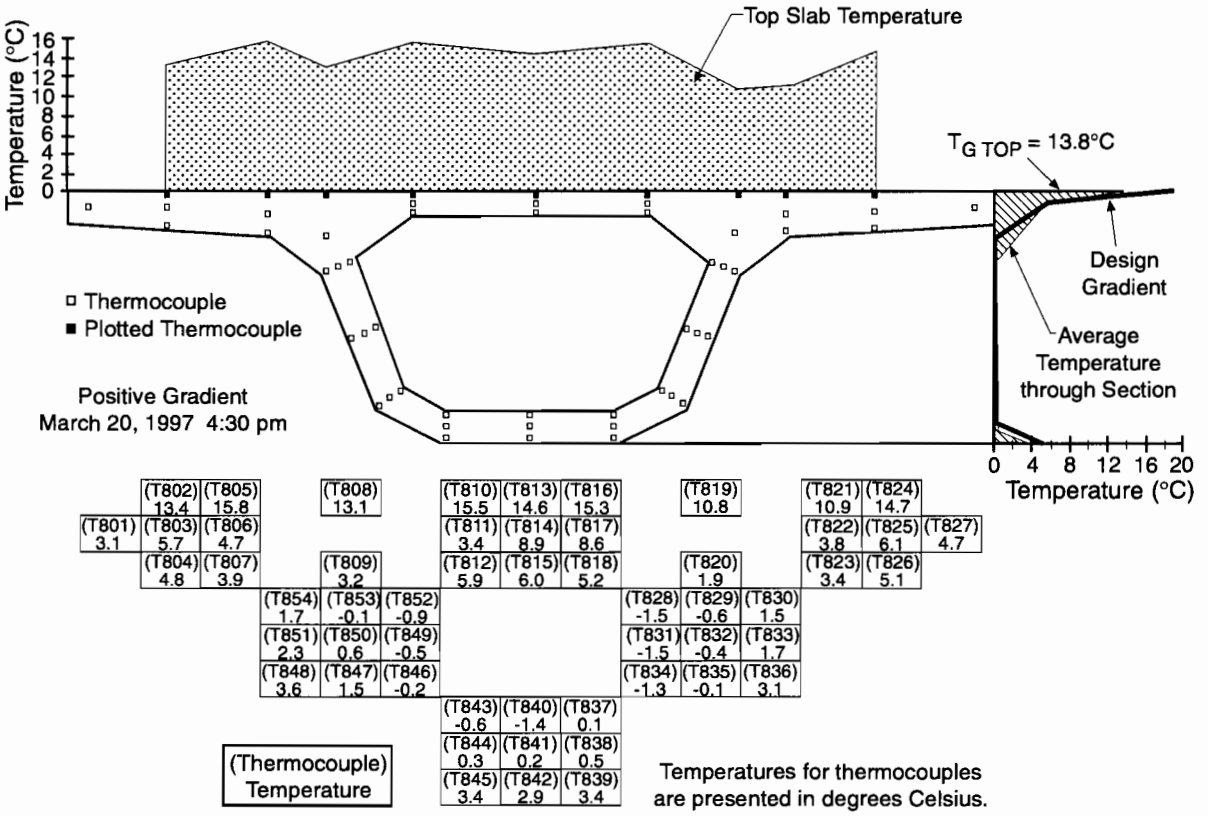

Figure 7.3 The maximum measured positive gradient (from March 20, 1997)

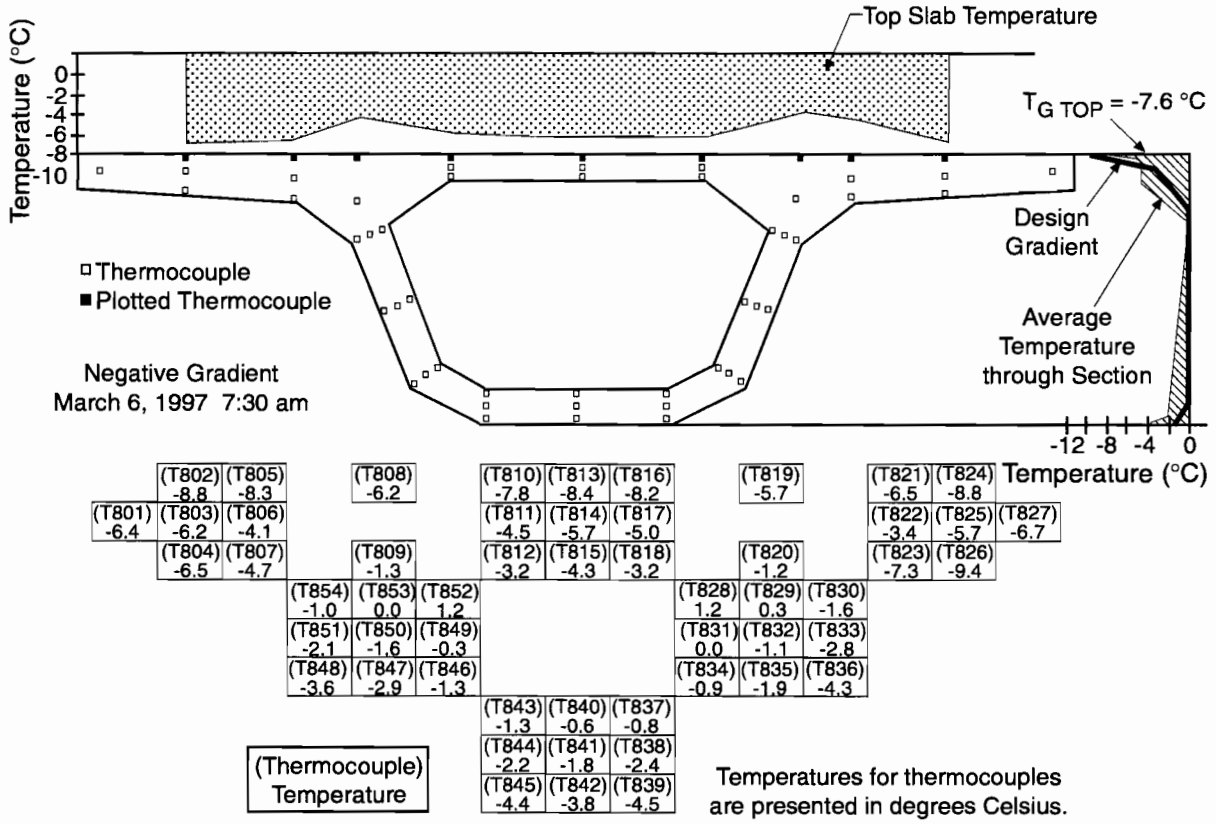

Figure 7.4 Measured thermal gradients for the month of March 1997

7.1.2 Statistical Occurrence of Gradients

Positive and negative gradient peaks were tabulated for the periods before and after application of the 5 cm (2 in.) thick asphalt blacktop. The peaks were taken from twenty-four hour daily time intervals. Occurrence ratios for different magnitudes of the gradients were calculated for the periods before and after the application of the asphalt blacktop. The range of data available before the application of the blacktop included only ninety-eight days of full data. The range of data after the application of the blacktop included 113 days from the date the asphalt was applied until Thompson's report (22). Neither of these ranges includes enough data to choose a definite design gradient. The ranges should include at least one year of complete data so that all of the seasonal effects can be included. Continued monitoring of the thermocouples is underway. It should be continued for a number of years because the statistical distribution can be unfairly weighted by the seasonal effects during a portion of an incomplete year. Each part of the year should be accounted for an equal number of times within the data range.

As an example of variations, the present limited statistical distributions for the positive and negative gradient daily peaks are plotted in Figures 7.5 through 7.8. The differences between the distributions before and after the asphalt was applied to the deck are because of seasonal weather changes between the times of the year when the sets of data were collected. If the data sets were more complete, design gradient magnitudes would be chosen based on the 95% fractile of the distributions. For example, values of -7°C and +11°C would be chosen for the top temperatures, respectively, of the negative and positive design gradients before the application of an asphalt overlay. Similarly, values of -3°C and 12°C would be the 95% fractiles of top temperatures for negative and positive design gradients after the asphalt overlay application. These values may change after longer sampling periods.

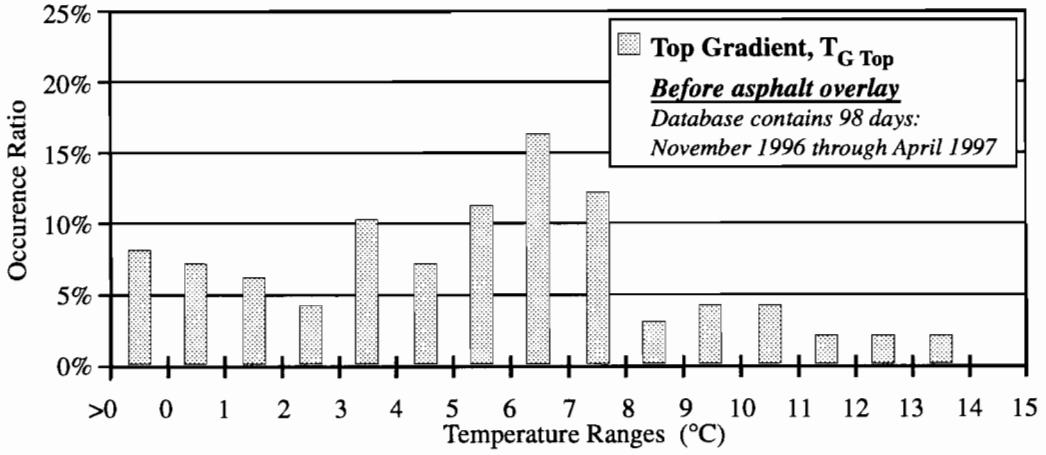

Figure 7.5 Statistical occurrence of daily peak positive gradients before application of the asphalt blacktop

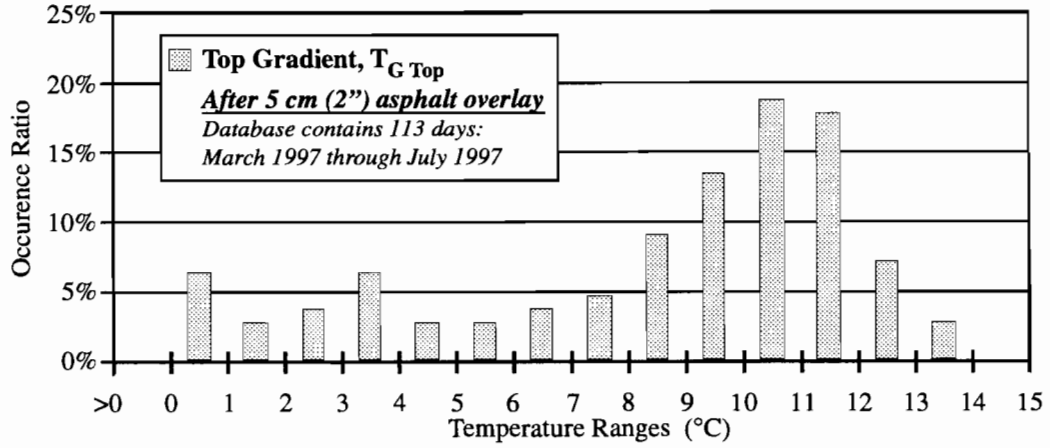

Figure 7.6 Statistical occurrence of daily peak positive gradients after application of the asphalt blacktop

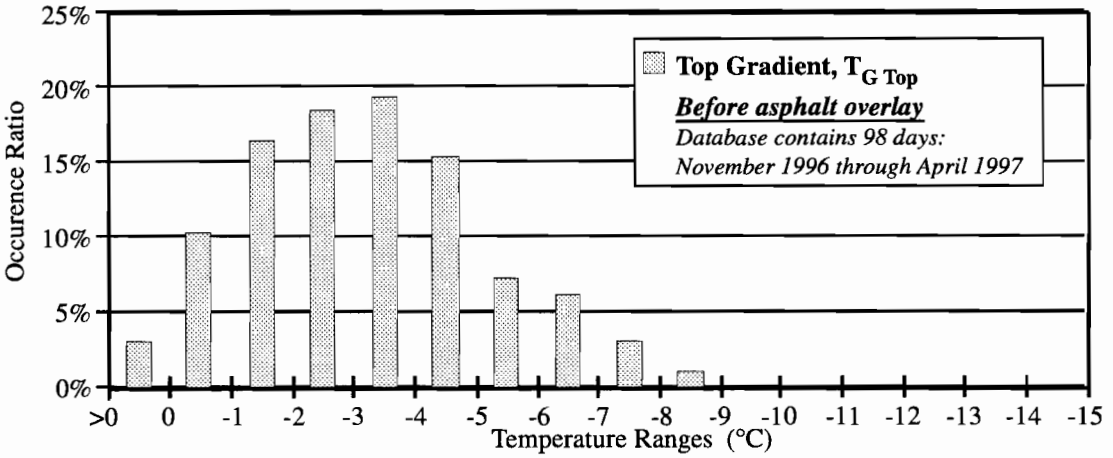

Figure 7.7 ***Statistical occurrence of daily peak negative gradients before application of the asphalt blacktop***

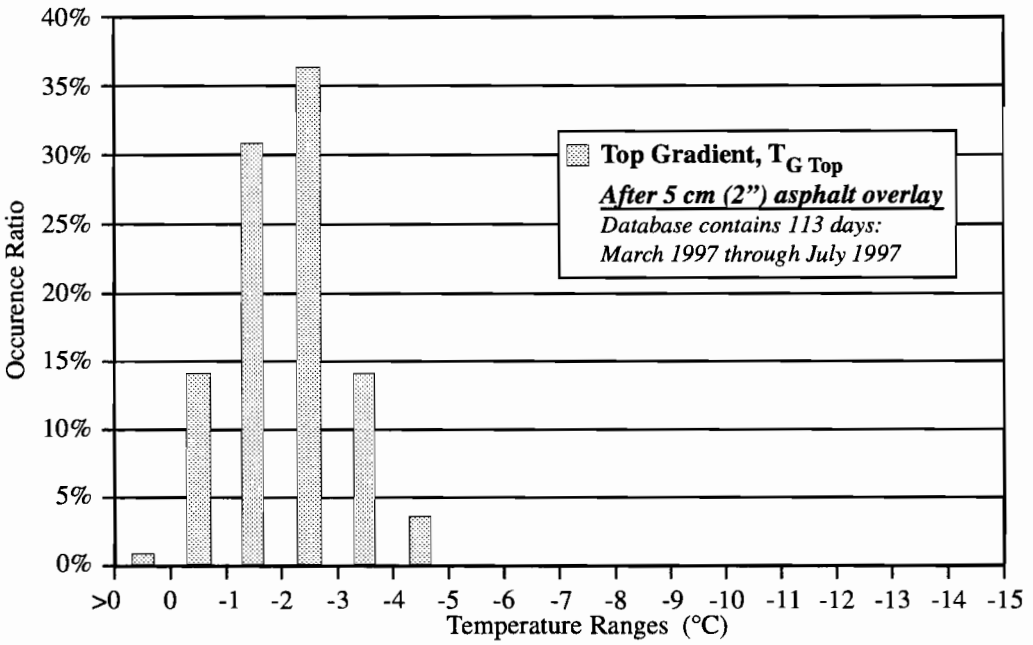

Figure 7.8 ***Statistical occurrence of daily peak negative gradients after application of the asphalt blacktop***

7.1.3 Stresses Caused By Thermal Gradients

Longitudinal Stresses

Two sets of thermal gradient stresses were calculated to compare with the measured thermal gradient stresses: the stresses from the design gradient and the stresses from the maximum measured gradient. Both of these sets of stresses were calculated using the recommended design technique in Section 4.6.6 of the *AASHTO LRFD Bridge Design Specifications* (2). This method relies on the assumptions that the box girder is prismatic and that the cross section does not warp (i.e. plane sections remain plane). To apply the AASHTO method to the measured temperature distribution, the cross section was divided into areas surrounding each thermocouple. The temperature measured by the thermocouple in a given area was assumed to be constant through that area. The stresses at the centroids of each of these areas were then calculated using the standard method. Figure 7.9 shows how the cross section was divided.

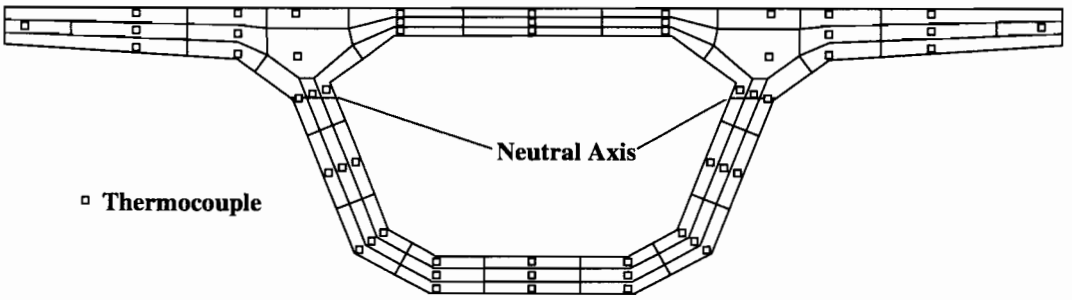

Figure 7.9 Division of the Ramp P cross section into tributary areas for each thermocouple gauge

To make the calculated results comparable to the measured data, a uniform temperature had to be added to the nonlinear gradients. The measured results come from the change in stress in the gauges between the time of the peak gradient occurrence and some baseline time where the temperature distribution through the cross section was fairly uniform. Between the time of the baseline and the time of the peak gradient occurrence there is also some uniform change in temperature in the ramp that contributes to the measured stresses. Thus, it is necessary to add some uniform temperature into the calculations to make the comparison between calculated and measured stresses reasonable. Utilizing the difference in measurements between the dates of the peak gradients and the dates on which the temperature was uniform throughout the section, uniform temperatures of 3.3°C and -6.4°C were added to the maximum positive and negative gradients (presented in Figures 7.3 and 7.4), respectively. The thermal gradient calculations are given in Appendix E (22). The measured and calculated longitudinal stresses in P16-2, P16-10, and P16-17 from the design positive gradient and the measured positive gradient are presented in Figures 7.10 through

7.12. The analogous plots for the negative gradient are presented in Figures 7.13 through 7.15.

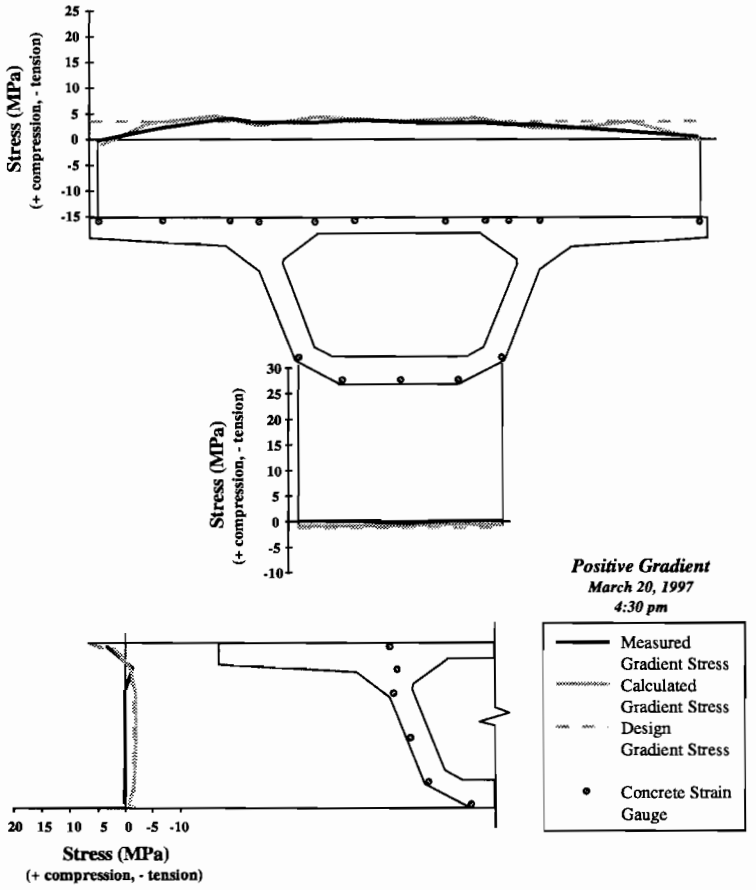

Figure 7.10 Comparison of measured and calculated positive thermal gradient stresses for P16-2

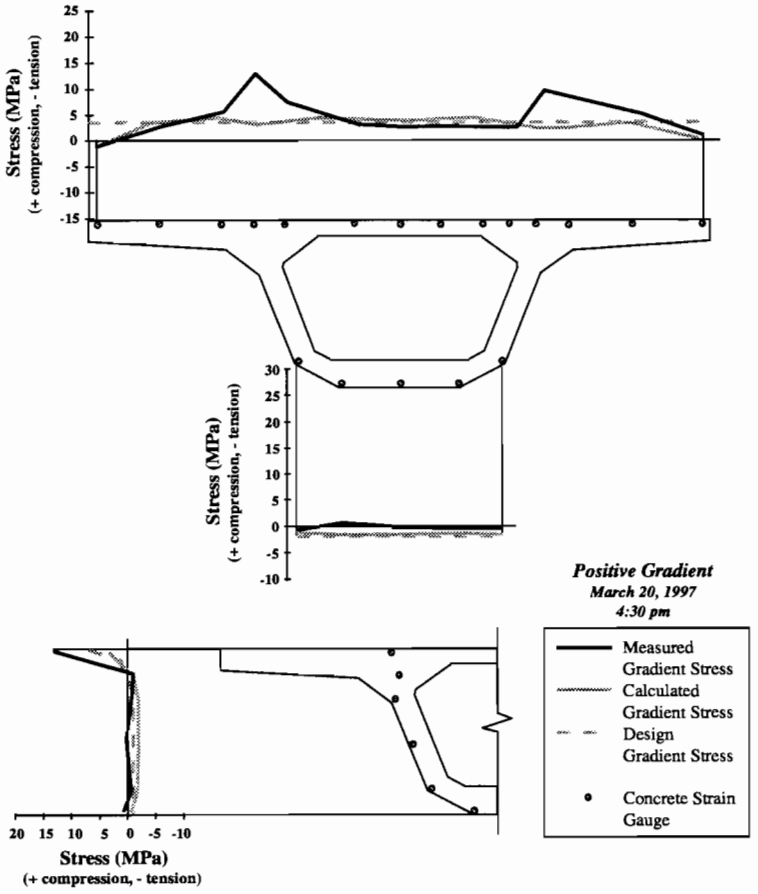

Figure 7.11 Comparison of measured and calculated positive thermal gradient stresses for P16-10

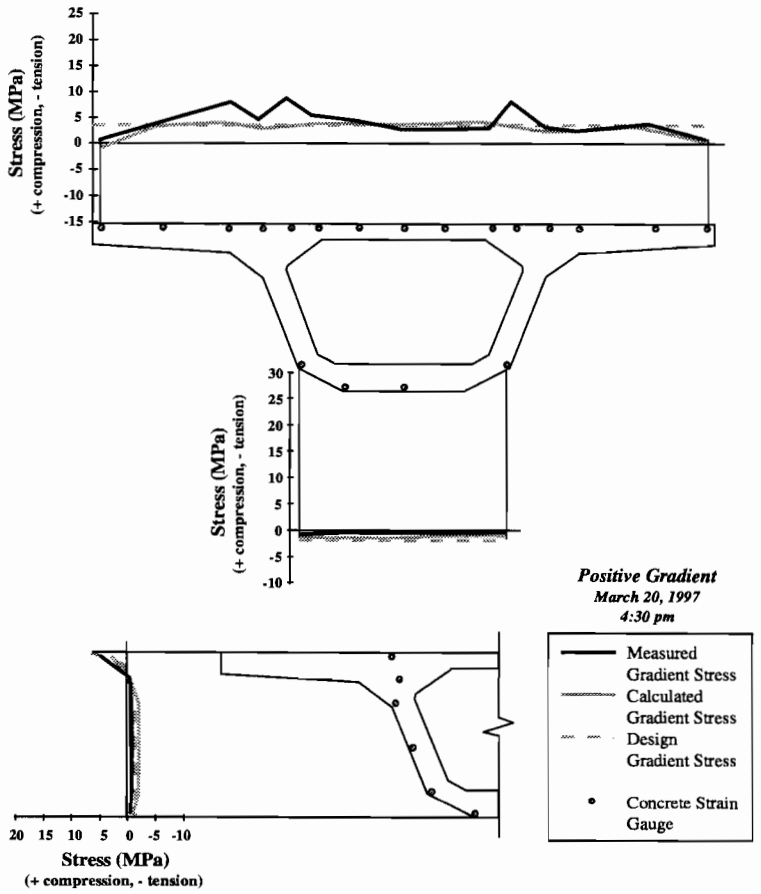

Figure 7.12 Comparison of measured and calculated positive thermal gradient stresses for P16-17

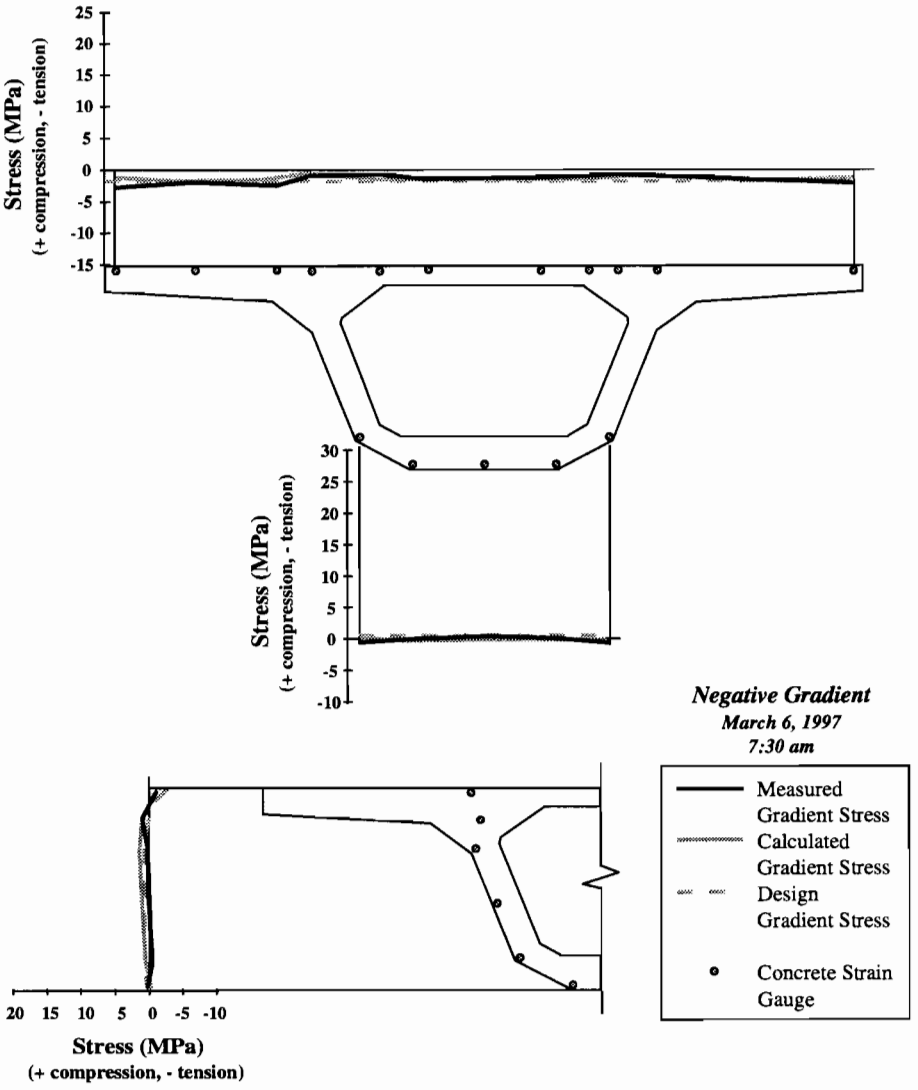

Figure 7.13 Comparison of measured and calculated negative thermal gradient stresses for P16-2

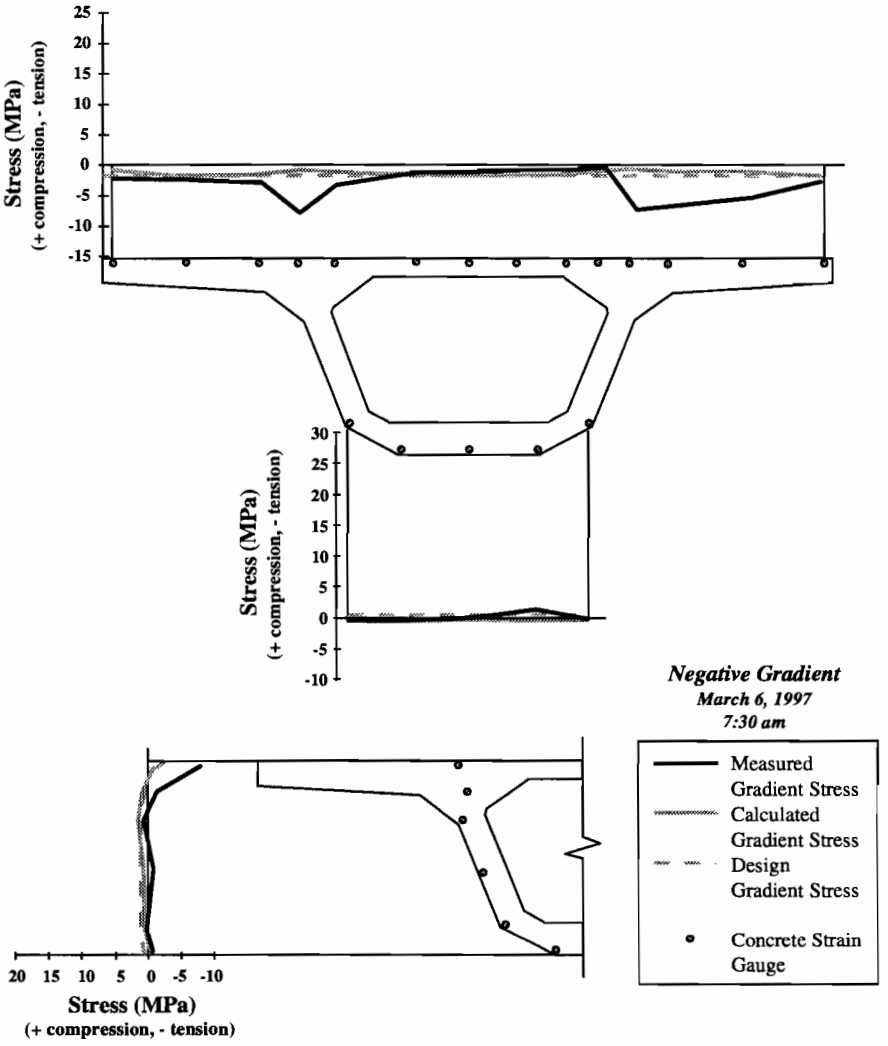

Figure 7.14 Comparison of measured and calculated negative thermal gradient stresses for P16-10

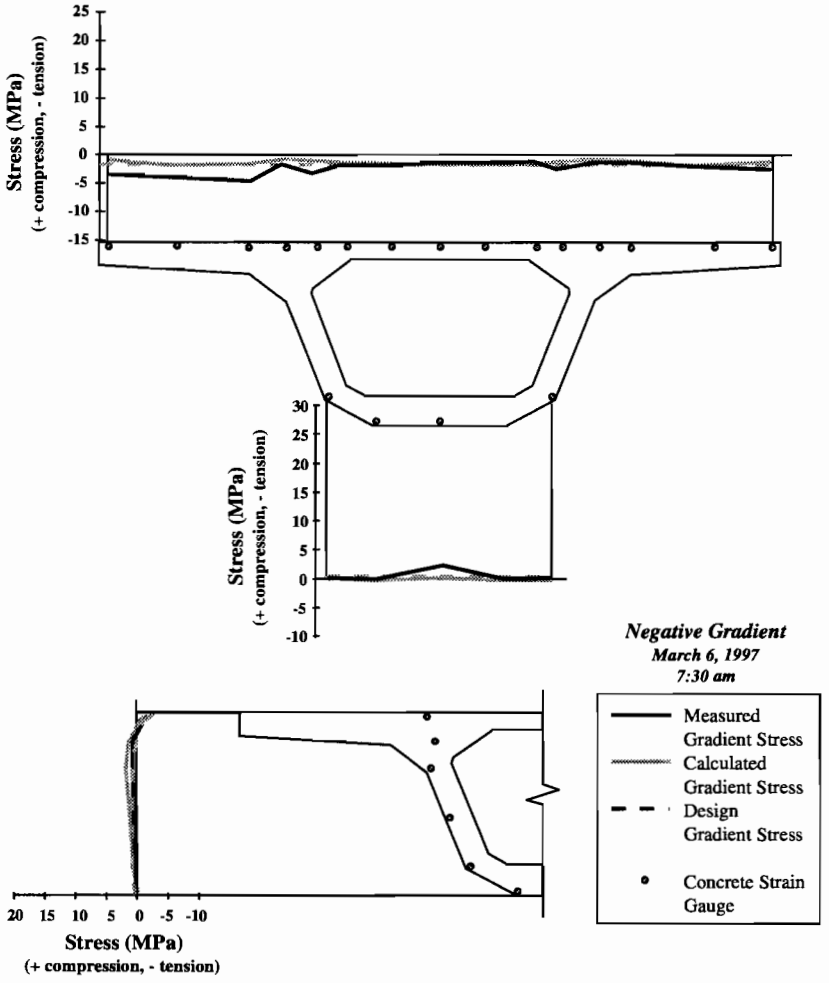

Figure 7.15 Comparison of measured and calculated negative thermal gradient stresses for P16-17

The plots of the measured stress distributions indicate peaks over the webs of P16-10 and P16-17, but not P16-2. This response indicates that the box girder is warping. P16-2 is restrained by the anchorage diaphragm from distortion of its section, so the absence of peaks over the webs at that section is consistent. The recommended method from the *AASHTO LRFD Bridge Design Specifications* (2) assumes the section will not warp. Thus, the stresses calculated from that method would be expected to match measured results better at P16-2 than at P16-10 and P16-17.

Table 7.1 compares measured stresses with stresses that were calculated using the recommended AASHTO method with the measured applied gradients. Table 7.2 compares measured stresses with the stresses calculated from the application of the design gradients.

Table 7.1 Comparison of measured and calculated stresses from measured thermal gradients

	Positive Thermal Gradient			Negative Thermal Gradient		
Segment	Average Measured	Average Calculated	Measured Calculated	Average Measured	Average Calculated	Measured Calculated
P16-2	2.54 MPa	3.04 MPa	0.836	-1.73 MPa	-1.52 MPa	1.138
P16-10	4.61 MPa	3.16 MPa	1.459	-3.21 MPa	-1.55 MPa	2.071
P16-17	4.20 MPa	3.11 MPa	1.350	-2.18 MPa	-1.51 MPa	1.444
	Peak Measured	Peak Calculated	Measured Calculated	Peak Measured	Peak Calculated	Measured Calculated
P16-2	4.03 MPa	4.30 MPa	0.937	-2.94 MPa	-2.01 MPa	1.463
P16-10	12.92 MPa	4.41 MPa	2.930	-7.89 MPa	-2.05 MPa	3.849
P16-17	8.90 MPa	4.32 MPa	2.060	-3.33 MPa	-1.98 MPa	1.682

Table 7.2 Comparison of measured and design stresses

	Positive Thermal Gradient			Negative Thermal Gradient		
Segment	Peak Measured	Peak Design	Measured Design	Peak Measured	Peak Design	Measured Design
P16-2	4.03 MPa	3.57 MPa	1.129	-2.94 MPa	-1.82 MPa	1.615
P16-10	12.92 MPa	3.57 MPa	3.619	-7.89 MPa	-1.81 MPa	4.359
P16-17	8.90 MPa	3.55 MPa	2.507	-3.33 MPa	-1.79 MPa	1.860

No distress has been observed in the Ramp P structure that can be attributed to thermal effects. In order to understand why no such distress has been observed despite the high stresses indicated in Figures 7.10 through 7.15, the total stress state of each segment was examined. Load combinations of dead load, prestress, live load, and thermal gradient were combined to produce minimum and maximum stresses for each instrumented segment. These stress distribution are plotted in Figures 7.16 and 7.17. Figure 7.16 shows the measured and calculated load combinations that produced the minimum stresses in each of the cross sections. These load combinations were not necessarily the same for each cross section. As can be seen in Figure 7.16, no tension occurs in any of the cross sections. Figure 7.17 shows the measured and calculated load combinations that produced the maximum stresses in each of the cross sections. Again, these load combinations were not necessarily the same for each location.

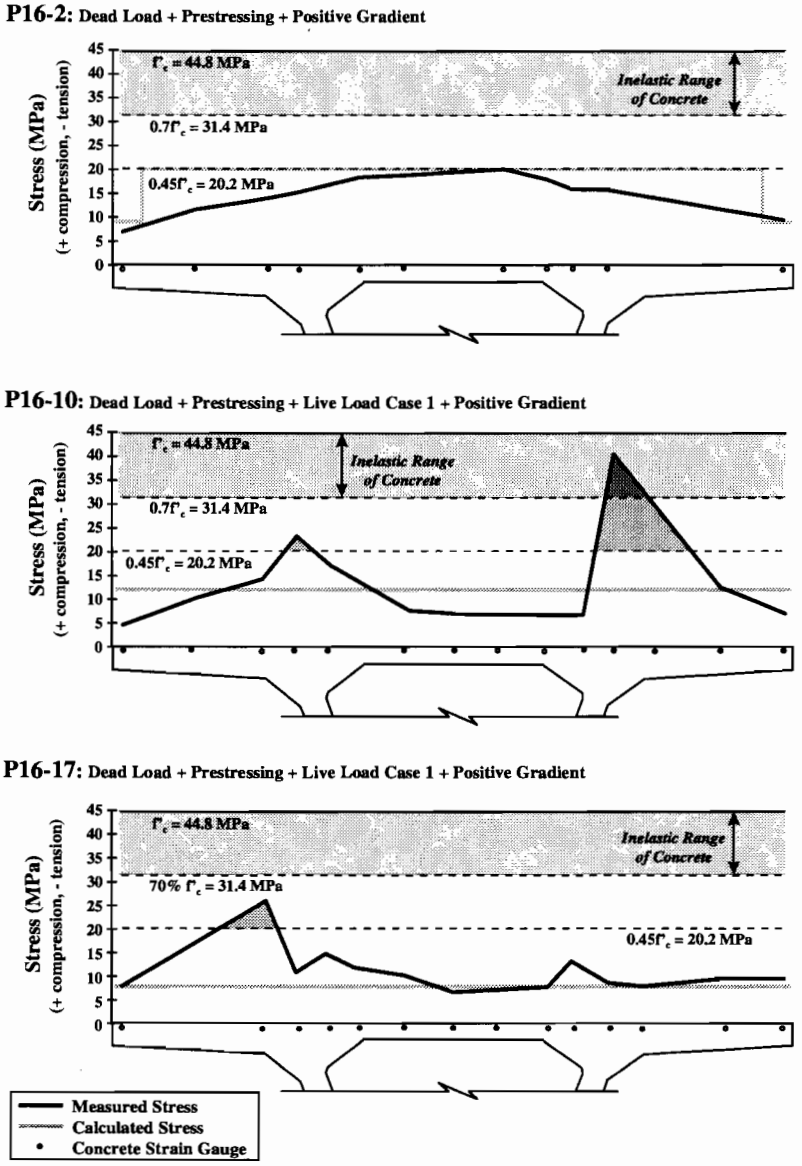

Figure 7.16 Maximum top flange stress load combinations for P16-2, P16-10, and P16-17

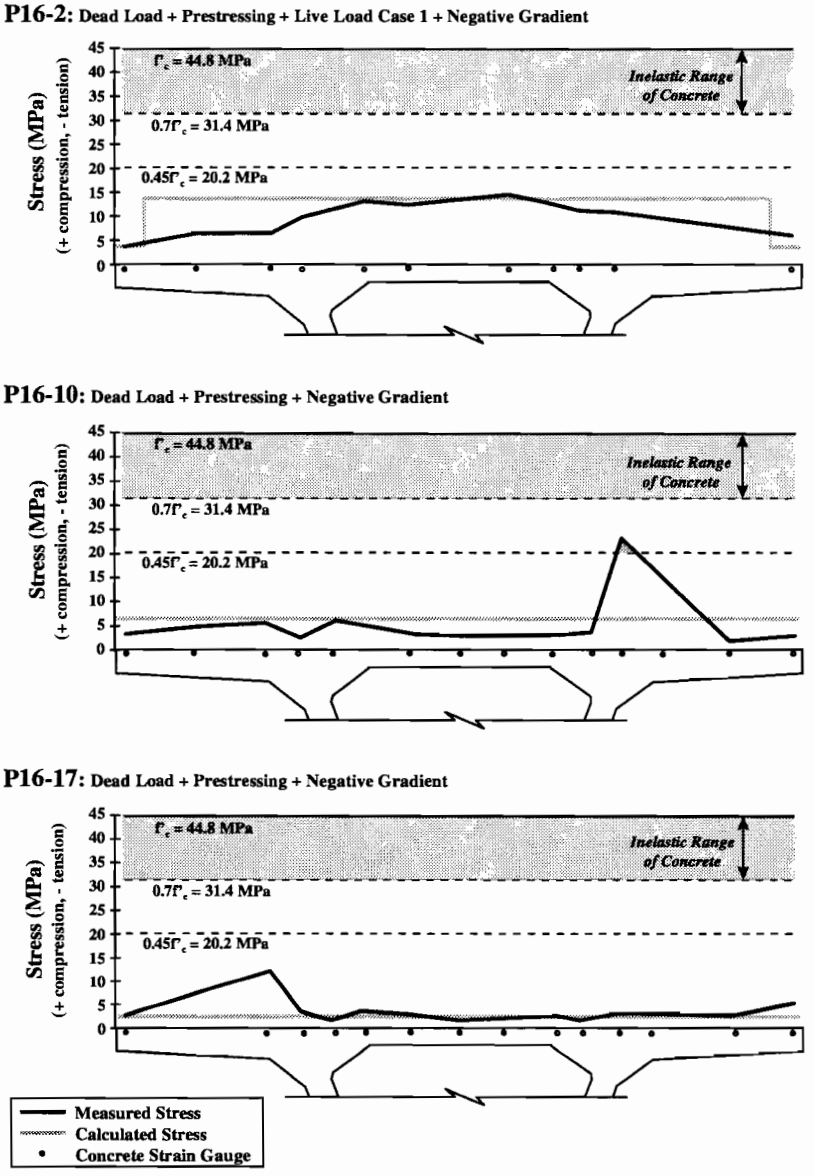

Figure 7.17 Minimum top flange stress load combinations for P16-2, P16-10, and P16-17

The design twenty-eight day compressive strength of the concrete, f'_c, was 44.8 MPa (6.5 ksi). The actual twenty-eight day compressive strengths of the concrete in the segments are unknown but are sure to be greater than the design strength. The precaster found that he was easily reaching his design strengths within the first week of curing. Cylinder tests of the concrete in the segments were generally abandoned once the tests indicated that the design

strength was achieved. However, the twenty-eight day tests from mainlane segments that were performed indicated concrete strengths around 69 MPa (10 ksi) were quite common.

Values of the design f'_c, $0.7f'_c$ (the approximate limit of linear elastic behavior in concrete), and $0.45f'_c$ (the maximum allowable compressive stress for segmental bridges from Section 5.9.4.2.1 of the *AASHTO LRFD Bridge Design Specifications* (2)) are also plotted in Figures 7.16 and 7.17. As can be seen in Figure 7.17, the maximum allowable compressive strength, $0.45f'_c$, was exceeded in P16-10 and P16-17 under combinations of dead load, prestress, live load, and positive thermal gradient. The elastic limit of the concrete was even exceeded in P16-10 near the top of the right web. Under such conditions, the stress data that is presented would no longer be valid because the modulus of elasticity that was used to transform the strain gauge data into stress values could no longer be used. However, because the true compressive strengths of the concrete in the segments was probably much greater than what is indicated in the figures, the plotted stress distribution should need no adjustment.

The load combination plots indicate very fine performance from the bridge. No tension is indicated, and only a small amount of over-compression can be seen. The over-compression should not pose any concern because the AASHTO allowable compression limit is actually somewhat conservative. Only where the linear elastic range of the concrete is exceeded is there a need for concern, but this only occurs over a small width of the top flange, approximately 30 cm (1 ft) at one cross section. Much of the rest of the top flange has stresses well below the AASHTO allowable limit.

Transverse Stresses

A simple transverse calculation model for the Ramp P cross section was created and the measured temperatures for the positive and negative thermal gradients were applied to it. The model consisted of a symmetric two-dimensional frame made up of standard beam elements. The gradients measured through the thickness of the flanges and the webs of the ramp were applied to the beam members of the model using the AASHTO recommended method for each member of the model. A description of the model and calculations for this transverse analysis are given in Appendix E (22). The results from the model are plotted next to measured transverse stresses from P16-17 in Figure 7.16. Though transverse stresses were measured in P16-2, P16-10, and P16-17, only the stresses from P16-17 were compared with the frame analysis because the P16-2 gauges were too close to the anchorage diaphragm, and the P16-10 gauges were too close to the heavy vertical deviator beam, both of which would effect those sections by providing restraint against transverse deformations. The stress plots in Figure 7.18 show that the model did a poor job of predicting the actual transverse stresses caused by the thermal gradients. The percent error for the top flange, top fiber stress was as high as 65% for the negative gradient. If warping of the box girder is occurring as was suggested by the longitudinal stresses, the transverse response of the cross section to applied thermal gradients would be affected as well. This may account for much of the difference.

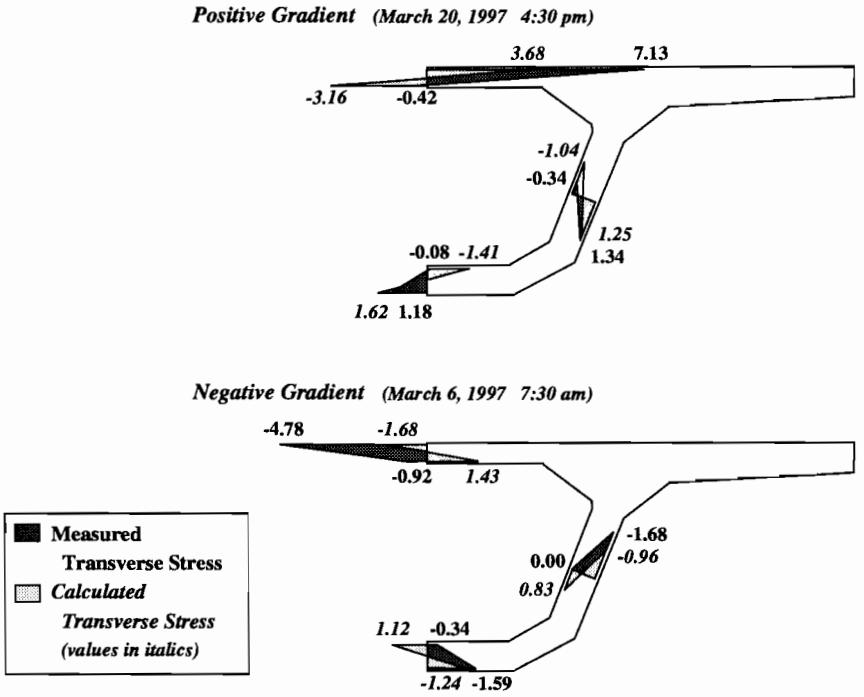

Figure 7.18 ***Comparison of measured and calculated transverse flexural stresses from positive and negative thermal gradients for P16-17***

External Tendon Stresses

Figures 7.19 and 7.20 show the external tendon stresses caused by the maximum measured positive and negative thermal gradients. As in the longitudinal and transverse stress sections, a small amount of linear temperature change is reflected in the measured stresses (3.3°C and -6.4°C for the positive and negative gradient cases, respectively). The highest tensile stress change was produced by the positive gradient. The peak stress change was 10.5 MPa tension in tendon T1 on the right side of the girder. The T2 tendon on the same side underwent almost the exact same stress change. A change of 10.5 MPa (1.5 ksi) is about 0.6% of the guaranteed ultimate tensile strength (GUTS) of 1860 MPa (270 ksi). Fatigue of the tendons due to daily thermal trends should not be a problem. Ryals (20) recommends a fatigue limit of 69 MPa (10ksi).

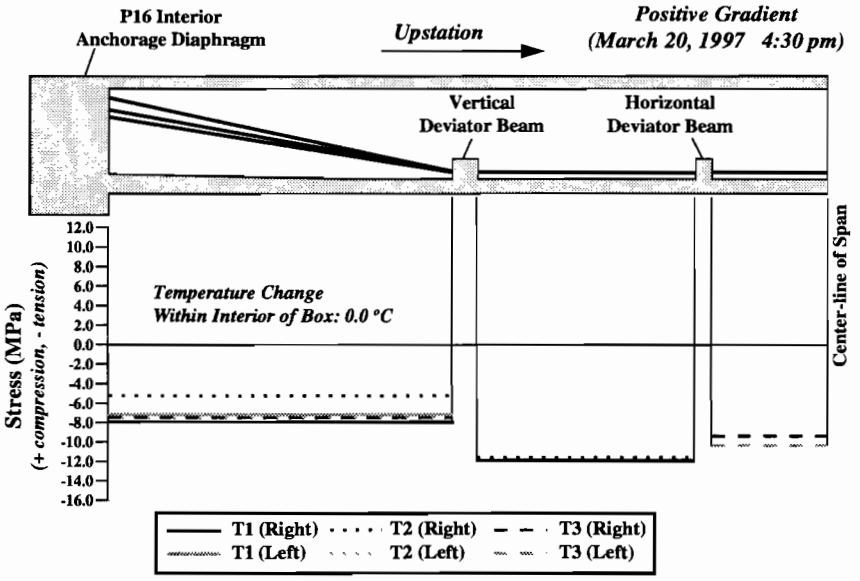

Figure 7.19 Measured stress changes in the external tendons from the maximum positive gradient

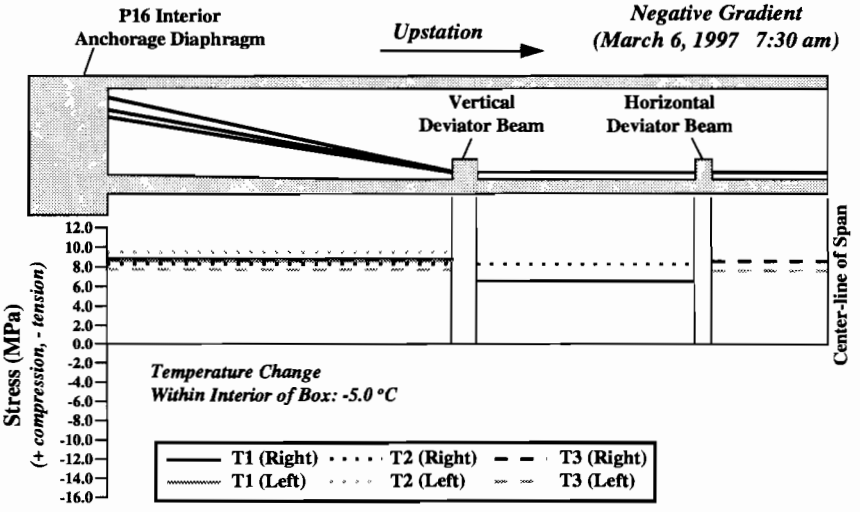

Figure 7.20 Measured stress changes in the external tendons from the maximum negative gradient

7.1.4 Conclusions and Recommendations

Design Gradients

Conclusions

The temperature distributions of the maximum measured positive and negative thermal gradients indicate that the shape of the design gradient from the *AASHTO LRFD Bridge Design Specifications* (2) fits the measured data best when the bottom fiber T_3 temperature is specified at the maximum allowed temperature (2.8°C for the positive gradient and -1.4°C for the negative gradient). The code specifies that the "temperature value T_3 shall be taken as 0.0, unless a site-specific study is made to determine an appropriate value, but shall not exceed 5°F (2.8°C)." Since it is doubtful that any designer could economically perform an appropriate site-specific study for a full box girder section or would go to the trouble anyway, only one value should be specified for the bottom fiber T_3 temperature. Preferably this value should be greater than 0.0°C. The conclusions regarding the shape of the design gradient in this report may not be applicable for types of bridge structures other than concrete box girders. The shape of the cross section of the bridge undoubtedly affects the distribution of the temperature through the depth of the section.

Temperature gradients not only occurred through the depth of the girder cross section, but through the thickness of the flanges and web walls of the box girder. The *Proposed AASHTO LRFD Guide Specifications for the Design of Segmental Concrete Bridges* (17) currently recommend in Section 6.4.4 of the commentary that transverse analysis for shallow cross sections may be necessary and that a gradient of plus or minus 5.6°C (10°F) from the exterior of the box section to the interior may be appropriate. The Ramp P study measured gradients has high as 8.6°C (15.5°F) through the top flange during the maximum positive gradient and -4.1°C (7.4°F) during the maximum negative gradient. Stresses of 7.1 Mpa (1.0 ksi) compression and 4.8 MPa (0.7 ksi) tension, respectively, were recorded in the top flange with these gradients.

The peak top fiber thermal gradient magnitudes measured in Ramp P were less than the specified design gradient top fiber temperatures for the positive and negative gradients. Furthermore, statistical distributions of the measured gradients show that the peak measured gradient occurs less than 5% out of the range of measured gradients. Ideally, the magnitudes of the design gradient temperatures should be based from measured gradient temperatures that reflect the 95th percentile to match other margins of safety. This would allow for a substantial reduction in the magnitude of the design gradient. At the time of this writing, the ranges of the measured thermal gradients from Ramp P are too incomplete to allow a conclusive recommendation of design gradients for temperature zone 4. Ongoing data collection within the next year should allow for a preliminary recommendation of design gradients for box girder sections in temperature zone 4.

Recommendations

The AASHTO recommended design gradients should be based on instrumentation studies of actual bridge structures. Such studies should produce at least one year of measured data including all seasonal effects. The design gradient should be statistically determined from the gradient that provides the 95th percentile fractile. The shape of the gradient is likely to vary based on the shape and size of the bridge cross section. Instrumentation studies of temperature trends in bridge structures should examine thermal distributions across the full cross section.

The *AASHTO LRFD Bridge Design Specifications* (2) should recommend a transverse gradient for all box girder sections. Recommendations for the shapes and magnitudes of such gradients based on the Ramp P study cannot be made at this time. As stated for the longitudinal design gradients, the recommended gradients should be chosen based on instrumentation studies of actual bridge structures. The transverse gradients that are suggested in Section 6.4.4 of the commentary from the *Proposed AASHTO LRFD Guide Specifications for Design of Segmental Concrete Bridges* (17) should be used for design until definitive transverse gradients are determined.

The maximum values that are allowed for T_3, the bottom fiber temperature from the design gradients in the *AASHTO LRFD Bridge Design Specifications* (2) should be applied to make the design gradients best match the shapes of the thermal gradients measured in Ramp P.

Analysis Methods

Conclusions

Measured longitudinal stresses from the Ramp P superstructure indicate that the cross section of the box may be warping under thermally induced strains. Such warping makes the recommended analysis method from Section 4.6.6 of the *AASHTO LRFD Bridge Design Specifications* (2) unsuitable for determination of the stresses caused by thermal gradients in box girder sections. The peak measured stresses were much greater than the peak stresses predicted by the recommended method. The peak measured compressive stress from the positive gradient was 2.9 times the peak calculated value at the same cross section. The peak measured tensile stress from the negative gradient was 3.8 times the calculated value at the same cross section.

Examination of the structure under load combinations including dead load, prestress, live load, and thermal gradient indicated that no tension is occurring in the structure. However, the maximum allowable compression stress from Section 5.9.4.2.1 of the *AASHTO LRFD Bridge Design Specifications* (2) was exceeded for some portions of the top flange in segments P16-10 and P16-17. The portion of the top flange over the right web in segment P16-10 showed stresses exceeding 70% of the specified concrete design strength, f'_c. $0.7f'_c$ is the approximate limit for linear elastic behavior of the concrete. The peak stress only occurs only a small width of the top flange in P16-10, about 30 cm (1 ft). Additionally, cylinder tests of the concrete used to precast the segments in Ramp P generally indicated higher

concrete strengths than the required design strength, 44.8 MPa (6.5 ksi). Much of the concrete used in the US 183 project achieved twenty-eight day strengths of up to 69 MPa (10ksi). Thus, the true elastic range of the concrete would extend to a much higher stress than is plotted in Figures 7.16 and 7.17. No distress has been observed in Ramp P that can be attributed to thermal gradients or to any other load. This indicates that the maximum allowable compression limit from Section 5.9.4.2.1 of the *AASHTO LRFD Bridge Design Specifications* could be overconservative.

Recommendations

Use of the recommended thermal analysis technique from Section 4.6.6 of the *AASHTO LRFD Bridge Design Specifications* (2) should be re-evaluated. This method is entirely based on the assumption that plane sections remain plane within the loaded cross section that will not be true if warping occurs. Further study of the problem may yield an effective flange width solution similar to the method commonly used to deal with shear lag. Appropriate methods for the solution of transverse stresses should also be examined. Instrumentation studies that examine stress behavior as well as temperatures through box girder cross sections are necessary. Until such time, however, advanced methods such as finite element or folded plate analysis techniques could be used to examine thermal behavior in box girders.

The maximum stress limits in Section 5.9.4.2.1 should allow less restrictive stress limitations for maximum stresses that only occur over a small portion across the width of a girder cross section. Data from Ramp P would tend to suggest that no serious detriment will occur to a bridge if overcompression of concrete only occurs in a small portion of the width of a cross section.

CHAPTER 8. CONCLUSIONS AND RECOMMENDATIONS

8.1 Overview

This study represents one phase of field instrumentation and monitoring of the new US 183 elevated highway in Austin, Texas. This phase includes the instrumentation of a five-span continuous precast segmental horizontally curved concrete box girder ramp bridge built in balanced cantilever. The behavior of this bridge was monitored during construction, under a service level live load test, and under daily applied thermal gradients.

This study included installation of concrete strain gauge devices in three full cross sections of one of the spans of the bridge. In each instrumented cross section, thirty-two concrete strain gauges were placed longitudinally to monitor the flexural and axial behavior at that section, twenty-four concrete gauges were grouped by threes into rosette patterns to monitor shear and transverse tensile stresses. The concrete strain gauges provided reliable information on the moments, shears, torsions, and axial loads occurring at the three-instrumented cross sections. An additional thirty-six strain gauges were placed on external post-tensioning tendons inside the box girder to monitor their structural contribution to the service level performance of the bridge. Finally, fifty-four thermocouple gauges were placed across one full cross section to determine the daily thermal gradients occurring in the bridge. A detailed description of the instrumentation placed in the bridge is given in Chapter 3 of this report.

Data presentation as well as observations of the construction process are given in Chapters 4 through 7 of this report. Conclusions and recommendations from each of those chapters are summarized in this chapter.

8.2 Lessons from the Construction Process

Conclusions and recommendations concerning design and construction practices were drawn from the observations of the construction process made by researchers at the site. The conclusions were divided into three categories: design related, construction related, and inspection related.

8.2.1 Design-Related Issues

Conclusions

1. Overall measured behavior of the bridge during erection and load tests indicated excellent structural design. No major problems exist. The bridge has substantial reserve strength.
2. Some lack of sensitivity to the construction process was demonstrated by the positioning of the access holes at the midspan of the girder, the inadequate space allocated for stressing rams, and the overall working conditions inside the box

girder that include such details as no permanent lighting and the placement of the drainage pipes along the midline of the girder cross section. Neglect in the planning of these details can result in work delays and a decline in the quality of the construction because the skills of the workers are impaired by the difficulties of their work environment.

3. Substantial difficulty in stressing of the external tendons occurred because of their long length, between 90 m (300 ft) and 160 m (525 ft) stretched over multiple spans. A combination of factors related to the length of these tendons probably resulted in the failure of three external tendons during stressing. The long length of the tendons required a large amount of slack and elongation, about 1.2 m (4 ft), to be pulled through the ram before the final tendon force was reached. The large number of strokes required from the stressing ram made power seating after each stroke necessary to avoid large nonuniform seating losses among the strands. The large length of tendon pulled through the ram probably contributed to formation of a knot in the area of the saddle next to the live end of the tendon. The tendons may have been rubbing against deviation and saddle pipes, thus resulting in high friction losses that would be critical over long tendon lengths. Trumpets on the ends of these pipes could have prevented such rubbing. Lastly, the external tendons were very difficult to grout because of their long length. For this bridge the tendons should have been limited to single span lengths, between 38 m (125 ft) and 55 m (180 ft). In no case should tendon lengths exceed 75 m (250 ft) unless special installation methods are used to eliminate the possibility of tangling.
4. Uplift of the superstructure from the bearing pads was recorded. The uplift may have been due to torsional effects caused by the external tendons.
5. The ability of the contractor to adjust vertical or horizontal alignment problems of the spans by adjusting the bearings at the piers was seen as a great advantage of the system of construction. This facet of the system that allows corrections frees designers and contractors from uncertain variables during the planning stages of the bridge.

Recommendations

1. Structural designers should consider all facets of the construction of a bridge with extra appreciation for the tasks that workers need to perform, where they need to perform the task, what tools and materials they will need to manipulate to perform the task, and under what environmental pressures. This consideration should extend not just to the construction process, but to foreseeable long-term inspection and maintenance tasks as well. For segmental projects, particular emphasis should be placed on stressing operations and the space allowed for rams. Detailed records of construction methods used by contractors and the advantages and disadvantages of particular methods should be kept by on-site inspectors and passed on through structural design departments to a centralized information

clearinghouse (possibly maintained by the American Segmental Bridge Institute) to benefit the knowledge and experience of the designers in regard to construction issues.

2. The length of tendon (3 to 5 m) immediately adjacent to the live end anchorage of long post-tensioning tendons should be left straight and free of deviation saddles to help prevent potential tangling and/or knotting problems in the strands of the tendon. Deviation pipes for external tendons should have trumpeted ends (diabolos ends) to prevent rubbing of the strands against the edges of the pipe. On-site inspectors should measure tendon elongations across several strands to verify that all strands elongate the same amount. Project documents and inspectors should also require power seating of the wedges every time the ram is stroked for long tendons that require multiple strokes of the ram to reach the design force. Finally, the lengths of tendons should be limited to stretch across no more than two spans or a maximum length of about 75 m (250 ft) unless special installation procedures are used to eliminate tangling.
3. Designers should consider the uncertainties of the design process and evaluate design concepts based on the adaptability of details to possible change.

Currently nothing can be recommended concerning the uplift of the superstructure off of the bearing pad until the problem is further observed and analyzed. Most likely, the solution lies in a better understanding of the effects of external tendons on horizontally curved bridges.

8.2.2 Construction-Related Issues

Conclusions

1. Many of the erection schemes utilized for the construction of Ramp P demonstrated lax construction planning. Particular schemes with significant difficulty included the erection and subsequent alignment of the interior anchorage segment in two halves and the erection of the first two cantilever segments off of the interior anchorage segment. Possible improvements are suggested in Section 4.5.2.2.
2. Poor visualization of the three-dimensional geometry of the bridge was demonstrated in the design of the bottom flange temporary post-tensioning blisters. The location and size of these blisters consistently conflicted with the alignment of the external tendons

Recommendations

1. Contractors should perform dry test runs of novel construction schemes at the precasting yard if time and space permit. Such tests would immediately make apparent flaws in a proposed scheme and would test the workability of any special construction equipment necessary for a certain task.

2. Erection schemes for precast segments must include measures to correct alignment problems in a quick and easy manner at the time of erection. As already stated, these measures should be pretested in such a manner that their viability is guaranteed.
3. Temporary post-tensioning details should allow free access to the components of the stressing system. External systems are best for this. Systems that require internal ducts may not allow such access, and removal of the temporary prestress after its use is no longer required may be difficult. Thus, the contractor should either plan on sacrificing the temporary prestress steel or providing blockouts at coupler points to allow access to the couplers. Ducts should be generously sized so that plenty of space is available for bars and couplers to easily be pulled through them.
4. Contractors should provide detailed shop or working drawings of structural details that demonstrate that no conflicts exist with other components of the bridge structure. Drawings that clearly demonstrate the details of a proposed erection scheme would also help to indicate any flaws in the idealization of a procedure.

8.2.3 Inspection-Related Issues

Conclusions

1. A construction delay of one night occurred because two segments of a Ramp P cantilever had their labels switched. The incident could have been avoided had either the contractor's or state's quality assurance personnel verified the labeling of the segments prior to their being trucked to the erection site. It is unknown if such checks were routinely performed at the precasting yard by either team of inspectors.
2. A problem occurred when grout from a transverse post-tensioning duct flowed into a longitudinal post-tensioning duct and obstructed the empty duct. Breaches must have been present in each of the ducts at the time of casting. The inspector present at the time of the casting could have closely inspected all of the ducts, noticed the problem, and directed it to be fixed. The incident that occurred and the subsequent damage to the concrete deck of the box girder to free the duct of grout demonstrate the importance that post-tensioning ducts be kept free of obstructions and thoroughly inspected for breaches before concrete is placed.
3. One of the segmental joints in the ramp demonstrated poor squeeze out of joint epoxy. The gap was noticed by an on-site inspector who directed it to be fixed by injection of epoxy. A similar problem in a mainline joint was not noticed and fixed, and some spalling in the bottom slab of the girder has been attributed to the voids that were present in the epoxy.

Recommendations

1. Quality assurance personnel can easily verify segment labels prior to transport to the site by checking the details of post-tensioning duct locations or special features such as anchorage blisters or deviator beams. Construction and inspection records should be logged verifying the quality and identity of the segment prior to transport to the construction site.
2. Verification of the integrity of post-tensioning ducts should be a priority task before casting of the segment because correction of flaws after placement of the concrete can be difficult. The presence of stiffening pipes in the ducts should be confirmed.
3. Full attention should be given to epoxy squeeze out between joints during erection. The cross section of the box girder should be as homogeneous as possible for complete and uniform transfer of stress as well as integrity against environmental forces.

8.3 Behavior Under Construction and Live Loads

The conclusions and recommendations presented in Chapters 5 and 6 are summarized here under two topic headings: stress distributions in box girders and structural behavior. The conclusions and recommendations grouped under the topic of stress distributions are all pertinent to the provisions of Section 4.6.2.6.2 of the *AASHTO LRFD Bridge Design Specifications* (2) concerning effective flange widths for box beam bridges. The conclusions and recommendations grouped under the topic of structural behavior concern other aspects of the bridge's behavior under dead and live loads.

8.3.1 Stress Distributions in Box Girders

Conclusions

1. The AASHTO effective flange method for normal forces was used to calculate peak stresses from the diffusion of cantilever post-tensioning that were close to measured values. In order to predict the tension that was measured at the bottom of the cross section, the compatibility induced tensile zone bounded by the line of inclination of the compressive force distribution had to be included in the effective cross section.
2. Shear lag under prestressing and live loads was noticed next to the support at pier P16 in both the free cantilever and fully continuous configurations of the structure. Reduction of the top flange width at P16-2 for analysis of stresses had been required under Section 4.6.2.6.2 of the *AASHTO LRFD Bridge Design Specifications* (2). The data did not suggest that any changes needed to be made to the code provisions.
3. Measured slopes from the live load test of Ramp P compared quite favorably with calculated values. These slopes were quite small. The calculated values were

based on full section properties of the bridge. The presence of significant shear lag would have caused a reduction in the effective area of the cross section in many parts of the bridge. Thus, greater than anticipated deformations of the bridge would have occurred under applied live load.

Recommendations

Based on the data gathered from the Ramp P study that includes information on stresses and bridge deformations under applied loading, no changes need to be made to the provisions of Section 4.6.2.6.2 of the *AASHTO LRFD Bridge Design Specifications* (2) for handling shear lag. However, the specifications pertaining to the analysis of normal force effects should be changed to indicate that compatibility induced stresses and edge tensile stresses must still be considered near the end of the member just as in post-tensioned anchorage zones. Figure 4.6.2.6.2-4 should be redrawn to clarify that the compressive force spreads out in a 30° cone that acts across the width and depth of the girder. However, the end of the flange cannot be neglected where possible tensile effects occur. Further research to clarify this application is recommended.

8.3.2 Structural Response

Conclusions

1. Insignificant transverse splitting stresses were measured during the stressing process of the cantilever tendons. This includes symmetrical and unsymmetrical loading from the tendons.
2. A sharp peak in stress from the stressing of external post-tensioning tendons was measured in P16-10. Segment P16-10 contained the deviation block for the external post-tensioning tendons, and the peak in stress was probably due to local zone effects.
3. Longitudinal stresses measured for the determinate cantilever were much closer to calculated values than the stresses measured in the fully continuous structure. The difference was probably due to over-idealization of the bearing pads and the omission of the stiffness contribution from the external tendons in the calculation model used for the continuous structure.
4. Measured live load stresses were much less than the measured dead load stresses indicating that the bridge structure has a high reserve for additional live load.
5. Shear stresses measured in the bridge structure under dead, live, and prestressing loads were small. The torsional components of these shear stresses were insignificant.
6. No effect from the horizontal curvature was measured in the longitudinal stresses or the stresses in the external tendons. This indicates that the torsional effect on the moment can be safely ignored for bridges that subtend central angles of up to 15°.

7. The stress changes in the external tendons under live load were very small. Fatigue of these tendons from applied live loads should not be a problem.

Recommendations

1. Section 4.6.1.2.1 of the *AASHTO LRFD Bridge Design Specifications* (2) allows structures with torsionally stiff closed cross sections whose central angle subtended by a span is 12° or less to be analyzed as straight. This provision of the code may be overly conservative. Data from Ramp P suggests that the angle limit may be increased to 15° or maybe even more. For a bridge such as Ramp P with a horizontal radius of curvature of 221 m (726 ft) the current span length limit for straight bridge analysis would be 46.3 m (152 ft). The instrumented span of Ramp P, which demonstrated insignificant torsional effects, was 54.9 m (180 ft). This recommendation cannot be assigned to the analysis of substructure forces. It is unknown from the current data what transverse moments and shears may have been transmitted into the Ramp P substructure from the horizontal curvature of the bridge.
2. A poor comparison between calculated and measured stresses from the continuity stressing indicates that a more advanced calculation model should have been used for the analysis. Some factors that were not accounted for in the calculations were modeling of the actual bearing pad conditions, modeling of the true age and stiffness of the concrete at the closure pores, and modeling of the external tendons as they were placed in the structure. Structural designers should remember that these details may be too important to neglect for an accurate analysis of a continuous box girder structure.

8.4 Thermal Behavior

8.4.1 Shape and Magnitude of Design Gradients

Conclusions

1. The shape of the specified positive and negative design gradients from Section 3.12.3 of the *AASHTO LRFD Bridge Design Specifications* (2) matched the shape of the measured gradients in the Ramp P superstructure best when the maximum allowable magnitude was used for T_3 (the temperature at the bottom of the gradient).
2. The maximum measured gradients in the Ramp P superstructure were significantly less in magnitude than the AASHTO design gradients. Furthermore, the actual maximum gradient has occurred less than 5% out of the total period of measurement. This data would indicate that the design gradients from the AASHTO code are oversevere.

3. Transverse thermal gradients were measured through the thickness of the flanges and webs of the box girder cross section. The magnitudes of these gradients were higher than the magnitudes suggested for segmental box girder bridges (but not required) by Section 6.4.4 of the commentary of the *Proposed AASHTO LRFD Guide Specifications for Design of Segmental Concrete Bridges* (17). The *Guide Specifications* suggest a linear temperature difference of ±5.6°C (10°F) from the exterior to the interior of the box. Measurements from Ramp P showed transverse gradients as high as +8.6°C (15.5°F) and as low as -4.1°C (-7.4°F). Corresponding peak transverse stresses of 7.1 MPa (1.0 ksi) compression and 4.8 MPa (0.7 ksi) tension caused by the transverse temperature gradients were measured in the top flange.

Recommendations

1. The bottom temperature of the required design gradients, T_3, should be set at the maximum allowed temperature, 2.8°C (5°F) for the positive gradient and -1.4°C (-2.5°F) for the negative gradient to best match the shapes for positive and negative thermal gradients that were measured in Ramp P.
2. The design thermal gradients should be based on statistical data from a variety of actual bridge structures under a variety of climatic conditions. In order to accomplish this, instrumentation of bridge superstructure cross sections using thermister or thermocouple gauges will have to become a standard practice for new bridges.
3. Transverse design of box girder cross sections should include analysis of a thermal gradient from the interior to the exterior of the box cross section. Until such time that a thorough statistical database of bridge temperature studies permits the definition of realistic design gradients, the suggested gradients from Section 6.4.4 of the commentary from the *Proposed AASHTO LRFD Guide Specifications for Design of Segmental Concrete Bridges* (17) should be used.

8.4.2 Analysis Methods

Conclusions

1. The recommended method for the analysis of nonlinear thermal gradients from Section 4.6.6 of the *AASHTO LRFD Bridge Design Specifications* (2) did a poor job of predicting the thermally induced stresses in Ramp P. The flaw in the AASHTO recommended method is the assumption that plane sections remain plane. Peak stresses measured in Ramp P were as much as 2.9 times the calculated peak compression for the maximum positive gradient, and as much as 3.8 times the calculated peak tension for the maximum negative gradient.
2. Warping of the box cross section affects not only the longitudinal stresses but the transverse stresses from applied thermal gradients as well.

3. Service load combinations of dead load, prestress, live load, and thermal gradients indicated that no tension was occurring in the bridge. The prestress was adequate for applied negative gradients. However, some overcompression was indicated under applied positive gradients. No distress has been observed in the bridge that can be attributed to thermal gradients.

Recommendations

The method that is recommended in Section 4.6.6 of the *AASHTO LRFD Bridge Design Specifications* (2) needs to be re-evaluated. The effects of applied nonlinear thermal gradients on box girder bridges are not as well understood as are other aspects of box girder behavior. Research studies should be implemented to investigate the problem both analytically and experimentally. Analytical studies should use advanced finite element studies to probe the response of a variety of box girder bridges to applied climatic conditions. Such an approach would allow an understanding of what shapes and magnitudes of thermal gradients occur in different bridge structures under the same climatic stimuli and what structural response occurs in the different bridge structures. Experimental studies should use instrumentation methods to measure both temperatures and stresses occurring in actual bridge structures. This data could be used to verify that a true analytical understanding of the problem is being developed. Additionally, the data would supply statistical information for the selection of realistic design criteria including not only the shapes and magnitudes for design gradients, but reasonable stress limits for thermal gradient loading conditions.

REFERENCES

1. *AASHTO Guide Specifications for Design and Construction of Segmental Concrete Bridges*. American Association of State Highway and Transportation Officials (AASHTO). 1989.

2. *AASHTO LRFD Bridge Design Specifications*. 1st ed. AASHTO. 1994.

3. *AASHTO Standard Specifications for Highway Bridges*. AASHTO. 1989.

4. Andres, V. A. "Verification of Force Distribution in an Innovative Bridge Pier." MSE Thesis. The University of Texas at Austin. December 1995.

5. Arréllaga, J. A. "Instrumentation Systems for Post-Tensioned Segmental Box Girder Bridges." MSE Thesis. The University of Texas at Austin. December 1991.

6. Bonzon, W. S. "Thermal Gradients in Segmentally Constructed Hollow Box Bridge Piers." MSE Thesis. The University of Texas at Austin. December 1996.

7. Davis, R. T. "Measurement Based Performance Evaluation of a Segmental Concrete Bridge." Ph.D. Dissertation. The University of Texas at Austin. May 1998.

8. Hyzak, M. D. "Bridge Deformation Monitoring." MSE Thesis. The University of Texas at Austin. May 1998.

9. Kollbrunner, C. F., and K. Basler. *Torsion in Structures*. Springer-Verlag Berlin/Heidelburg. New York. 1969.

10. Kristek, V. *Theory of Box Girders*. John Wiley and Sons. New York. 1979.

11. Menn, C. *Prestressed Concrete Bridges*. Bérkhäuser Verlag. Basel, Germany. 1990.

12. Nakai, H., and C. H. Yoo. *Analysis and Design of Curved Steel Bridges*. McGraw-Hill, Inc. New York. 1988.

13. *1983 Ontario Highway Bridge Design Code*. Highway Engineering Division. Toronto, Ontario. 1983.

14. Petroski, H. *Engineers of Dreams*. Alfred A. Knopf. New York. 1995.

15. Podolny, W., Jr., and J. M. Muller. *Construction and Design of Prestressed Concrete Segmental Bridges*. John Wiley and Sons, Inc. New York. 1982.

16. Potgieter, I. C., and W. L. Gamble. "Response of Highway Bridges to Nonlinear Temperature Distributions." Report No. FHWA/IL/UI-201. University of Illinois at Urbana-Champaign. Urbana, IL. April 1983.

17. *Proposed AASHTO Guide Specifications for Design and Construction of Segmental Concrete Bridges*. AASHTO. March 1997.

18. RISA2D. v3.03. Program for DOS. RISA Technologies. Lake Forest, CA. 1993.

19. Roberts, C. L., J. E. Breen, and M. E. Kreger. "Measurement-Based Revisions for Segmental Bridge Design and Construction Criteria." Report No. CTR 0-1234-3F. Center for Transportation Research. The University of Texas at Austin. August 1993.

20. Ryals, K. K., J. E. Breen, and M. E. Kreger. "Fretting Fatigue in External Post-Tensioned Tendons." Report No. CTR 3-5-89/2-1211-1F. Center for Transportation Research. The University of Texas at Austin. December 1992.

21. "Steel, Concrete and Composite Bridges, Part I, General Statement." British Standard BS 5400. British Standards Institution. Crowthorne. Berkshire, England. 1978.

22. Thompson, M. K. "Measured Behavior of a Balanced Cantilever Erected Curved Segmental Concrete Bridge." MSE Thesis. The University of Texas at Austin. December 1997.

23. Wood, B. A. "Thermal Gradients and Their Effects on Segmental Concrete Box Girder Bridges." MSE Thesis. The University of Texas at Austin. August 1997.